Analytische Chemie

Dissertationsthema

Development of Separation Methods and Chemical Transformations for Structural Elucidation of Large Organic Compounds in Petroleum Fractions

Inaugural-Dissertation
zur Erlangung des Doktorgrades
der Naturwissenschaften
in der NRW Graduate School of Chemistry
im Fachbereich Chemie und Pharmazie
der Mathematisch-Naturwissenschaftlichen Fakultät
der Westfälischen Wilhelms-Universität Münster

Vorgelegt von
Magdalena Ulman, geb. Olszewska
aus Białystok
-2008-

Dekanin/Dekan:	Prof. Dr. F. Ekkehardt Hahn
Erste Gutachterin/ Erster Gutachter:	Prof. Dr. Jan T. Andersson
Zweite Gutachterin/ Zweiter Gutachter:	Prof. Dr. Uwe Karst
Tag der mündlichen Prüfung(en):	10.11.2008……..
Tag der Promotion:	10.11.2008...……..

To my family

Table of Contents

1 Introduction ... 1
1.1 Energy Supply ... 1
1.2 Fossil Fuel Formation ... 2
1.3 Introduction of Sulfur into Crude Oil ... 4
1.4 Forms of Sulfur Compounds in Crude Oil ... 7
1.5 Refining Process ... 8
1.6 Legal Limits of Sulfur in Fuels ... 11
1.7 Desulfurization Process ... 12
1.7.1 Hydrodesulfurization ... 13
1.7.2 Other Methods of Desulfurization ... 16
1.8 Summary ... 18
2 Analytical Techniques for PASH Separation and Investigation ... 19
2.1 Liquid Chromatography ... 19
2.2 Gas Chromatography ... 22
2.3 Mass Spectrometry ... 23
2.4 Other Techniques ... 29
3 ESI FT-ICR MS ... 31
3.1 Data Interpretation ... 31
3.1.1 “Hydrogen Deficiency” (z) ... 33
3.1.2 Nominal Mass Series (z^*) ... 33
3.1.3 Double Bond Equivalent (DBE) ... 34
3.1.4 Kendrick Mass Defect (KMD) ... 34
3.1.5 Multiple Sorting ... 35
3.1.6 Kendrick Plot ... 37
3.1.7 Generation of Pseudograms ... 38
4 Objectives ... 39
5 Pattern of PASHs in Vacuum Gas Oil (VGO) ... 40
5.1 Experimental Section ... 40
5.1.1 Sample ... 40
5.1.2 Liquid Chromatography of PASHs ... 41
5.1.2.1 SARA Fractionation ... 41
5.1.2.2 Ligand Exchange Chromatography ... 42
5.1.2.3 Separation on β-Cyclodextrin ... 42
5.1.2.4 Charge Transfer Chromatography ... 43
5.1.3 PASH Methylation ... 43
5.1.4 Analysis ... 44
5.2 Results and Discussion ... 45
5.2.1 Separation ... 45
5.2.2 CD Fractions Analysis ... 58
5.3 Summary ... 67
6 Oxidation ... 68
6.1 Dehydrogenation ... 70
6.1.1 DDQ ... 72
6.1.1.1 Experimental Procedure ... 73
6.1.1.2 Results and Discussion (Standard Mixture) ... 73
6.1.1.3 Mass Spectra (Standard Mixture) ... 82
6.1.1.4 Results and Discussion (Real-World Sample) ... 90
6.1.1.5 Results and Discussion (Standard Mixture, Chloranil) ... 102
6.1.1.6 Summary ... 103

6.1.2 Palladium 104
6.1.2.1 Experimental Section 105
6.1.2.2 Results and Discussion (Standard Mixture) 105
6.1.2.3 Results and Discussion (Real-World Sample) 107
6.1.2.4 Summary 115
6.1.3 Selenium 116
6.1.3.1 Experimental Section 118
6.1.3.2 Results and Discussion (Standard Mixture) 119
6.1.3.3 Results and Discussion (Real-World Sample) 121
6.1.3.4 Summary 128
6.2 Summary 129
7 Hydrodesulfurization of VGO 134
7.1 Experimental Section 134
7.1.1 Sample 134
7.1.2 Liquid chromatography of PASHs 135
7.1.3 PASH Methylation 135
7.1.4 Analysis 135
7.2 Results and Discussion 135
7.3 Summary 142
8 Summary 143
9 Zusammenfassung 146
10 Appendix 150
10.1 Synthesis of Model Thiophenic Compounds 150
10.1.1 Synthesis of Tetrahydrodibenzothiophene 150
10.1.1.1 Synthesis of 2-Bromocyclohexanone 150
10.1.1.2 Sythesis of Tetrahydrodibenzothiophene (One-Pot Synthesis) 150
10.1.1.2.1 Preparation of Na_2CO_3/SiO_2 150
10.1.1.2.2 Preparation of PPA/SiO_2 151
10.1.1.2.3 Procedure 151
10.1.2 Synthesis of 2-Cyclohexylmethanobenzothiophene 152
10.1.3 Synthesis of 2-Cyclohexylethanobenzothiophene 153
10.1.4 Synthesis of 2-Benzylbenzothiophene 154
10.1.5 Synthesis of 4-Decyldibenzothiophene 155
10.1.6 Synthesis of 2-Decylbenzothiophene 156
10.1.7 Synthesis of 2-Eicosylbenzothiophene 157
10.2 Synthesis of Pd(II)-Mercaptopropano Silica Gel 158
10.3 Synthesis of Tetrachlorophthalimide Silica Gel 159
10.3.1 Synthesis of Tetrachlorophthalicmonoallylamide-allylammonium Salt 159
10.3.2 Synthesis of Tetrachlorophthalicallylimide 159
10.3.3 Synthesis of Tetrachlorophthalimidopropanotrichlorosilane 159
10.3.4 Synthesis of Tetrachlorophthalimidopropanosilica 160
10.4 Instrumental Parameters 161
10.4.1 High-Performance Liquid Chromatography 161
10.4.2 Gas Chromatography 162
10.4.3 Fourier Transform Ion Cyclotron Resonance Mass Spectrometry 163
10.4.4 Nuclear Magnetic Resonance 164
10.4.5 Elemental CHN Analyses 164
10.4.6 Fluorescence spectroscopy 164
10.5 Materials 165
10.6 Abbreviations and Symbols 168
11 References 171

1 Introduction

1.1 Energy Supply

Energy supply and demand play an increasingly vital role in our national security and for the economic output. The fossil fuels (coal, oil and gas) have been formed from organic remains of prehistoric plants and animals. They are a non-renewable source of energy. Over 85 % of our energy demand is met by the combustion of fossil fuels. In the 1970s, oil shortages pushed the development of alternative energy sources. The renewable energy sources like wind, solar, geothermal, hydropower and biomass will play an important role in the future. Overall consumption of renewable resources in the United States in 2006, for example, was about 7 % of all the energy used nationally [1, 2].

The energy in wind can be used for practical purposes like generating electricity. In 2005, wind mills in the United States generated a total of 17.8 billion kWh of electricity, enough to serve more than 1.6 million households. However, it was only a small fraction of the nation's total electricity production, about 0.4 %.

Solar energy can be converted into others forms of energy, like heat and electricity. Electricity can be obtained using photovoltaic cells or solar power plants.

Geothermal energy is simply the heat from the Earth. The three main uses of geothermal energy are: direct use and district heating systems using hot water near the surface (a district heating system provides heat for 95 % of the buildings in Reykjavik, Iceland), electricity generation and geothermal heat pumps.

Hydro-energy uses running water as the energy source. Of the renewable energy sources that generate electricity, hydropower is the most often used. It accounted for 7 % of total U.S. electricity generation and 73 % of generation from the renewables in 2005.

Biomass, simply organic material from plants and animals, is renewable, as we are going to carry on making waste products. Biomass fuels provide about 3 % of the energy used in the United States.

The use of renewable energy is not new. 125 years ago, wood supplied up to 90 % of our energy needs. The use of these sources is limited by the fact that they are not always available. Despite this the use of renewable fuels grows quickly, due to higher prices for the non-renewable fuels [1, 2].

1.2 Fossil Fuel Formation

In the earlier days of Earth, millions of years ago, the majority of life forms were phytoplankton and zooplankton. The beginning of our fossil fuel reserves took place after the death of these life forms and the accumulation on the bottom of a seabed. The age they were created is called Carboniferous Period. It was part of the Paleozoic Era.

Pressure, heat, bacteria and time played an important role in the formation of fossil fuel. Mineral sedimentation embedded the organisms in rock and the continued sedimentation caused an increase of pressure and temperature. Under oxic conditions an efficient bacterial breakdown took place, returning the material into the carbon cycle as carbon dioxide. Under anoxic conditions (like the marine environment) the material was transformed into fossil material by chemical transformation [3-5].

Three stages of transformation can be named during fossil fuel formation: diagenesis, catagenesis and metagenesis.

Diagenesis is a process affecting the primary products under conditions of relatively low temperature and pressure. The main product of this first step is kerogen, insoluble in common organic solvents, with a high amount of oxygen in form of esters, carbonyls, hydroxyl groups etc. (with considered elemental composition $C_{1000}H_{500-1800}O_{25-300}N_{10-35}S_{5-30}$), formed by polycondensation of the biological degradation products. Kerogen can be classified into high-sulfur or low-sulfur kerogens. The main factor is availability of low-valent sulfur species (H_2S and polysulfides) for the incorporation into the organic material. A high amount of

iron minerals can capture the sulfide and form iron(II) sulfides and thus is a competitive reaction to this incorporation.

Decomposition of kerogen into bitumen, which is later cracked into oil, takes place during catagenesis. A lot of heteroatoms and water are lost, aromatic systems are stacked, side chains are cleaved, and methane and hydrogen sulfide are released during this stage. Catagenesis can be divided into two parts: the oil window (liquid oil formation) and the wet gas zone (wet gases with condensate formation).

The degree of aromaticity increases during the last stage, metagenesis, with the ratio of hydrogen-to-carbon falling to 0.25 (for comparison, *n*-hexane shows a ratio of 2.33 and benzene of 1) [6].

Oil and gas are not able to penetrate the rocks and because of that they are found not freely drifting in the ground, only between the folds of a rock and in the areas of a rock that are porous. The folds are created when the continental plates shift and move. Antarctica is the only continent where oil fields are not known [3-5].

Coal was formed in a comparable way as fossil material. The first product in the coalification process is peat. Next, the peat is transformed into lignite and then into subbituminous coal and finally into bituminous coal, which is jet black and has a high heating value. The last stage is anthracite [6].

The average elemental distribution in fossil materials is presented in Table 1 [5-8]. All crude oils are mainly composed of carbon and hydrogen. Minor amounts of heteroatoms like sulfur, oxygen and nitrogen, and trace amount of metals like vanadium and nickel can be found. Sulfur is the third most abundant element in crude oil. The introduction of sulfur into the crude oil is explained later.

The average composition of the crude oil is 57 % aliphatics, 29 % aromatic hydrocarbons and 14 % resins and asphaltenes. The aliphatic hydrocarbons can be divided into linear and branched ones and the aromatic into mono-, polycyclic aromatic hydrocarbons and aromatic compounds with heteroatoms [6].

Table 1 Elemental distribution in fossil materials [5-8]

	Oil, %	Coal, %
Carbon	83 - 87	73 - 94
Hydrogen	10 - 14	2.4 - 5.6
Sulfur	0.05 - 13.9	0.5 - 2.1
Nitrogen	0.1 - 2	0.9 - 1.9
Oxygen	0.05 - 1.5	2.1 - 21.3

1.3 Introduction of Sulfur into Crude Oil

The origin of sulfur in the crude oil is not clear. It cannot be completely explained by sulfur from biota. This amount is not present in the living organisms. Thus, the source of sulfur from inorganic sources like sulfate from the sea water can be considered as a major source. The sulfur cycle in sea water involves continuous oxidation and reduction processes, caused by microorganisms like *Desulfovibrio*, *Desulfobacter* (which reduce sulfate to sulfide) and *Thiobacillus* (oxidize reduced sulfur to elemental sulfur) [9].

The origin of Organic Sulfur Compounds (OSC) can be explained by three major pathways, namely biosynthesis, formation during early diagenesis and by reaction of elemental sulfur and hydrocarbons, but none of them has been proved to conclusively occur in fossil material.

Biosynthesis

Cyr *et al.* suggested the biosynthetic origin for bicyclic, tetracyclic and hopane sulfides present in petroleum [10]. The sulfur atom is attached to the second carbon atom of the alkyl side chain of the hydrocarbon. That was thought to reflect the site specificity of the biosynthetic pathway, where sulfur is incorporated into the hydrocarbon framework [10, 11].

Formation during early diagenesis

Brassel *et al.* identified a number of isoprenoid thiophenes in shallow, immature sediments [12]. The origin of these compounds was suggested to occur via incorporation of inorganic sulfur species (H_2S, HS^-, HS_x^-) into chlorophyll derived phytol, archaebacterial phytenes or their diagenetic products. Also Sinninghe Damsté *et al.* confirmed this hypothesis [13, 14]. They attributed the OSC identified to sulfur incorporation into the specific precursors. The sediments and the source rock of the oil, from which the OSC were isolated, were deposited under anoxic conditions with low amount of Fe ions. These kinds of conditions are thought to favor such reactions. Normally bacterial sulfate reduction leads to the production of H_2S which readily reacts with Fe ions to form inorganic sulfur compounds (FeS and FeS_2). In an environment of low Fe content (such as carbonate environments), H_2S is available for sulfur incorporation reactions. The organic-sulfur rich kerogens and exctractable OSC can thus be generated. The sulfur incorporation into mono- and polyunsaturated C_{20} isoprenoid alcohols or their diagenetic products was proposed to lead to the formation of thiophenes. Additional double bonds in the alkyl side chain of these thiophenes may result in the incorporation of another sulfur atom and lead to the creation of bithiophenes and (thienyl)alkylthiophenes, or a ring closure reaction followed by the aromatization and creation of isoprenoid benzothiophenes. The intermediate compounds may be thiolanes and thienylthiolanes. The other isoprenoid OSC can be formed by the same mechanism but derived from with other substances. Unsaturated fatty acids or alcohols might also play a role as precursors for di-*n*-alkylthiolanes and di-*n*-alkylthianes. Vairavamurthy and Mopper presented the formation of 3-mercaptopropionic acid by an abiotic reaction between hydrogen sulfide and acrylic acid in recent marine sediments [15]. They suggested a pathway for incorporation of sulfur during early diagenesis [11-16].

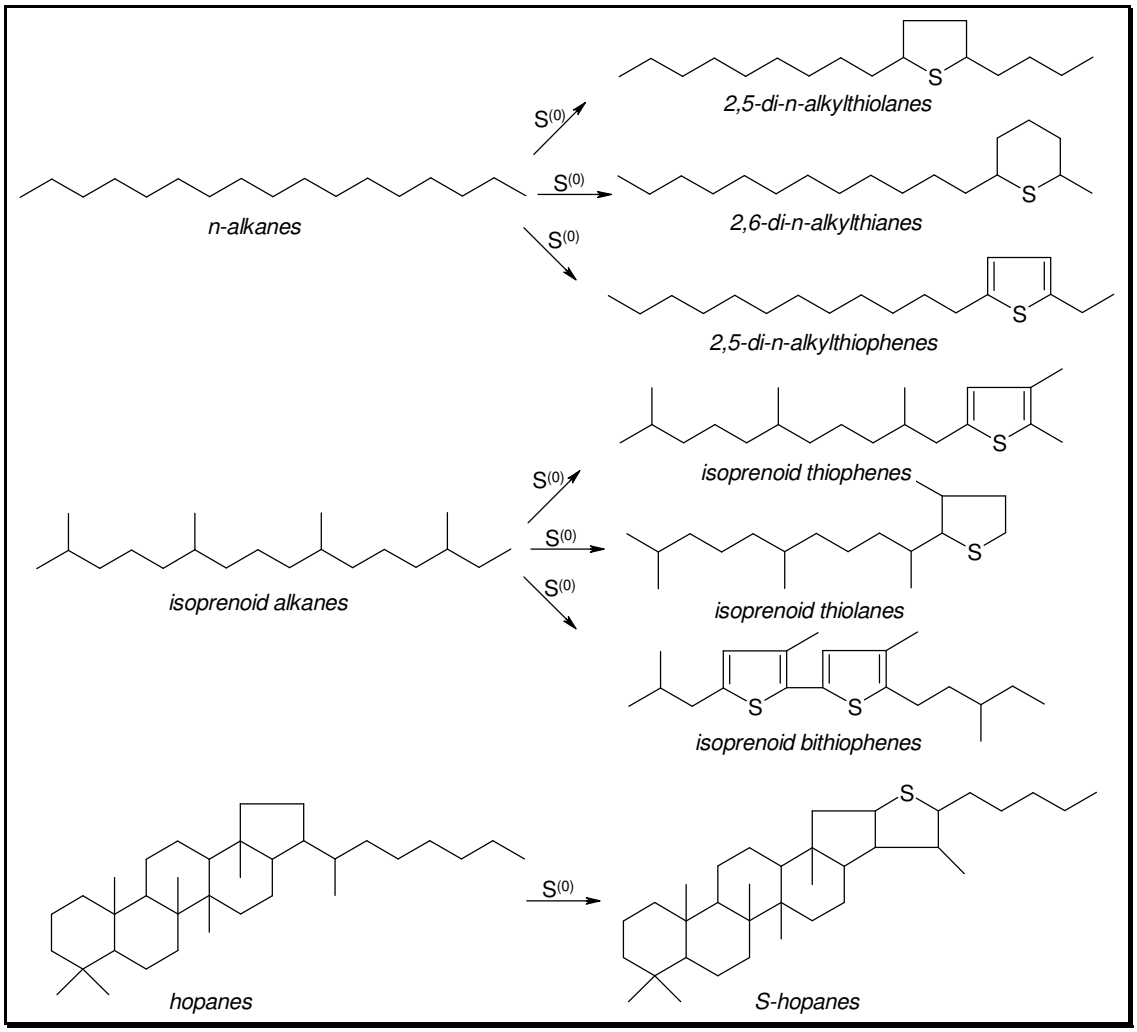

Figure 1 Possible origin of OSC in sediments and immature crude oils [11]

Formation by reaction of elemental sulfur and hydrocarbons

Schmid *et al.* suggested that 2,5-di-*n*-alkylthiolanes present in petroleum might originate from reactions of the *n*-alkanes with elemental sulfur during early maturation [17]. The hypothesis was partly supported by experiments. Heating of *n*-octadecane in the presence of elemental sulfur at 200 - 250 °C for 62 h produced C_{18} 2,5-di-*n*-alkylthiophenes, although the C_{18} 2,5-di-*n*-thiolanes were not present. The above hypothesis was negated by Sinninghte Damsté *et al.* [11]. They proposed sulfur incorporation into the functionalized precursors during the early stage of diagenesis as the major origin for the OSC [11, 17].

Further studies of Sinninghte Damsté *et al.* indicated two types of sulfur incorporation reactions with suitably functionalized precursors at the early stage of diagenesis, that is intramolecular and intermolecular. Intermolecular reactions can give rise to the formation of sulfur-containing high molecular weight substances [11].

1.4 Forms of Sulfur Compounds in Crude Oil

Sulfur exists in both aliphatic and aromatic forms in the crude oil.

The fractions boiling below 150 °C are composed mainly of alkane- and cycloalkanethiols, dialkyl and alkyl cycloalkyl sulfides, disulfides, monocyclic sulfides, thiophene and thiophenes with one or two short side chains.

The fractions boiling between 150 - 250 °C are comprised of alkane-, arene- and cycloalkanethiols, dialkyl, alkyl cycloalkyl and alkyl aryl sulfides, polysulfides, mono-, bi- and tricyclic sulfides, thiaindanes, thiophenes with up to four short side chains and thiophenes with one annealed ring (benzothiophenes, thienothiophenes and thienopyridines).

The fractions boiling above 250 °C contain thiophenes, isothiaindanes, dithienyls, thiazoles, thiochinolones, annealed thiophenes (benzothiophene, indenothiophenes, dibenzothiophenes, naphtho-, benzonaphtho- and phenanthrothiophenes, benzodithiophenes).

The fractions boiling above 540 °C contain around half of the total amount of sulfur in crudes. The sulfur compounds consist of thiophenes up to 80 %, in polycyclic systems and with the side chains attached, which can comprise heteroatoms [8].

A few typical parent structures of sulfur compounds are presented in Table 2.

Table 2 Typical structures of sulfur compounds in crude oils

Structure	Name
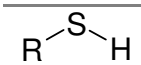	thiol
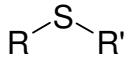	sulfide
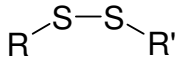	disulfide
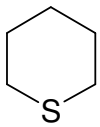	thiane
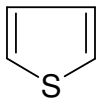	thiophene
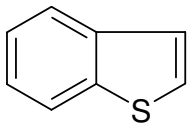	benzothiophene
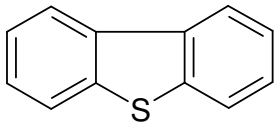	dibenzothiophene
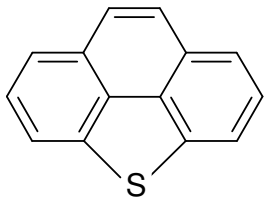	phenanthro[4,5-*bcd*]thiophene

1.5 Refining Process

Crude oil is a mixture not suitable for direct use and it has to be refined, that is broken down into smaller fractions, before using. A typical crude oil contains only 15 - 20 % of straight-run gasoline with low octane number (explained further in this chapter).

There are a few basic steps in the refining process: distillation, cracking, treating and reforming.

Distillation

Modern distillation separates light hydrocarbon molecules from heavy ones in the distillation towers. During the process, the lightest materials, like propane and butane, vaporize and rise to the top of the atmospheric column. Medium weight materials, including gasoline, jet and diesel fuels, condense in the middle. Heavy materials, called gas oils, condense in the lower part of the atmospheric column. The heaviest tar-like material, called residuum, never really rises. In some cases, the distillation columns are operated under reduced pressure. Vacuum distillation reduces the chance of thermal decomposition (cracking) due to overheating of the mixture.

The fractions obtained from a distillation unit with the respective boiling ranges are presented in Table 3.

Table 3 Classification of the refinery cuts according to the boiling ranges [18]

	Boiling range [°C]	Carbon number	Usage
Petroleum Gas	<40	1 - 4	heating, cooking
Naphtha	60 - 100	5 - 9	intermediate of gasoline
Gasoline	40 - 205	5 - 12	motor fuels
Kerosene	175 - 325	10 - 18	fuel for jet and tractor engines
Gas Oil	250 - 350	>12	diesel fuel, heating oil
Lubricating Oil	300 - 370	20 - 50	motor oil, grease
Heavy Gas Oil	370 - 550	20 - 70	industrial oil
Residuals	>550	>70	coke, tar, wax

Cracking

Heat and catalysts are used to convert the heavier oils to lighter products and in this way improve the yield of the lighter fractions. There are three cracking methods: fluid catalytic cracking (FCC), hydrocracking (Isomax), coking (thermal-cracking).

FCC uses high temperature and a catalyst to crack heavy gas oils into gasoline. Hydrocracking applies a catalyst to react gas oil and hydrogen into jet fuel and gasoline under high pressure and high temperature. By using the coking, high

value light products are obtained. The large molecules are broken down into smaller molecules when the residuum is held in a coke drum at a high temperature for a period of time.

Treating

The crude products contain impurities like sulfur and nitrogen. By a process called hydrotreating, a milder version of hydrocracking, these impurities can be removed and thus reduce the air pollution formed when the fuels are burnt. Sulfur is converted into hydrogen sulfide and then into elemental sulfur. Nitrogen is transformed into ammonia and removed by water-washing.

Reforming

The straight run gasoline, that has a low octane rating, is sent to a reforming unit which can increase the octane level.

To determine the octane number for different gasolines, the knocking characteristics (premature ignition produces knocking) are compared to a mixture of 2,2,4-trimethylpentane (isooctane, octane) and *n*-heptane. Heptane knocks considerably and by definition has the octane number zero. Isooctane burns smoothly and has the octane number 100. Thus, the 87-octane rating has knocking characteristics similar to a mixture of 87 % isooctane and 13 % *n*-heptane.

The reforming unit employs noble metal catalysts, platinum and rhenium (rheniformers). Hydrocarbon molecules are reformed into high octane gasoline components. Methylcyclohexane is reformed for example into toluene. The reforming process removes hydrogen from low-octane gasoline, which is then used in the various cracking and treating units.

A schematic diagram showing all the processes involved in the refinery unit is presented in Figure 2.

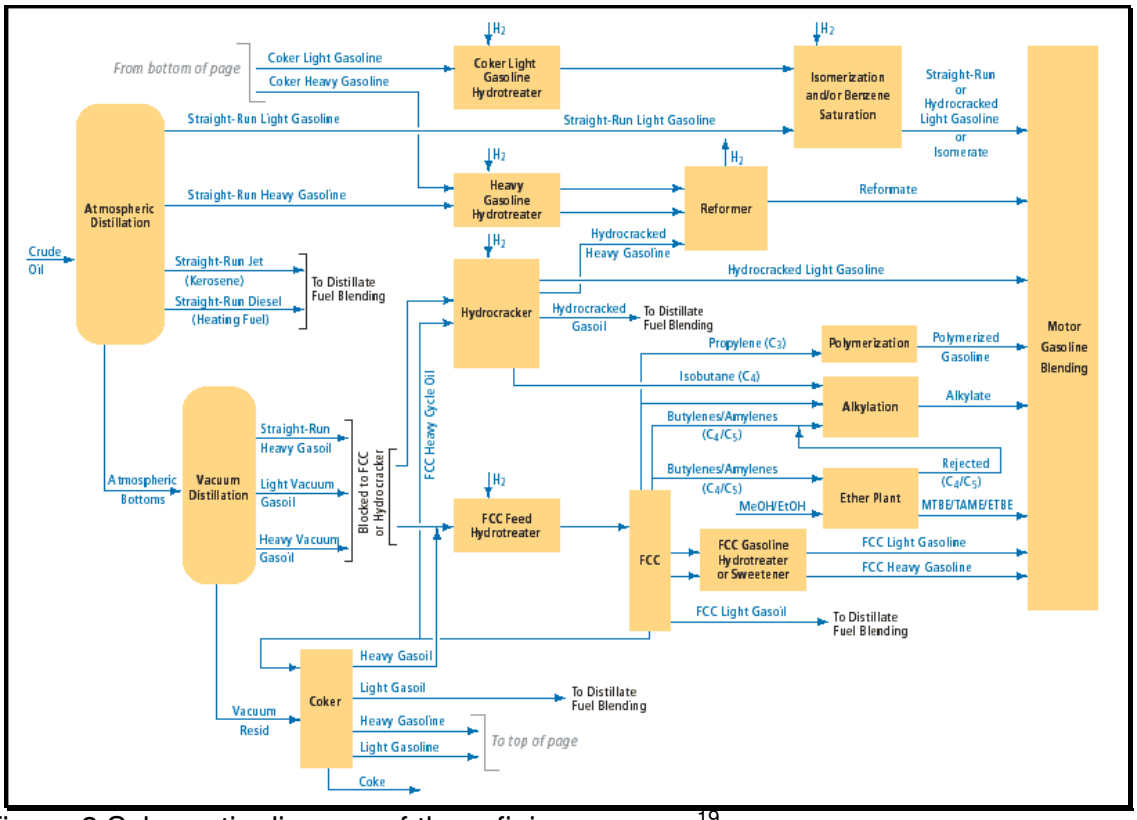

Figure 2 Schematic diagram of the refining process [19]

Blending and combining cannot be overlooked in the refining process. In the first process gasoline is blended from the components made in several processes in order to obtain higher octane number, and other better specification. The second process combines, in the presence of sulfuric acid catalyst, the light molecules, lighter than gasoline, to obtain high octane level gasoline [19].

1.6 Legal Limits of Sulfur in Fuels

The environmental regulations exert pressure to reduce the maximum allowed sulfur content in the fuel [20]. The primary goal of the recently proposed regulations by the Directive of the European Parliament and the Environmental Protection Agency (EPA) Clean Air Act (Tier 2) is to reduce the sulfur content of transportation fuels. To minimize the negative health and environmental effects of automotive exhaust

emission, the sulfur level in motor fuels is minimized [21]. All industrial catalysts based on nobel metals suffer from the inhibitory effect of sulfur [22].

In 1998 the European directive on transportation fuels put limits on sulfur in gasoline and diesel fuel of 150 ppm and 350 ppm respectively. In 2005 Europe restricted its diesel sulfur content to less than 50 ppm [21].

In January 2001 EPA issued regulations requiring refiners to reduce sulfur content in highways diesel fuels by 97 % and leave no more than 15 ppm by June 2006 [23]. EPA issued new rules in June 2004 that require refiners to reduce the sulfur content in non-road diesel in steps. First, a 500 ppm sulfur cap is effective by June 2007. Second, a 15 ppm sulfur cap is effective in June 2010 (for non-road diesel other than locomotive and marine). Third, a 15 ppm sulfur cap is effective in June 2012 (for locomotive and marine diesel). Fourth, a 15 ppm sulfur cap is effective in June 2014 (for small-refiners non-road diesel) [24].

In Japan the sulfur content in diesel fuels has been reduced in several steps since 1990: a 2000 ppm sulfur limit became effective in 1994, 500 ppm sulfur limit in 1997, 50 ppm sulfur limit in 2005 and 10 ppm sulfur limit is effective from 2007 [25, 26].

Germany has passed legislation limiting the sulfur in diesel and gasoline to 10 ppm as of November 2001 [21].

Additional sulfur regulations are expected in the future, therefore numerous studies on deep desulfurization of diesel fuel continue in an intensive way [27].

1.7 Desulfurization Process

The exhaust gases from motor vehicles contribute to air pollution through release of SO_x [21, 28, 29]. Sulfur is also a well-known poison for catalytic converters. Therefore there is a need to reduce sulfur level in fuels. More and more severe environmental legislations are introduced [20-22, 27, 30-32]. Industrial research is aimed at finding the best methods and catalysts for ultra-deep desulfurization. The challenge is to remove the sulfur impurities with a minimal olefin saturation since olefins provide a fairly good octane number [22, 33].

1.7.1 Hydrodesulfurization

The hydrodesulfurization (HDS) is a well documented process. It has been common in the refining of crude oil for over 60 years. It is a process in which sulfur is removed from sulfur compounds by reaction with hydrogen, releasing H_2S, which can be next absorbed by reaction with ZnO to form ZnS and in this way removed from the hydrocarbon feedstock. The HDS is a catalyzed reaction usually involving a metal sulfide catalyst, in particular molybdenum sulfide promoted by cobalt or nickel, supported on porous alumina ($Co/Mo/Al_2O_3$ or $Ni/Mo/Al_2O_3$). Its performance depends on the properties of the specific catalyst (active species concentration, support properties, synthesis route), the reaction condition, the nature and concentration of the sulfur compounds, as well as the reactor and process design [21, 34]. The HDS reaction is usually operated at moderately high temperature and pressure, typically 300 - 350 °C and 50 - 100 atm [21, 27, 29, 30, 33, 35-37].

The reactivity depends on the local environment of the sulfur atom in the molecule and the overall shape of the molecule. The first step of the process is the coordination of the molecule onto the active site on the catalyst surface. There are two possibilities for the coordination for dibenzothiophene (DBT), via the π-system or via the p-orbital sticking out of the molecule). For 4,6-dimethyldibenzothiophene , the methyl groups inhibit the coordination via the p-orbital and the coordination via the π-system is favored.

The aliphatic organosulfur compounds (mercaptans, sulfides, disulfides) are very reactive in conventional HDS. They can be easily removed (Figure 3) [21].

$$R-S-H + H_2 \longrightarrow R-H + H_2S$$
$$R^1-S-R^2 + 2H_2 \longrightarrow R^1-H + R^2-H + H_2S$$
$$R^1-S-S-R^2 + 3H_2 \longrightarrow R^1-H + R^2-H + 2H_2S$$

Figure 3 Aliphatic organosulfur compounds HDS reaction pathways [21]

The HDS reaction pathways of thiophene are presented in Figure 4. The thiophenic ring is hydrogenated prior to the desulfurization (hydrogenation pathway). The thiophenic ring can also be split due to attack by surface adsorbed hydrogen at the sulfur atom (hydrogenolysis pathway). Both pathways are possible and which reaction pathway dominates depends on the nature of the sulfur compound, the reaction conditions and the catalyst used. Thiophene and H_2S are inhibitors for the HDS. The reactivity is affected by the degree of substitution of the thiophenic ring. It was found, that the reactivity varies in the following order: thiophene > 2-methylthiophene > 2,5-dimethylthiophene [33, 38].

Figure 5 presents the HDS reaction pathways for benzothiophene. Again H_2S was proposed to inhibit hydrogenolysis, but not hydrogenation. It was observed, that a methyl substitution of benzothiophene reduces its rate of partial hydrogenation. The hydrogenolysis route becomes more favorable. The reactivities with respect to hydrogenation are in the order: benzothiophene > 2-methylbenzothiophene > 3-methylbenzothiophene > 2,3-dimethylbenzothiophene. The effect is proposed to be due to electronic factors [33, 39].

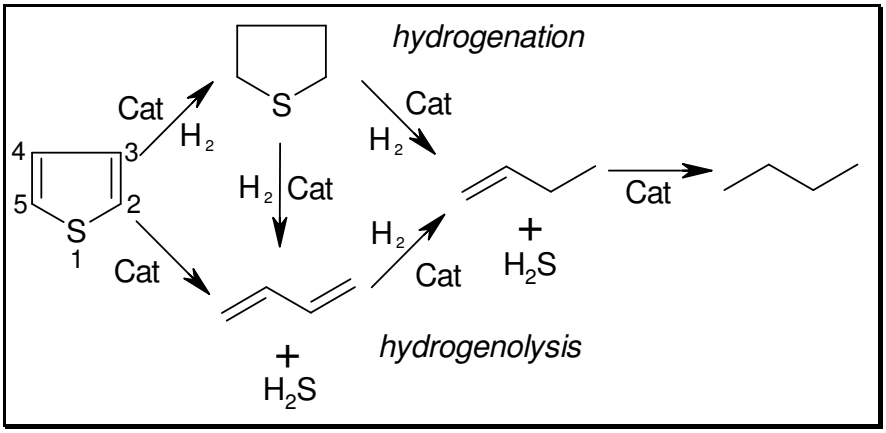

Figure 4 Thiophene HDS reaction pathways [21]

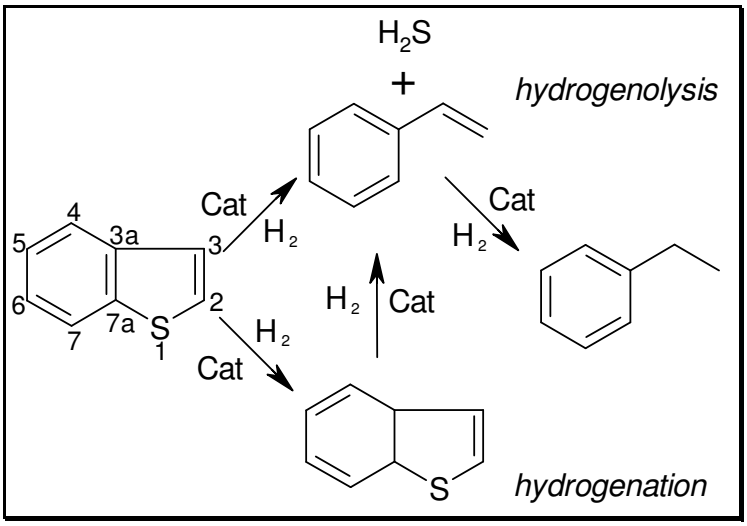

Figure 5 Benzothiophene HDS reaction pathways [21]

Figure 6 presents the HDS reaction pathways for dibenzothiophene. The conversion proceeds via least hydrogen consumption (hydrogenation of biphenyl and cyclohexylbenzene is slow). The rate of hydrogenation of dibenzothiophene increases when the H_2S concentration increases [33, 40]. Under the same condition dibenzothiophene reacts preferably via the hydrogenolysis pathway whereas 4,6-dimethyldibenzothiophene via both, the hydrogenation and the hydrogenolysis routes [21].

The HDS reactivity of substituted dibenzothiophenes decreases as follows: 2,8-dimethyldibenzothiophene > dibenzothiophene > 4-methyldibenzothiophene > 4,6-dimethyldibenzothiophene. The enhancement in reactivity can be explained by the electronic effects. Methyl groups *para* to the α-carbons (4a and 4b) enrich the electron density on the sulfur atom and increase the activity. The decrease in the HDS reactivity is explained by steric effects [41]. Adsorption of the substrate onto the catalyst surface via the sulfur atom is hindered by the methyl groups [20, 33, 42-44]. It is possible to enhance the reactivity of 4,6-dimethyldibenzothiophene by removing the steric hindrance of the methyl groups by hydrogenation of one of the phenyl rings, isomerization (shifting methyl groups from position 4,6 to 3,7 or 2,8), demethylation or C-C bond scission. The saturation depends on the hydrogenation capabilities of

the catalyst (suitable metal for example). All other routes depend on the acidic property of the catalyst [20, 35].

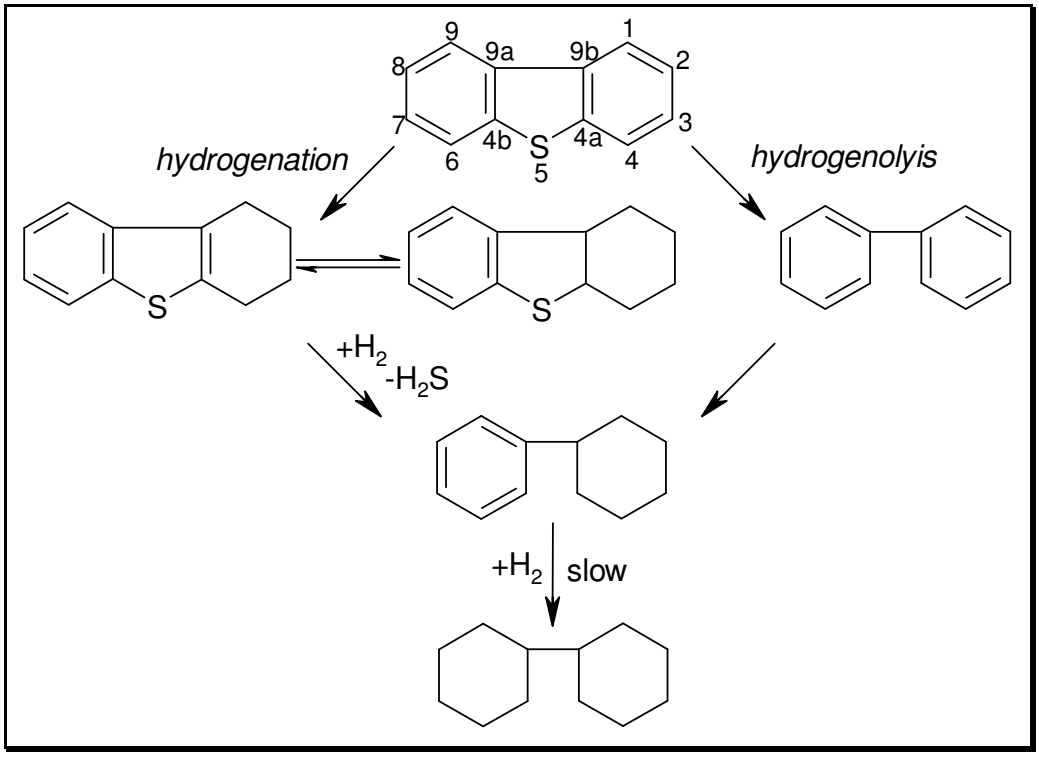

Figure 6 Dibenzothiophene HDS reaction pathways [21]

Polynuclear organic sulfur compounds are the least reactive sulfur compounds in the HDS reaction. The reactivity of alkylbenzonaphthothiophenes and alkylphenanthrothiophenes are much higher than those of the alkyldibenzothiophenes with one of the alkyl substituents at the 4 position, but lower than those for alkylbenzothiophenes [34].

1.7.2 Other Methods of Desulfurization

Non-HDS technologies for efficient removal of sulfur molecules include: shifting the boiling point of sulfur compounds, oxidative desulfurization, desulfurization via extraction, precipitation, adsorption, etc [20, 21].

Shifting the boiling point by alkylation

When boiling temperatures of sulfur compounds are shifted to a higher value, they can be removed by distillation. The sulfur compounds remain in the distillation residue and can be removed by the HDS when the octane number is not an issue. The process employs alkylation of thiophenic compounds via reaction with olefins present in the stream, for example like in Figure 7 [21].

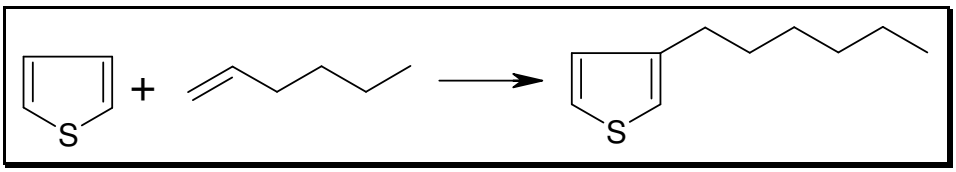

Figure 7 Shifting the boiling point by alkylation [21]

Selective oxidative desulfurization

Generally the process of selective oxidative desulfurization is composed of oxidation and purification. The example can be oxidation of the sulfur compounds with oxidizing agents like peroxides, which is then followed by thermal decomposition of the oxidized products. Sulfur is released mainly as SO_2 [21].

Desulfurization via extraction

Desulfurization via extraction is based on the better solubility of the organosulfur compounds compared to sulfur-free hydrocarbons in an appropriate solvent (for example acetone, ethanol). The solvent-fuel mixture is separated and this way hydrocarbons are separated from the solvent. The organosulfur compounds are separated through distillation and the solvent is recycled.

The photochemical oxidation (also oxidation with special oxidant, for example peroxoacetic acid) can be applied before the extraction (desulfurization via extractive photochemical oxidation). The sulfur containing hydrocarbons are suspended in an aqueous-soluble solvent and irradiated by UV or visible light. This results in the oxidation of the sulfur compounds to polar compounds (sulfoxides, sulfones), which are then rejected by the nonpolar hydrocarbon phase. Acetonitrile which possesses

high solubility for both initial and oxidized sulfur compounds, was found to be most suitable [21, 29, 45, 46].

Desulfurization by precipitation

Desulfurization by precipitation is achieved by formation and removal of insoluble charge-transfer complexes between π-acceptor and DBT derivatives in hexane for example. The consecutive steps include filtration in order to remove the formed complex. Currently the efficiency is very low. One treatment results in the removal of 20 % of the sulfur present. There is also a problem with a competition in complex formation between DBT compounds and non-sulfur aromatics [21, 31, 47, 48].

Desulfurization by adsorption on a solid sorbent

The process of desulfurization by adsorption on a solid sorbent employs either physical adsorption of organosulfur compound on the sorbent (for example activated carbon) or chemical interaction of the organosulfur compounds and the sorbent. Sulfur is fixed in the sorbent and free hydrocarbon, without sulfur, is released into the purified fuel. There is a need for a sorbent regeneration. Efficiency is mainly determined by the sorbent properties (capacity, selectivity, durability and regenerability) [21, 49].

1.8 Summary

Knowledge about the sulfur species is essential to improve the methods of removal to meet the legislation limits. Sulfur oxides produced during fossil fuel combustion are the major air pollutant causing acid rain. The sulfur compounds are moreover catalytic poisons in processes like fluid catalytic cracking, hydrocracking and catalytic reforming to produce lighter and cleaner motor or diesel fuel. Moreover, many PASHs are suspected to possess mutagenic or carcinogenic properties. The mechnism of the HDS process for some PASHs is still not fully understood [50].

2 Analytical Techniques for PASH Separation and Investigation

2.1 Liquid Chromatography

Because of the complexity of the higher boiling fractions of the crude oils, an off-line separation is usually required for the sample simplification. Initially the oil sample can be separated on silica and alumina according to the SARA scheme, into saturates, aromatics, resins and asphaltenes [51] or even more fractions using solvents of different polarity [50, 52-55].

Further separation of PAHs and PASHs is often required. The separation of these two groups by means of oxidation has been investigated. The oxidation of PASHs to sulfones can be achieved for example using hydrogen peroxide or *m*-chloroperbenzoic acid. These products, being more polar than PAHs, are easily separated on silica or alumina. The sulfones are then reduced back to PASHs, for example with lithium aluminium hydride. Unfortunately this method appeared not efficient [53, 56-59].

Modified silica gel can simplify and enhance the separation of PAHs and PASHs. For example complexation of PASHs with metal ions is less time consuming than oxidation. Different metals like Cu, Ag, Hg and Pd, were investigated for the so called ligand exchange chromatography (LEC) [60]. LEC has been first suggested by Helfferich in 1961 [61]. It is based on the principle of a complex formation between the sulfur compounds, which can donate a lone pair of electrons, and a metal ion, which has a vacant d-orbital to accept the lone pairs [62]. Palladium shows strong selectivity towards PASHs [63-67], which can be eluted by addition of a competitive ligand (e.g. isopropanol) to the mobile phase [68]. Compounds with a thiophene ring that is not condensed with other aromatic systems are weakly retained and elute together with PAHs. If the sulfur is in a non-aromatic ring, the compound is irreversibly retained by the Pd(II) ions. The nitrogen heterocycles are also irreversibly retained, but the oxygen heterocycles do not interact strongly with Pd(II) [69].

Further separation can be achieved according to the number of aromatic rings on a β-cyclodextrin stationary phase [70], or (and) electron-acceptor stationary phases in normal-phase HPLC (donor-acceptor liquid chromatography) [71]. The acceptors for donor-acceptor liquid chromatography can be represented by nitro compounds like 3,5-dinitrobenzoic acid (DNB), halogeno compounds like tetrachlorophthalimide (TCP), or cyano compounds like 4-aminophthalodinitrile (PDN) [55, 72-74]. In NP-HPLC with these kinds of stationary phases, the retention is based primarily on the interaction between the aromatic π-electrons and the electron-poor stationary phase. Holstein [75] demonstrated, that the TCP-modified silica separated aromatic compounds according to the number of fused aromatic rings. This kind of stationary phase interacts strongly with electron-rich species. The mechanism involves a delocalization of electrons between the support material and the analyte. A reversible complex by electron transfer is formed [76]. It was also found, that substituted PAHs and PASHs are retained more strongly on the TCP phase, as alkyl chains are electron donors. When an alkyl chain is long, we have to consider an interaction with the mobile phase and a steric hindrance. A decrease in retention is observed then [77].

The presence of alkyl side chains on the aromatic rings significantly increases the retention time on the reversed-phase material. In case of RP-HPLC (with C_{18} packing material for example), there is a dependence of the relative solubilities of the components in the polar mobile phases. An addition of alkyl chains reduces the solubility in the mobile phase and causes more efficient interactions with the stationary phase. Thus the increase in the retention volume can be observed. RP-HPLC can lead to misleading results due to overlapping of alkyl homologues [78].

An efficient separation can also be achieved using gel permeation chromatography (GPC) [79]. This method allows the separation of the sample compounds according to the molecular size [80]. Larger molecules cannot access some of the pores and exit the column faster. Smaller molecules penetrate more into the porous structure and elute later. In the ideal case there is no interaction between

the stationary phase and the sample [81, 82]. GPC is a useful experiment for the investigation of the molecular weight of very heavy hydrocarbons [83-85].

Typical detectors used for HPLC of PASHs are UV-visible absorption (specially diode array detector, DAD) [86, 87], fluorescence [56, 88-90], refractive index (RI) detectors [83] and nowadays MS (mass spectrometry, chapter 2.3).

UV-vis absorption detectors, used in this work, respond to those substances, that absorb light in the range of 180 - 800 nm. For these wavelengths to be absorbed, the molecule has to carry a chromophore (π-electron functions or hetero atoms with non-bonding valence-shell electron pairs). A UV-vis detector consists of a cell through which the analyte passes. The light passes through the cell and falls onto a photo-electric cell. The resulting electric signal is amplified and recorded. In the diode array detector light is collimated by an achromatic lens system and the total light passes through the detector cell onto a holographic grating. The dispersed light falls onto a diode array. The array may contain hundreds of diodes. The output of any diode can be selected. The relation between the intensity of the transmitted light and the concentration of solute is given by Beer's Law:

$$I = I_0 e^{-klc}$$

where: I - transmitted light, I_0 - intensity of the light entering the cell, k - molar extinction coefficient of the solute for the specific wavelength, c - solute concentration, l - path length of the cell.

UV detection has been widely used in PAH and PASH analysis [66, 76, 91-93].

Fluorescence detector, also tried here for PASH investigation, is based on a luminescence in which the molecular absorption of a photon is followed by an emission of a photon with a longer wavelength. Fluorescence and UV-vis detectors are sensitive, nondestructive and can be placed in series, as presented by Winger *at el.* [88, 93].

The refractive index detector uses the change of the speed of light when passing through liquids of different optical densities. It can be useful for those compounds that are nonionic, do not absorb in UV, and do not fluoresce. The refractive index increases with increasing molecular weight and aromaticity [83]. This kind of detector was successfully used during the HPLC fractionation procedure of sulfur compounds [94].

2.2 Gas Chromatography

PASH identification can be done using gas chromatography, also GC x GC [95], with different detectors. Especially useful are selective ones, like the flame photometric detector (FPD), the sulfur chemoluminescence detector (SCD) and the atomic emission detector (AED) [53, 96-98]. GC provides information about boiling point and polarity, which leads to more reliable identification [95]. The only limitation is the volatility of the sample in GC. This technique cannot be used for the high boiling fraction of the crude oil. Masses up to 400 amu were resolved [99].

The FPD is based on a chemiluminescent reaction of the sulfur (or phosphorus) containing compounds, in a hydrogen/air flame. During the combustion, sulfur is reduced to the S_2 molecule in an excited state. The excess energy can be emitted as light in a broad band (λ_{max} for emission of excited S_2 is 394 nm). The signal is not a linear function of sulfur concentration [57, 100, 101]. Yin and Xia [102], Schulz *et al.* [41] used this kind of detector for sulfur compound investigation in gasoline. Pulsed FPD allows more precise quadratic response towards the sulfur compounds, being equimolar for different sulfur compounds [97].

In the SCD sulfur monoxide is first generated from the sample in air and hydrogen under a vacuum. SO is further carried to the reaction chamber, where it reacts with ozone, to generate sulfur dioxide and light. The light is measured by a photomultiplier tube [100]. The signal is proportional to the quantity of sulfur in the sample [95, 97]. SCD was successfully used for petroleum product investigation [32].

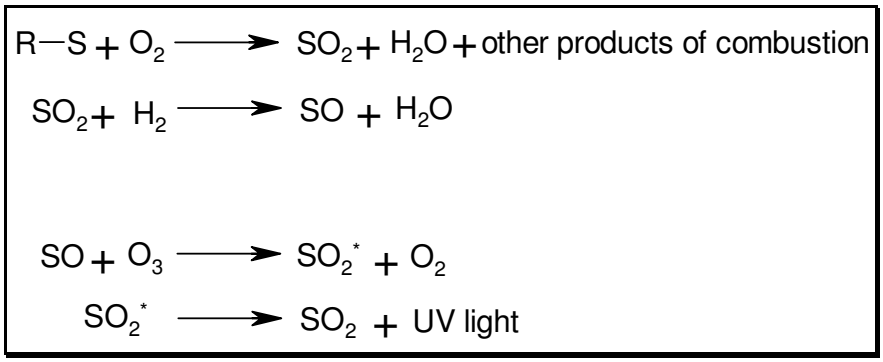

Figure 8 Reactions in SCD

The AED, introduced commercially in 1989 [103], is based on the detection of the atomic emission of many different elements in analytes that elute from a GC column. The elements are fed into a microwave powered plasma cavity and atomized. The atoms are excited by the energy of the plasma. The light emitted by these excited atoms is separated into lines via a photodiode array. The individual emission lines are sorted and a chromatogram can be produced consisting of only such peaks that contain a specific element. The AED is a selective and a sensitive multi-element detector [97]. The detectable minimum for sulfur is in the low picogram range [99, 104]. AED is selective also for the isotopes of several elements, like $^{12}C/^{13}C$ [103].

The GC-AED was applied for PASHs investigation in crude oils by Hegazi *et al.* [105] and many others for PASH investigation in different samples [92, 94, 106, 107].

2.3 Mass Spectrometry

In mass spectrometry we do not specify the response to the element sulfur but rather to the predominant molecular mass [108]. Mass spectrometry with conventional ionization methods is not applicable to large molecules due to the fragmentation [85]. By lowering the electron ionization energy it is possible to reduce the fragmentation of the petroleum molecules. Different soft ionizations should satisfy such criteria for thorough petroleum composition investigation as effective ionization for saturate and aromatics, compatible with high-resolution mass spectrometry and on-line chromatography for the separation of petroleum [109].

Different ionization sources can be applied to PASHs analysis. Due to the complexity of the petroleum fractions, it is desirable to produce only molecular or pseudomolecular ions (protonated, hydride-abstracted, adduct molecular ions) to simplify the determination of the compounds types. Conventional electron impact ionization (EI), which ionizes molecules using emitted electrons, can result in extensive fragmentation. Numerous soft ionization techniques have been developed to diminish fragmentation [110]. Chemical ionization (CI), which differs from EI by applying a reagent gas, unfortunately can be applied only for the lighter fractions, as it proceeds in the gas phase. The high-boiling petroleum fractions have been analyzed employing field ionization (FI) and field desorption (FD), but neither FI nor FD is suitable for on-line LC-MS. Atmospheric pressure ionizations were developed especially for LC-MS. LC-MS combined with thermospray (TSP) was used by Hsu and Qian for the high-boiling hydrocarbon characterization [110, 111]. Matrix-assisted laser desorption ionization in combination with time-of-flight mass spectrometry (MALDI-TOF MS) was used for investigation of high boiling crude oil fractions by Robins and Limbach [112]. The ions observed consist mainly of molecular and quasimolecular ions. The M+1 peak is contributed from ^{13}C and possibly from $[M + H]^+$ [112, 113]. The upper mass limit is beyond m/z 100,000 for MALDI-MS [99].

The ionization process in FI results in less electronic excitation than in conventional electron impact ionization (EI), giving rise to more abundant molecular ion species [85] for aromatic and saturated petroleum molecules [109, 114], but it also requires that the samples are heated to high temperature for vaporization, which could make them suffer from a thermal decomposition [110]. The upper mass range is limited to m/z 1200 - 1500 [99]. The combination of GC-FI-TOF HRMS was applied to an analysis of petroleum products in the carbon range C_6 - C_{44} by Qian and Dechert [109]. FD ionization is often chosen for non-volatile, high molecular weight compounds [85]. The upper mass range is about 2000 to 3000 Da. A huge advantage of FD and FI is that they are free from matrix interferences [114].

Atmospheric pressure ionization (API) was the first technique for direct connection of a solution phase and MS. API-MS has been particularly used for the analysis of the non-volatile and thermally labile compounds. API coupled to Fourier transform ion cyclotron resonance mass spectrometry (FT-ICR MS) offers high resolution and accuracy [23].

Originally proposed by Dole and later pioneered by Fenn electrospray ionization (ESI), used in this work, is a leading member of API and the method of choice for many applications in LC-MS. In ESI a liquid is pushed through a charged, usually metal capillary. A mist of electrically charged droplets is generated. A neutral carrier gas is used to help evaporate the solvent. The charge density increases to a point at which the repulsion becomes of the same order as the the surface tension. The charged analyte droplets explode, a phenomenon that is explained by the Coulomb forces between the charged analyte molecules. The process is repeated until an analyte is free of solvent and is a lone ion. The analytes are ionized by ESI only if they are ionic in a solution. Neutral, nonpolar analytes are not amenable to the technique. ESI produces a variety of ions depending on the polarity of the analyte, the characteristic of the solvent and presence of impurities such as alkali metal ions. ESI can produce intact ions with multiple charges from large, complex molecules [115-117]. The upper mass limit in ESI mode is around 1200 m/z for singly charged ions [99].

Atomospheric pressure chemical ionization (APCI) is a soft ionization, not useful for completely nonpolar compounds. Because of the required heat, it is applied only for stable analytes up to 1000 - 1500 Da. Lafleur *et al.* [118] investigated different PAHs using APCI-MS. Also Marvin *et al.* investigated PAHs with masses higher than 300 u using LC-APCI-MS [119]. APCI generated protonated molecular ions [M + 1] for PAHs. The mass range for PAHs was extended to 448 u when using LC-MS. Atmospheric pressure chemical ionization mass spectrometry (APCI-MS) was used together with RPLC for PASHs analysis in environmental samples by Thomas *et al.*[96].

Atmospheric pressure photoionization (APPI) is potentially interesting and can be used for many compounds which cannot be ionized by ESI or APCI. Simultaneous production of protonated, deprotonated molecules and molecular ion complicates the analysis [120, 121].

Atmospheric pressure laser ionization (APLI) is useful for compounds with very low polarity and nonpolar aromatic hydrocarbons. For benzonaphthothiophene no fragmentation was observed, only the radical cation with the natural isotope distribution [122]. An upper mass limit of m/z 12,000 was shown [99].

Many different analyzers can be used for PASHs analysis. Especially the higher boiling fractions require high resolution.

The magnetic sector is a momentum analyzer rather than a direct mass [123]. The resolution is around 25,000, with a maximum of 100,000 for the double-focusing instruments. The mass range goes up to 4000 m/z. It lacks the coupling possibility with the atmospheric ionization source and is not well combined with pulsed ionization methods like MALDI.

A linear quadrupole has a resolution up to 8000 [123]. The modern quadrupoles covers an m/z range up to 2000 - 4000. It is a kind of standard device in LC-MS. It can be used in MS/MS studies and is easily coupled with atmospheric ionization sources but not with pulsed ionization sources.

The quadrupole ion trap (QIT) [124] is characterized by a mass resolution in a similar range to that of a quadrupole. Modern QITs cover ranges up to m/z 3000. It finds application in GC/MS and LC/MS, is also easily coupled with MALDI source and useful for MS^n.

In time-of-flight (TOF), the resolution typically reaches 10,000 [123], but as high as 30,000 was also observed. The m/z range is unlimited. The mass accuracy is up

to 5 ppm and this makes accurate mass measurements possible. It is best suited to MALDI and can be also used in MS/MS [109].

Fourier transform ion cyclotron resonance mass spectrometry (FT-ICR MS), widely used in this work, has been first demonstrated by Comisarow and Marshall. FT-ICR MS has extremely high resolution (350,000) [125-127], accuracy (< 1 ppm) and it can be used for large masses. Using FT-ICR MS, C_3/SH_4, $^{13}C/CH$, $^{13}CH/N$, CH_2/N and other mass doublets were baseline resolved [128-130].

FT-ICR MS is a powerful tool for analyzing the high-boiling fractions of crude oils, but the analysis of FT-ICR MS data has to be augmented by different reference materials. It demands also a statistical evaluation of the huge amounts of data.

In the basic FT-MS instrument, the ions are generated in the source. The ions then pass through a series of pumping stages. When the ions enter the cell (ion trap), the pressure is in the range of 10^{-10} to 10^{-11} mbar with temperatures close to absolute zero. The cell is located inside a magnet field (typically 4.7 to 12 Tesla) cooled by liquid helium and liquid nitrogen. When the ions pass into the magnetic field they are bent into a circular motion in a plane perpendicular to the field by the Lorentz force. They are prevented from escaping the cell by the trapping plates at each end. The frequency of rotation of the ions is dependent on their m/z ratio. At this stage, no signal is observed because the radius of the motion is very small. The excitation, the second step, of each individual m/z is achieved by a swept RF pulse across the excitation plates of the cell. Each individual excitation frequency will couple with the ions natural motion and excite them to a higher orbit where they induce an alternating current between the detector plates. The frequency of this current is the same as the cyclotron frequency of the ions and the intensity is proportional to the number of ions. When the RF goes off the resonance for that particular m/z value, the ions drop back down to their natural orbit (relax) and the next m/z packet is excited.

Although the RF sweep is made up of a series of stepped frequencies, it can be considered as all frequencies simultaneously. This results in the measurement of all the ions in one cycle producing a complex frequency vs. time spectrum containing all

the signals. The deconvolution of the signals by the FT methods results in the deconvoluted frequency vs. intensity spectrum which is then converted to the mass vs. intensity spectrum (the mass spectrum). FT-ICR MS allows the measurement of the ions without destroying them, and this enables further experiments to be performed on the ions [131-134].

Mass accuracy does not depend on already inherent kinetic energy of the ions. It depends only on the mass and charge of the ions and on the field-strength. This technique is very accurate, as frequencies can be measured exactly.

$$F_L = zvB$$

$$F_C = \frac{mv^2}{r}$$

$$zvB = \frac{mv^2}{r}$$

$$\omega = \frac{v}{r}$$

$$\omega = \frac{Bz}{m}$$

where: F_L - Lorentz force, z - charge, v - ion velocity, B - external magnetic field, m - mass of ion, r - radius of circular ion path, F_C - centripetal force, ω - angular frequency

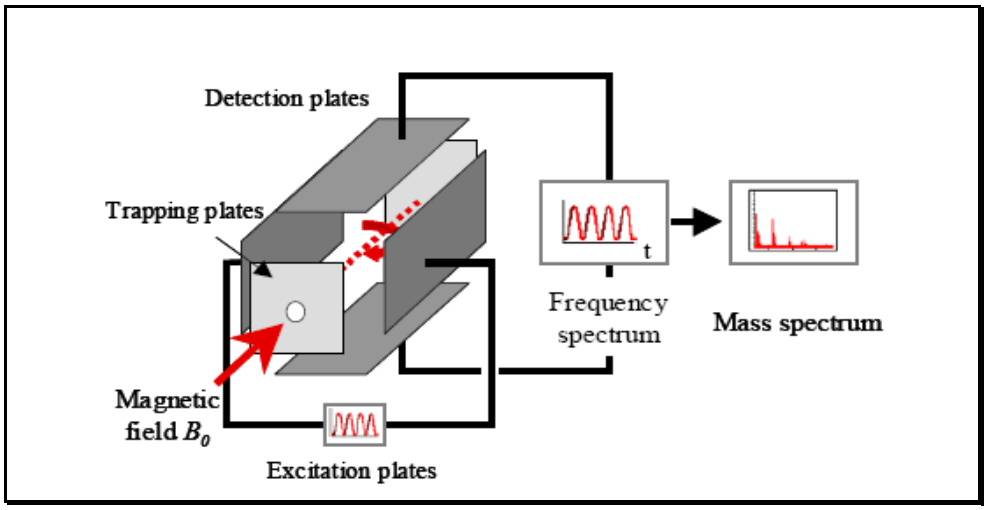

Figure 9 FT-ICR MS device [135]

Different soft ionization techniques, for example low-voltage electron ionization (restricted to volatile compounds) [136-138], electrosparay ionization (not suitable for nonpolar compounds) [117, 125, 126, 128, 139-146], field desorption/ionization [114, 147, 148], atmospheric pressure photoionization [149] and atmospheric pressure laser ionization [122] have been coupled to FT-ICR MS [120, 150-154].

2.4 Other Techniques

Other often used methods for PASH investigation are infrared spectroscopy (IR), nuclear magnetic resonance (NMR) [155] and X-Ray Photoelectron Spectroscopy (XPS). Capillary electrophoresis also seems to be suitable and was applied in PASHs analysis [156, 157].

Information regarding the number of the methyl groups per molecule was obtained from IR spectroscopy [83, 84]. This technique is particularly well suited for the finger-print changes in the structural group composition in the terms of aromatic, naphthenic and paraffinic molecular species [158]. The absorption bands at 1600 cm^{-1} (C-C multiple bond stretching due to aromatic ring) and 720 cm^{-1} (indicator of CH_2 groups in a hydrocarbon chain) were taken as representative of aromaticity and paraffinicity by Singh and Gulati [158]. Drushel and Sommers used IR for the analysis of the sulfur compounds of a high-boiling petroleum fraction [58].

^{1}H NMR can be applied in petroleum products investigation and was used for the structural specification of the hydrogen-type distribution. The chemical-shift regions can distinguish between hydrogens of aromatic rings, on α-carbon relative to aromatic rings, on β-groups to aromatic rings etc. [58, 83, 84]. The information derived from ^{1}H NMR is unfortunately limited, because of the close similarity of the aliphatic proton chemical shifts, which result in broad, unresolved signals. Also ^{13}C NMR found application in petroleum industry. Primary, secondary, tertiary and quaternary carbon atom in the saturate and aromatic moieties can be distinguished. S-methylation has been also applied for the sulfur compounds before NMR

measurement, and the shifts for the CH_3-group were measured for different model sulfonium salts [80, 87, 159-168].

X-Ray photoelectron spectroscopy (XPS) is a quantitative spectroscopic technique which can be used in measurements of an elemental composition, an empirical formula, a chemical state and an electronic state of the elements. The XPS sulfur 2p binding energy provides a sensitive measure of the electronic character of sulfur within a molecule [169]. This technique was used by Kelemen *et al*. for the determination and quantification of sulfur forms in petroleum and coals [170].

Capillary electrophoresis (CE) [171, 172] can be used for different PASH separations, as presented using standard PASH compounds, after methylation. A linear dependence between the migration time and the calculated molecular volumes was found [156, 157].

3 ESI FT-ICR MS

Figure 10 presents the FT-ICR MS instrument used in this work. All the measurements using FT-ICR MS were performed in collaboration with the Max-Planck-Institute of Coal Research in Mülheim an der Ruhr (Germany).

The ions are produced in ESI and accumulated to ion packages in an octapole. These ions are transferred through an array of tubes and half-tube lenses into a cyclotron cell. A magnetic field strength of 4.7 up to 12 T is currently employed. The magnet used here had a field strength of 7 T.

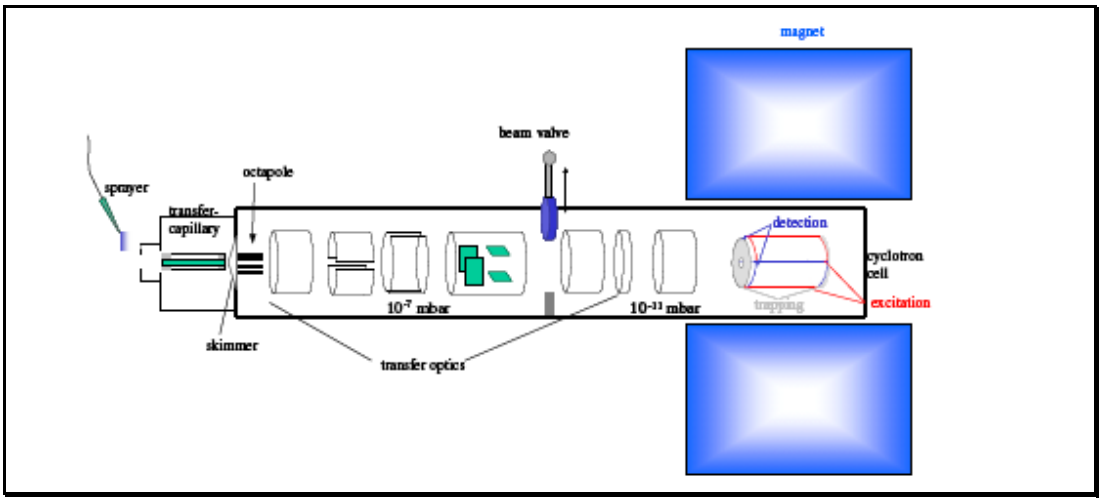

Figure 10 FT-ICR MS with ESI (Bruker Daltonics, Germany)

3.1 Data Interpretation

FT-ICR MS is a powerful tool for analyzing the high-boiling fractions of the crude oils. The ICR accurate mass measurements can provide an elemental composition for the thousands of petroleum components from a single mass spectrum [151]. FT-ICR MS provides ultra-high resolution [125-127] and ppm-level of accuracy. With FT-ICR MS, C_3/SH_4, $^{13}C/CH$, $^{13}CH/N$, CH_2/N and other mass doublets can be successfully resolved [128-130].

Although FT-ICR MS provides the best mass measurement of all MS techniques, it is difficult to assign the exact composition of found constituents without preliminary knowledge of the elements present. The knowledge from the previous investigations is essential. It is known that in the aromatic fractions, presence of a metal element is unusual, thus leaving elements like C, H, S, N, O as the main ones. The data interpretation is focused on the mentioned elements and their isotopes.

There is a demand for statistical evaluation of huge amounts of data. The mass spectrum of PASHs from VGO (fraction Pd-2) is presented in Figure 11. Any analysis directly from this kind of presentation is extremely difficult. The mass spectrum for fraction CD-1 (mainly benzothiophenes, explained in chapter 5) is presented in Figure 12. It is much simpler, but even after separation of fraction Pd-2 into three CD fractions, special methods of data interpretation are needed.

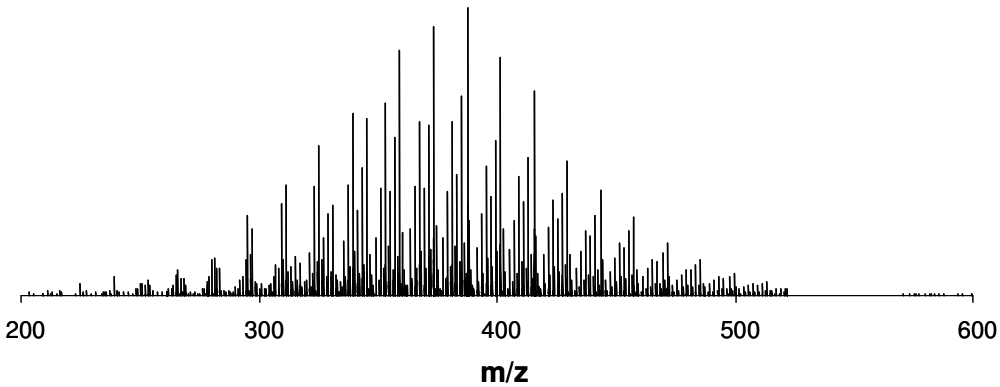

Figure 11 Mass spectrum (FT-ICR MS) of the PASHs (fraction Pd-2, VGO, IL)

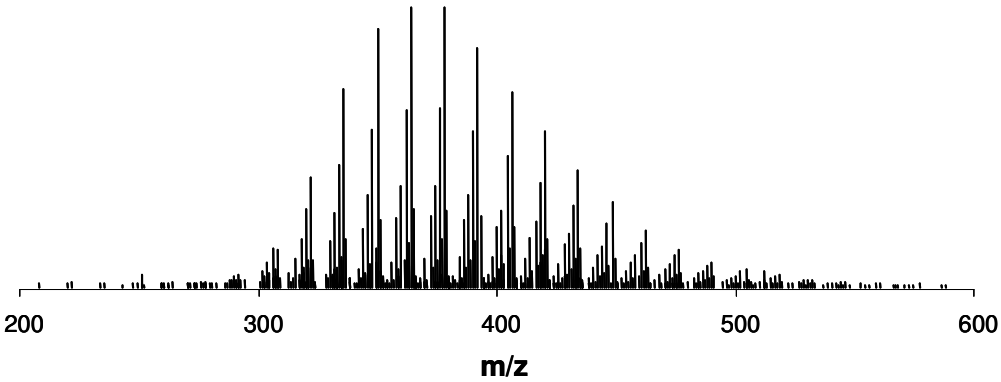

Figure 12 Mass spectrum (FT-ICR MS) of fraction CD-1 (VGO, IL)

The data reduction technique has been employed by using a few indices, like the nominal mass series, the Kendrick mass defect, in order to simplify the analysis and create better visualization of the obtained results, in form of the Kendrick plots (explained further). The simplification in the presentation of the huge amount of data is visible. The pseudograms are an other method of data presentation and they will be described below as well.

3.1.1 "Hydrogen Deficiency" (z)

A complete analysis of each individual molecular species in a heavy petroleum fraction is almost impossible because of the presence of an enormous number of compounds. An analysis is therefore based on the grouping of the compound series (types) according to their number of hydrogen relative to a number of carbons, that is:

$$C_nH_{2n+z}X$$

where: n - the number of carbon atoms, z - "hydrogen deficiency" relative to mono-olefins or 1-ring naphthenes, X - heteroatom like S, O, N, S_2 etc. [173].

Each addition of one ring or one double bond will make the z value more negative by 2. Thus a series of molecules like ethane C_2H_6, ethene C_2H_4 and ethyne C_2H_2 will have the z value of 2, 0 and -2 respectively [151]. Another example is a $z = -10S$ series that includes benzothiophene C_8H_6S, methylbenzothiophene C_9H_8S, C_2-substituted benzothiophenes C_9H_8S etc. [125, 173].

3.1.2 Nominal Mass Series (z^*)

All components in a fuel mixture can be grouped into 14 families according to their nominal molecular weight. The nominal mass series, z^*, of an ion is defined as the reminder of its nominal mass divided by 14, minus 14, that is the modulus of (nominal mass/14) -14. Each nominal mass yields a z^* value between -1 and -14. Several compounds types (compound type z series) are included in each nominal

mass series, z^*. For example the $z^* = -6$ series contains compound type of z = -6 (benzenes), -10S (benzothiophenes), -20 (cyclopentanophenanthrenes) etc. [173].

3.1.3 Double Bond Equivalent (DBE)

The double bond equivalent (DBE) is the sum of the number of rings and double bonds present in a molecule [150]. For the elemental composition $C_cH_hN_nO_oS_s$:

$$DBE = c - h/2 + n/2 + 1$$

The relation between z and DBE can be establish in the following way:

$$DBE = -(z/2) + (n/2) + 1$$

3.1.4 Kendrick Mass Defect (KMD)

In 1960 E. Kendrick introduced a mass scale based on the mass assignment of a methylene group as exactly 14 mass units, instead of 14.01565 on the C^{12} = 12.00000 scale to express the organic mass spectral data [174]. To convert a mass from the ^{12}C mass scale to the Kendrick mass scale, a mass has to be multiplied by a factor of (CH_2 value on the Kendrick scale)/(CH_2 value on the ^{12}C scale), that is 14.00000/14.01565. Each series has a unique mass defect and this simplifies the identification of the compound series. The mass defect of an ion is defined as the difference between its accurate mass and a nominal mass. The IUPAC masses are converted to the Kendrick mass scale in the following way:

$$KM = \text{IUPAC MASS} \times (14/14.01565)$$

$$KNM \text{ - nearest integer } KM$$

$$KMD = (KNM - KM) \times 1000$$

In Table 4 calculations are presented, as the example, for benzothiophene (BT) and dibenzothiophene (DBT) homologous series.

Table 4 KMD calculations for homologous series of BT and DBT

	BT	MeBT	EtBT	DBT	MeDBT	EtDBT
	C_8H_6S	C_9H_8S	$C_{10}H_{10}S$	$C_{12}H_8S$	$C_{13}H_{10}S$	$C_{14}H_{12}S$
IUPAC	134.01902	148.03467	162.05032	184.03467	198.05032	212.06597
NM	134	148	162	184	198	212
MD	19.0	34.7	50.3	34.7	50.3	66.0
KM	133.86938	147.86938	161.86938	183.82918	197.82918	211.82918
KNM	134	148	162	184	198	212
KMD	130.6	130.6	130.6	170.8	170.8	170.8

The Kendrick mass scale simplifies the compound identification. The mass peaks can be sorted and grouped into the homologous series according to their unique KMD [126, 130, 139, 143, 144, 148, 173].

3.1.5 Multiple Sorting

Hsu et al. have developed a multiple sorting technique based on the nominal mass series and the KMD in order to process the high resolution mass spectral data (Figure 13) [173]. The mass spectra with their accurate masses are sorted by z* and separated into 14 groups. Within the same z* group, the mass peaks are further sorted by their KMD. Pre-sorting by nominal mass series facilitates the sorting based on the KMD, as the difference in the KMD between, for example, $C_{11}H_8O$ and C_7H_6S is 0.5 mmu. It is thus difficult to distinguish between these two compounds. The value of this order is not uncommon for frequent errors. But $C_{11}H_8O$ and C_7H_6S have the nominal mass z* value of -12 and -4 respectively. The z* values are well separated and allow the better distinguishing between O- and S-containing compounds.

A general elemental composition of an individual compound can be calculated from the accurate mass measured. The compound type distribution is determined from the elemental distribution in the mixture. This procedure works well for the simple mixtures. For complex fuel mixtures it is very time-consuming and not

effective. The use of the average KMD of the series and the multiple sorting eliminate time-consuming procedure and increases the accuracy of a compound type identification.

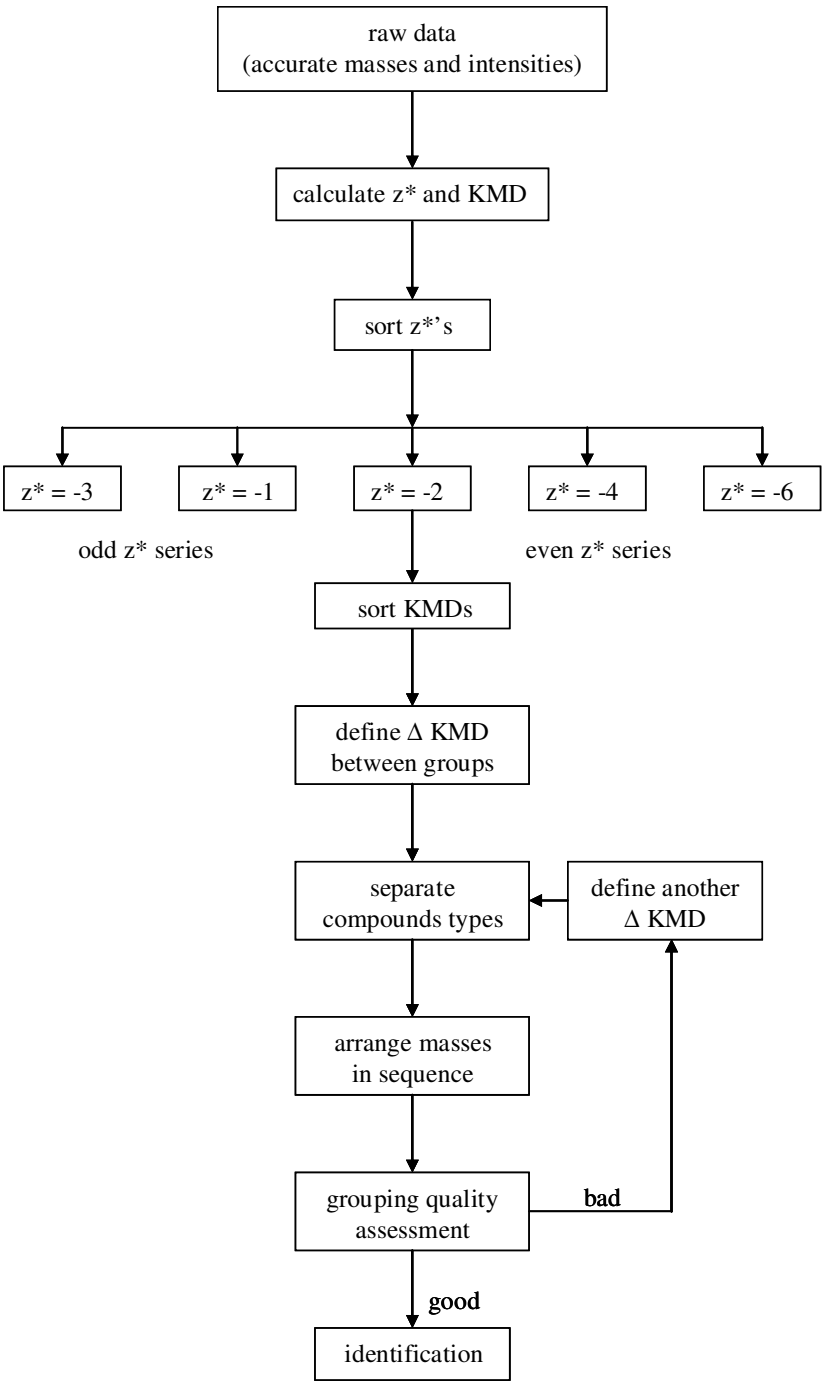

Figure 13 Flow diagram of a multiple sorting algorithm [173]

3.1.6 Kendrick Plot

The Kendrick mass scale allows the sorting of compounds into the homologous series according to the alkylation, classes (type of heteroatom) and types (ring plus double bond). As already mentioned, in the conversion of the IUPAC mass to the Kendrick mass, the IUPAC mass measured by MS is multiplied by a factor of 0.99888 (14.00000/14.01565, that is the ratio of the nominal mass to the accurate mass of CH_2). In this way compounds containing the same heteroatoms (N, S, O) and the same number of rings and double bonds, but different number of CH_2 groups in an alkyl side chain, have the same KMD and are plotted as a homologous series on one horizontal line [151].

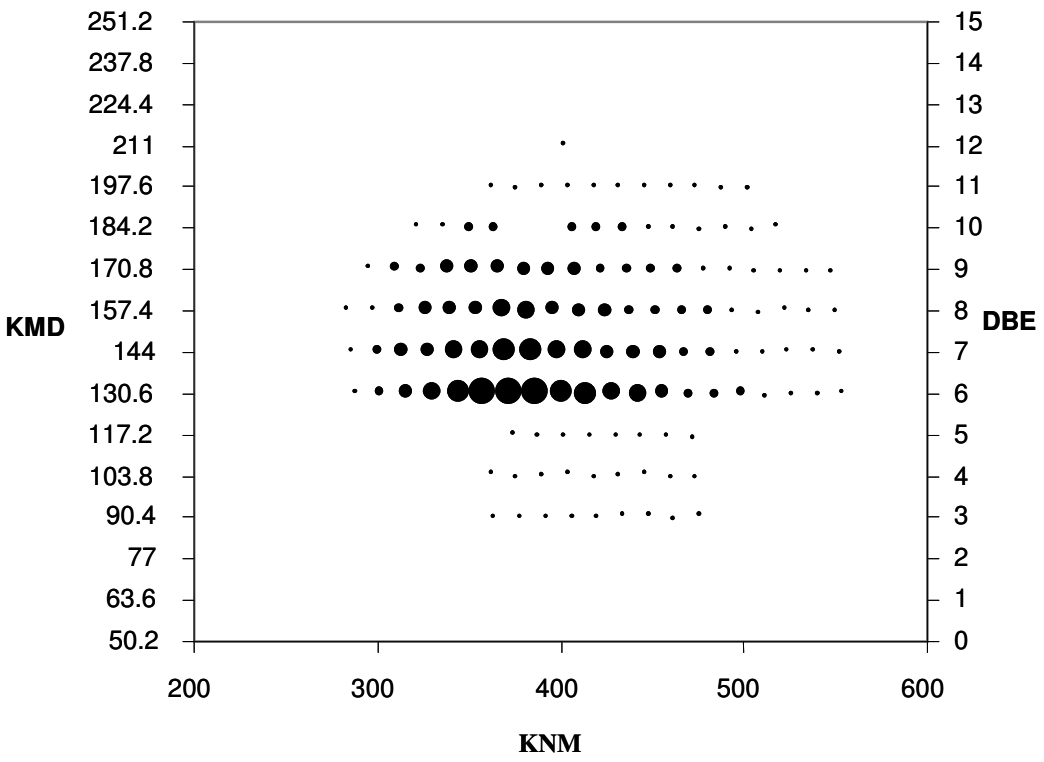

Figure 14 Kendrick plot of the compounds with one sulfur atom (IL, VGO, CD-1)

As presented in the Kendrick plot in Figure 14 (S1 class), all members of a homologous series can be presented in a horizontal line in a plot of the KMD (DBE) versus the KNM. The KMD increases with the DBE, so that the Kendrick plot gives

a simultaneous graphical picture of the degree of unsaturation (y-axis) and degree of alkylation (x-axis). The addition of one ring or one double bond (difference of H_2) is reflected by a vertical shift of 13.4 upward on the KMD scale [148, 151].

3.1.7 Generation of Pseudograms

Another method of a data visualization is the creation of a so-called pseudogram. Such a graphical presentation derived from mass data can be compared with a GC chromatogram. In the Kendrick plot, each compound is presented only as a single dot. In the pseudogram mass signals are depicted as peaks.

The individual peaks of a pseudogram are generated using the Gaussian function:

$$y(x) = a\exp(-([(x-b)/c]^2))$$

where: *a*,*b*,*c* - represent the relative abundance of the mass of interest, the particular mass, and the selected standard deviation, respectively, where the last of these can be selected to obtain a suitably looking pseudogram.

The advantage of the pseudogram is that a better overview of individual components within a crude oil fractions is obtained [120, 151].

4 Objectives

The objective of this work is to improve analytical methods for better separation of the sulfur containing high-boiling fractions of a crude oil. This is of major importance for the further simplification of the PASHs analysis. The fractions obtained will be characterized by means of different analytical methods.

The extensive chromatographic separation will also be combined with a chemical transformation (aromatization). Different oxidation agents will be applied and received products will be investigated. More information about PASH structures with one sulfur atom in the complex mixture of the higher-boiling cuts can be obtained by the combination of chromatographic separation, aromatization and oxidation products investigation.

As the heavier distillation fractions show a higher resistance to deep hydrodesulfurization, it is important to investigate the structures of these refractory PASHs. Here the samples of the vacuum gas oil before and after the HDS process will be separated, investigated and compared with respect to distribution of the parent structures, average mass and the degree of aromatization.

5 Pattern of PASHs in Vacuum Gas Oil (VGO)

The high-sulfur crudes are gaining more importance for the production of low-sulfur fuels, as availability of low-sulfur crudes is decreasing. Millions of tons of vacuum residues are produced every year in the refineries, but despite the fact that they can be a valuable resource for petrochemistry, their further processing is hampered by the large amount of sulfur [67]. An efficient desulfurization is essential to achieve a low content of sulfur, which will satisfy the legal limits regulations in transportation and the heating fuels in many countries. The HDS is generally used as the most effective method for this purpose. Unfortunately, it has not been shown to be as effective for the high-boiling fractions, like vacuum gas oil, as for the low- and middle-boiling ones. The reasons for that are not fully understood. More investigation is needed to explain the influence of the molecular characteristics on the HDS process.

In the present work the PASHs in a vacuum gas oil (VGO) distilled from an Iranian Light oil are investigated mainly by FT-ICR MS, after extensive separation and chemical transformation. The goal is to obtain knowledge about the structure of PASHs with one sulfur atom in a high-boiling fraction.

5.1 Experimental Section

5.1.1 Sample

The vacuum gas oil from the Iranian Light crude oil with a boiling range of 390 - 460 °C and a sulfur content of 1.12 % was supplied from Institut Français du Pétrole, Vernaison, France.

5.1.2 Liquid Chromatography of PASHs

5.1.2.1 SARA Fractionation

The aromatic fraction was first separated from the saturates [51]. For this purpose, 20 g of silica and 35 g of alumina were dried during 16 h at 180 °C. Silica and alumina were afterwards cooled in a desiccator. A column (200 mm x 28 mm) was filled with silica and afterwards with alumina in *n*-heptane. The adsorbents were used only once. For the separation, around 1.25 g of VGO was taken. The saturates were obtained by eluting with 120 mL of *n*-heptane and the aromatics by eluting with a mixture of 240 mL of *n*-heptane and 120 mL of toluene. The samples were concentrated under reduced pressure and in a nitrogen stream at 40 °C.

The whole separation scheme is presented in Figure 15.

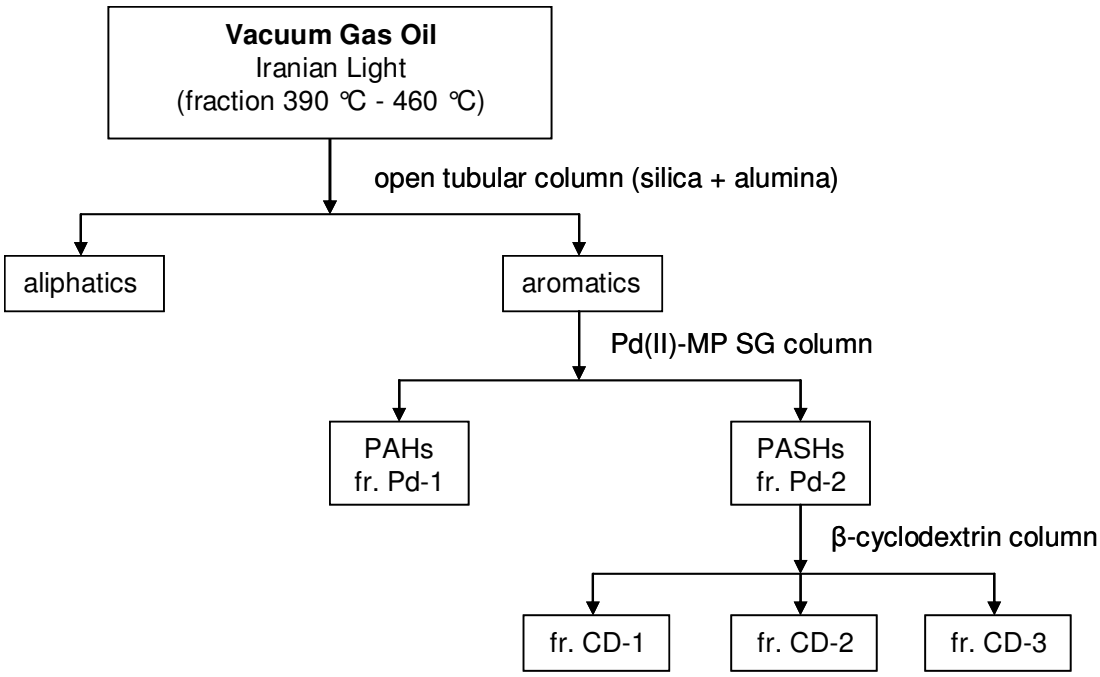

Figure 15 Separation scheme of the PASHs (VGO)

5.1.2.2 Ligand Exchange Chromatography

About 10 mg of Pd(II)-MP SG (for its synthesis, see appendix) were packed into a stainless steel column (250 mm x 8 mm, Knauer) according to the slurry packing technique with methanol at a pressure of around 300 bar using the Knauer pneumatic pump [175]. Afterwards the column was washed with 50 mL each of methanol, dichloromethane and cyclohexane.

Around 200 mg of aromatics were diluted in 3 mL of cyclohexane. 250 µL was used for every injection afterwards. HPLC separation gave two fractions. The first fraction (PAHs, fraction Pd-1) was eluted with cyclohexane:dichloromethane (7:3 v/v). After 15 min the solvents were changed to cyclohexane:dichloromethane (7:3 v/v) with addition of 1 % of isopropanol and the second fraction (PASHs, fraction Pd-2) could be collected (after 20 min). The separation was accomplished with a flow rate of 3 mL/min at room temperature.

5.1.2.3 Separation on β-Cyclodextrin

The β-cyclodextrin bonded silica phase (5 µm) was available from Merck (ChiraDex). About 1.5 g of modified silica was packed into a stainless steel column (150 mm x 4 mm, Knauer) according to the slurry packing technique with methanol at a pressure of around 400 bar using the Knauer pneumatic pump [175]. Afterwards the column was washed with 50 mL each of methanol, dichloromethane and cyclohexane.

Different combinations of columns and temperature were tested for optimal results. Finally the HPLC separation was done using two connected β-cyclodextrin columns at room temperature. Cyclohexane with 0.5 % of *tert*-butyl methyl ether (TBME) was used as the mobile phase with a flow rate of 1 mL/min.

The PASH fraction from the previous separation (43 mg of fraction Pd-2) was diluted with 3 mL of cyclohexane. A volume of 30 µL was used for every injection. Fraction Pd-2 was separated into three fractions, according to the number of condensed aromatic rings:

• CD-1 (two condensed aromatic rings)
• CD-2 (three condensed aromatic rings)
• CD-3 (four and more condensed aromatic rings)

5.1.2.4 Charge Transfer Chromatography

About 1.5 g of TCP SG (for its synthesis, see appendix) was packed into a stainless steel column (150 mm x 4 mm, Knauer) according to the slurry packing technique with methanol at a pressure of around 400 bar using the Knauer pneumatic pump [175]. Afterwards the column was washed with 50 mL each of methanol, dichloromethane and cyclohexane.

The HPLC separation was performed using two connected TCP columns. Cyclohexane was used as the mobile phase with a flow rate of 1 mL/min, at room temperature. Samples for the injection were diluted in cyclohexane.

5.1.3 PASH Methylation

Around 5 mg of every CD fraction was dissolved in 2 mL of 1,2-dichloroethane (DCE). 50 µL of methyl iodide and 40 mg of silver tetrafluoroborate were added and the mixture was allowed to stir for 48 h in the dark at room temperature, to ensure complete methylation of all sulfur compounds. Then the mixture was filtered and the solvent was evaporated in a stream of nitrogen at 40 °C to a volume of 2 mL. Methyl thiophenium salts were further investigated using FT-ICR MS [120]. The general procedure is illustrated in Figure 16. Dibenzothiophene gives the 5-methyldibenzothiophenium ion [67].

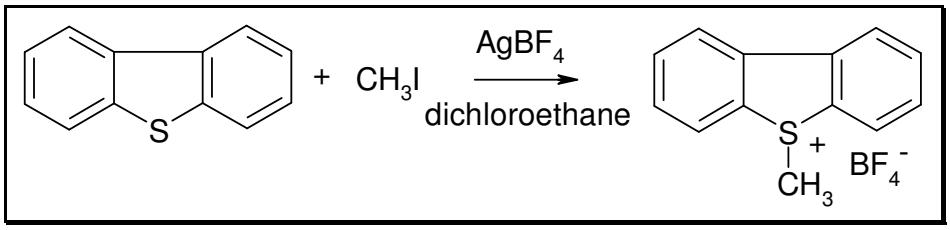

Figure 16 PASH methylation

5.1.4 Analysis

The data obtained from FT-ICR MS measurements were further interpreted after calculations and multiple sorting in an Excel spreadsheet (see chapter 3). Each mass corresponds to the methylated form of the parent molecule. To assign the elemental composition of the original components, the $[M + CH_3]^+$ ions were converted to neutral masses by subtracting 15.02293 from the measured values. Further, the IUPAC masses were converted to the Kendrick mass scale and further sorted. Mass peaks are first sorted by z* and divided into 14 groups. Within the same z* group, mass peaks are further sorted by the KMD. Only specific values of the z* and the KMD were taken into the further analysis, that is the values for the one-sulfur compounds.

Before methylation and measurement using FT-ICR MS, UV, fluorescence, NMR spectra and GC chromatograms were recorded.

UV spectra for the CD fractions were recorded during HPLC separation on 2 x TCP-columns using HP 1050 with DAD.

Fluorescence spectra were recorded on a luminescence spectrometer. Every CD fraction was diluted in cyclohexane for the analysis.

For NMR measurement, the CD fractions were dissolved in CD_2Cl_2. A Varian 600 unity plus (600 MHz) was used.

A GC chromatogram was recorded for fraction CD-1 only, using GC-MS (TIC), after dilution of the sample in cyclohexane.

The methodology and instrumental parameters are given in chapter 9.4.

5.2 Results and Discussion

5.2.1 Separation

Silica/alumina column

1.25 g of the vacuum gas oil (Iranian Light, 390 - 460 °C) after fractionation gave around 761 mg of saturates and 455 mg of aromatics.

Pd(II)-MP SG column

Around 200 mg of aromatics were separated into around 97 mg of PAHs (Pd-1) and 43 mg of PASHs (Pd-2), as presented in Figure 17.

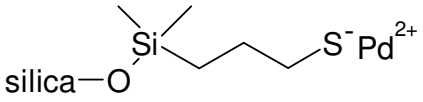

Pd(II)-MP SG

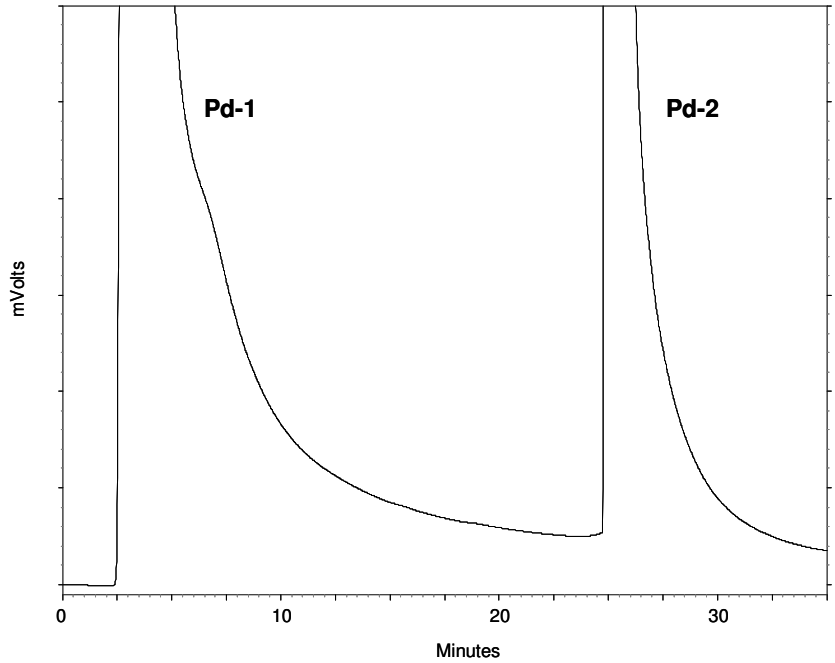

Figure 17 HPLC chromatogram of the aromatics separation on Pd(II)-MP SG (250 mm x 8 mm column, mobile phase - cyclohexane:dichloromethane 7:3, after 15 min cyclohexane:dichloromethane 7:3 with 1% isopropanol, a flow rate of 3 mL/min, room temperature)

As already mentioned in chapter 2.1, ligand exchange chromatography, which is the principle of this separation, is based on the complex formation between the

sulfur compounds, which can donate a lone pair of electrons, and a metal ion (here Pd), which has a vacant d orbital to accept the lone pairs of electrons [62]. Palladium shows strong selectivity towards PASHs [63-67] which can be eluted after addition of isopropanol to the mobile phase, which is a competitive ligand [68].

The strength of the interaction between Pd(II) and thiophenes is correlated with the Hückel π electron density on the sulfur atom. The interaction and density diminish in the order: dibenzothiophene > benzo[*b*]naphtho[2,1-*d*]thiophene > benzothiophene. The compounds with thiophene rings that are not condensed with any other aromatic system are very weakly retained and elute together with the PAHs in fraction Pd-1. Alkyl substituents increase the electron density and the alkyl derivatives are stronger retained than their parent compounds, unless a steric effect is in operation. The alkylation in the 4- and 6-position of a dibenzothiophene does not hinder the complexation and all DBTs elute in fraction Pd-2. Naphthothiophenes are a more complex case, as naphtho[1,2-*b*]- and naphtho[2,1-*b*]thiophene were found in fraction Pd-1, naphtho[2,3-*b*]thiophene in fraction Pd-2. The compounds with two sulfur atoms in the aromatic rings are well retained by Pd(II) and elute in fraction Pd-2. If the sulfur is in a non-aromatic ring, the compound is irreversibly retained by Pd(II) ions. The nitrogen heterocycles are irreversibly retained, but the oxygen heterocycles do not interact strongly with Pd(II). Olefins do not show strong interaction with Pd(II) and are eluted in the Pd-1 fraction [69].

Till now the standard separation was prepared on Pd(II)-MP SG using for synthesis silica LiChrosorb Si 100, 10 µm from Merck, with pore size of 10 nm and particle size of 10 µm. The specific surface area for this silica reaches 290 -340 m^2/g. Some other silica types were taken for Pd(II)-MP SG preparation, with larger pore size, to check if discrimination of some sulfur compounds with higher masses takes place. Many PASHs investigated here have molecular masses above 600 amu and may therefore be of such a lorge size that they cannot diffuse into the pores of the 10 nm material. The other tested silicas were: YMC Gel Silica 12 nm S-5 µm and YMC Gel Silica 20 nm S-5 µm, that is both with the particle size

of 5 µm and the pore size of 12 nm and 20 nm respectively. The specific surface area are 349 m^2/g ± 10% for pore size of 12 nm and 174 m^2/g ± 10% for pore size of 20 nm. The specific surface area is lower for bigger pore and particle size. A high Pd(II) loading is observed for silica with the particle size of 5 µm and the pore size of 12 nm important for good separation. A Pd(II) loading on silica with smaller particle size and smaller values of pore size is much easier than on silica with bigger pores and particle size. The metal loading for different silica types is presented in Table 5.

Table 5 The metal loading for Pd(II)-MP SG

Metal loading (µg Pd(II) / 1 mg Pd(II)-MP SG) *:		
for pore size 10 nm	for pore size 12 nm	for pore size 20 nm
particle size 10 µm	particle size 5 µm	particle size 5 µm
20.7	22.9	15.2

* The samples of Pd(II)-MP SG for metal loading measurement were mixed with HF in platinum crucible and left for one night. Next day H_2SO_4 was added and the samples were intensively heated to remove an excess of HF. The remains were dissolved in water, transported to a 50 mL volumetric flask and the Pd(II) concentration was measured using AAS.
The Pd(II) concentrations were as follows: 11.6 µg/mL (for pore size 10 nm, in 28 mg of Pd(II)-MP SG), 12.9 µg/mL (for pore size 12 nm, in 28.2 mg of Pd(II)-MP SG), 8.2 µg/mL (for pore size 20 nm, in 27 mg of Pd(II)-MP SG).
The measurement was repeated twice.

The Kendrick plots are shown below for fraction Pd-2 (S1 class), obtained on Pd(II)-SG MP synthesized from silica with different particle and pore size (Figures 18, 19, 20). A standard is chosen, so that all the intensity changes can be compared directly to that one-sulfur compound. As the standard, the compound with KNM of 358 amu and DBE of 6 is chosen, corresponding to benzothiophene with 16 aliphatic carbon atoms, as there should not be any problems with the complete elution of the compound for all silica types. It is the most abundant sulfur compound as seen in the Kendrick plot for Pd(II)-MP SG with pore size of 12 and 20 nm, and the second most abundant for pore size of 10 nm (for Pd(II)-MP SG 10 nm, the compound with mass

of 372 amu and DBE of 6, the next compound in the homologues series of DBE 6, has the highest intensity).

With larger pore size, a few compounds with higher masses are collected. The highest mass seen in Figure 18 (silica pore size of 10 nm) is 526 amu, for compound with DBE of 6. In Figure 19 (pore size of 12 nm), the highest mass is attributed for the compound with DBE 9 (mass of 548 amu). In Figure 20 (pore size of 20 nm) the highest masses belong to the aliphatic sulfur compounds with DBE of 1 and 2, which appear here. The highest mass for aromatic sulfur compound is attributed to 554 amu, for compound with DBE of 6. Some sulfur compounds with low DBE appear more efficiently with larger pore size, which can be explained by the low metal loading (Table 5) and less effective interactions, that is the complex formation between sulfur compounds and Pd ions. There is no change in the maximum of DBE (14) for different silica pore size. The DBE 6 series of compound is the most abundant for all different silica types.

As presented, discrimination of larger sulfur components takes place for smaller pore size material used for separation of aromatics. In order to collect PASHs with higher masses, silicas with larger pore sizes have to be used for synthesis of Pd(II)-MP SG.

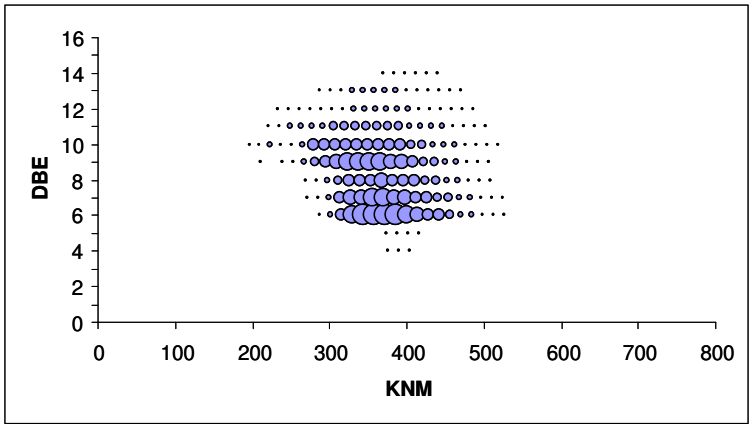

Figure 18 Kendrick plot of Pd-2 fraction (VGO, IL) from Pd(II)-MP SG (pore size 10 nm)

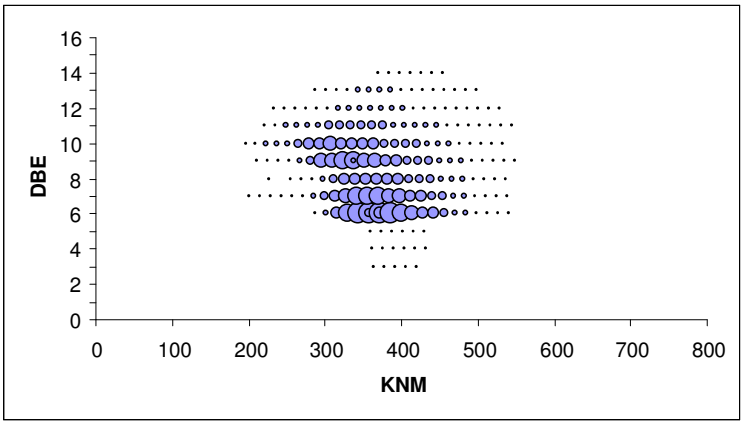

Figure 19 Kendrick plot of Pd-2 fraction (VGO, IL) from Pd(II)-MP SG (pore size 12 nm)

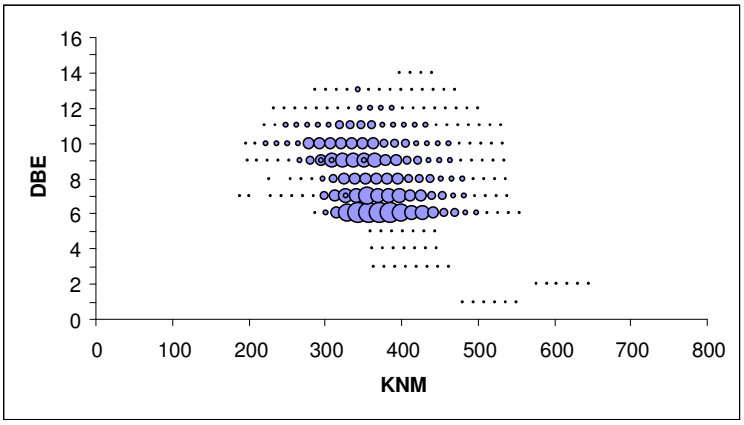

Figure 20 Kendrick plot of Pd-2 fraction (VGO, IL) from Pd(II)-MP SG (pore size 20 nm)

β-Cyclodextrin column

The Pd-2 fraction (43 mg) was separated on 2 x β-cyclodextrin columns (150 mm × 4 mm) into three CD fractions. Around 8 mg of fraction CD-1 (two condensed aromatic rings), 14 mg of fraction CD-2 (three condensed aromatic rings) and 3 mg of fraction CD-3 (four and more condensed aromatic rings) were collected. Figure 21 presents the separation of fraction Pd-2 on two connected β-cyclodextrin columns.

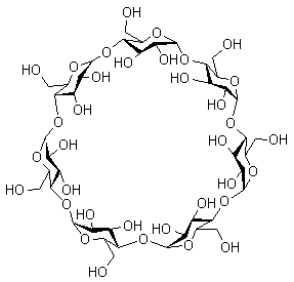

β-cyclodextrin

Cyclodextrins are oligoglucoses. The β-phase consists of seven glucose units in a ring connected to the silica. In NP chromatography the hydroxy groups are pointed outwards, so the cavity (7.8 Å) of the molecule is nonpolar. Probably the cavity is filled with the mobile phase and the interaction with the solutes is through the hydroxyl groups on the outer surface. For β-cyclodextrin mono- and disubstituted benzothiophenes elute earlier than benzothiophene. The same trend is observed for dibenzothiophene. Alkyl groups decrease the retention time in comparison to parent structure. Long alkyl chains significantly decrease the retention time [70, 71, 176].

In order to separate the fractions according to the number of fused aromatic rings completely, different combinations of column lengths, column numbers and temperature were tested for optimal results. The results are collected in Table 6. The best separation can be observed using three connected 150 mm x 4 mm columns at room temperature. The separation decreases with a temperature increase, from 40.3 % (the separation was calculated: height difference of CD-1 peak and the valley between CD-1 and CD-2 peaks / height of CD-1 peak) at room temperature, 23.1 % at 50 °C, till 17 % at 70 °C. The separation generally is more efficient when more columns were connected. For example one 150 mm x 4 mm column gives a separation of 32.3 % at room temperature, two columns - 33.1 % and three columns - 40.3 %. A longer column (250 mm × 4.6 mm) should give better separation than a shorter one (150 mm × 4 mm), but the results do not always support this assumption.

Finally the separation conditions were chosen. The separation using two connected β-cyclodextrin columns (150 mm x 4 mm) at room temperature gives a good value for the separation, 33.1 %. Higher values of separation are obtained using three connected columns (150 mm x 4 mm), or combinations with longer, 250 mm x 4.6 mm, column, but due to a very high back pressure, further work is precluded (Table 6).

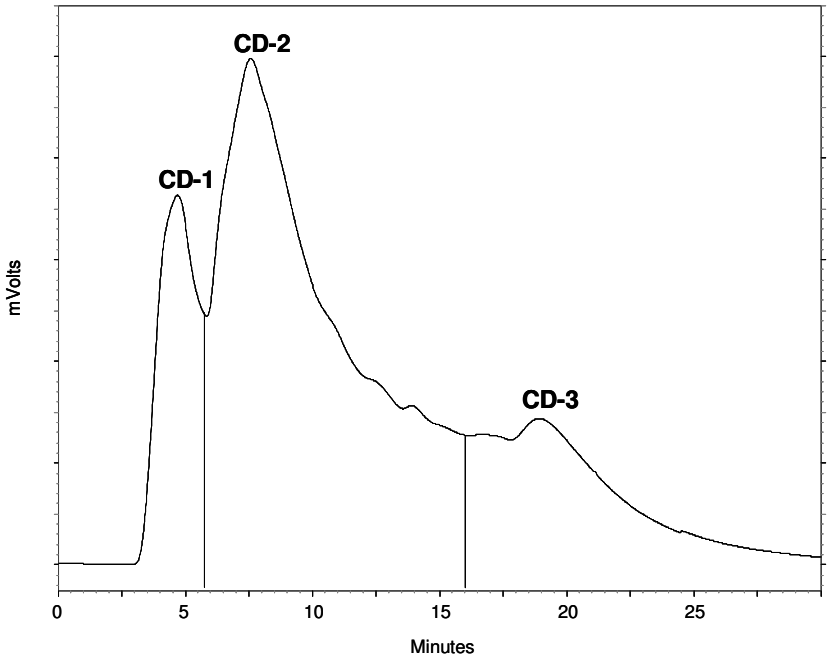

Figure 21 HPLC chromatogram of Pd-2 fraction separation on 2 x β-cyclodextrin columns 150 mm × 4 mm (mobile phase - cyclohexane with 0.5 % of *tert*-butyl methyl ether, a flow rate of 1 mL/min, room temperature)

Table 6 Optimization of Pd-2 fraction separation on β-cyclodextrin columns (mobile phase - cyclohexane with 0.5 % of *tert*-butyl methyl ether, a flow rate of 1 mL/min)

Column combination	Temperature	Separation *
1 x 150 mm × 4 mm	room temp.	32.3%
1 x 150 mm × 4 mm	50℃	29.1%
2 x 150 mm × 4 mm	**room temp.**	**33.1%**
2 x 150 mm × 4 mm	50℃	18.3%
3 x 150 mm × 4 mm	room temp.	40.3%
3 x 150 mm × 4 mm	50℃	23.1%
3 x 150 mm × 4 mm	70℃	17%
1 x 250 mm × 4.6 mm	room temp.	30.2%
1 x 250 mm × 4.6 mm	50℃	15.1%
2 x (150 mm × 4mm and 250 mm × 4.6 mm)	room temp.	36.5%
2 x (150 mm × 4 mm and 250 mm × 4.6 mm)	50℃	24%
2 x (250 mm × 4.6 mm and 150 mm × 4 mm)	50℃	24.9%
3 x (250 mm × 4.6 mm and 2 x 150 mm × 4 mm)	room temp.	36%
3 x (250 mm × 4.6 mm and 2 × 150 mm × 4 mm)	50℃	24.9%

* The separation was calculated: (height difference of CD-1 peak and the valley between CD-1 and CD-2 peaks / height of CD-1 peak.

Jordi Gel DVB Polyamino column

The commercially available stationary phase Jordi Gel DVB Polyamino resin was also investigated for Pd-2 fraction separation. The phase (100 nm, 5 µm, Jordi) was packed into a column (see Table 7) the same way as β-cyclodextrin. It separates the Pd-2 fraction in an analogous way to the β-cyclodextrin column, according to the number of condensed aromatic rings (Figure 22). Different solvents (cyclohexane or pentane) and column lengths were used to compare the separation efficiency. The best separation is achieved using pentane as the mobile phase, but because of the solvent flow problems and long time of separation, finally cyclohexane appears as the best solution (Table 7).

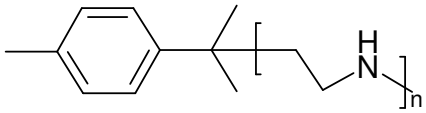

Jordi Gel DVB Polyamino Resin

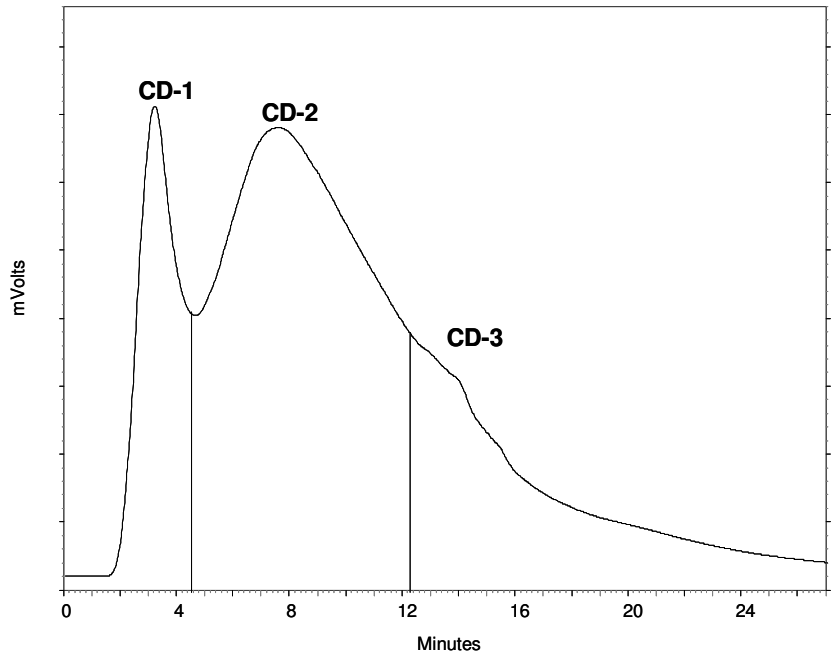

Figure 22 HPLC chromatogram of Pd-2 fraction separation on Jordi Gel DVB Polyamino column 250 mm x 4.6 mm (mobile phase - cyclohexane, a flow rate of 1 mL/min, room temperature)

The separation achieved on Jordi Gel DVB Polyamino Resin is comparable to the separation achieved using β-cyclodextrin column. Both can be used for fractionation of Pd-2 according to the number of condensed aromatic rings.

Table 7. Separation of Pd-2 fraction using Jordi Gel DVB Polyamino Resin (room temperature, flow 1 mL/min)

Column	Solvent	Separation
Jordi, 150mm x 4 mm	cyclohexane	30.8 %
Jordi, 150 mm x 4 mm	pentane	44.1 %
Jordi, 250 mm x 4.6 mm	cyclohexane	41 %
Jordi, 250 mm x 4.6 mm	pentane	58.1 %

TCP column

For the next step of separation, tetrachlorophthalimide silica gel was chosen. It is an electron-acceptor stationary phase [71]. Holstein demonstrated that TCP-modified silica separates the aromatic compounds according to the number of fused aromatic rings [75]. The reversible complex by electron transfer is formed (charge transfer mechanism) [76].

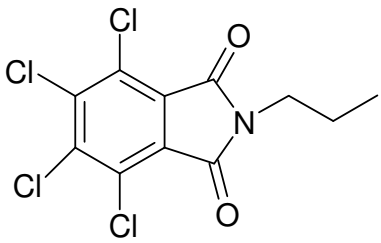

TCP phase

The chromatograms for fraction CD-1, CD-2 and CD-3 are presented further (Figures 23, 24, 25) obtained on two connected TCP columns. Every next fraction contains more aromatic rings and has a longer elution time. Fraction CD-1 is composed mainly of benzothiophenes with many different alkyl substituents which cause the peak broadening. Because of the incomplete separation on β-cyclodextrin, it is contaminated with dibenzothiophenes, visible in the chromatogram as a broad peak over 4.5 min. Fraction CD-2 is composed mainly of dibenzothiophenes with different alkylation pattern. It starts to elute already below 4 min, as it still contains some benzothiophenes. By retention time over 10 min, possibly other PASHs containing more aromatic rings, are eluted. Fraction CD-3 is the most differentiated in shape, because of different number of aromatic rings (at least four aromatic rings in the structures) and various alkylations. The signals below 10 min probably come from dibenzothiophenes.

The influence of an alkyl substituent on the retention time is much higher than in the case of the β-cyclodextrin columns. That is the reason why the separation according to the number of fused aromatic rings on β-cyclodextrin columns is preferred. That does not exclude the further use of TCP columns as the fourth dimension of the separation, which unfortunately still is not efficient enough. A fairly extensive overlap of peaks is observed under the present conditions.

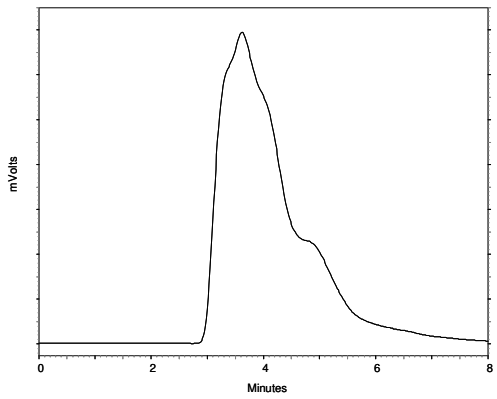

Figure 23 HPLC chromatogram of CD-1 fraction on 2 x TCP columns 150 mm × 4 mm (mobile phase - cyclohexane, a flow rate of 1 mL/min, room temperature)

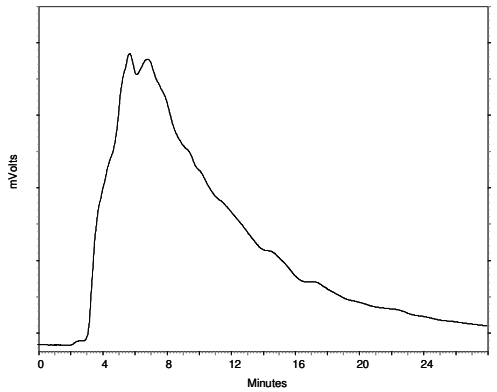

Figure 24 HPLC chromatogram of CD-2 fraction on 2 x TCP columns 150 mm × 4 mm (mobile phase - cyclohexane, a flow rate of 1 mL/min, room temperature)

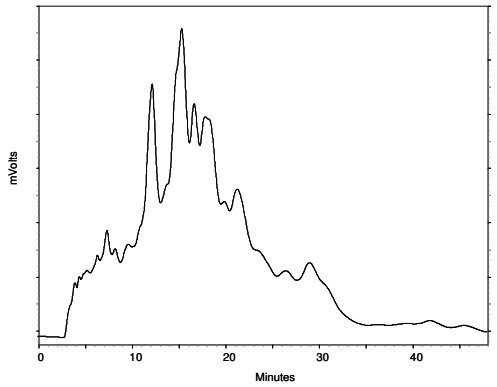

Figure 25 HPLC chromatogram of CD-3 fraction on 2 x TCP columns 150 mm × 4 mm (mobile phase - cyclohexane, a flow rate of 1 mL/min, room temperature)

Other stationary phases, like aminopropano silica gel or 2,4-dinitroanilino-N-propano silica gel, were also investigated for CD fractions separation possibility. They do not show any good separation. The packing with TCP SG (10 µm) longer columns 250 mm x 4.6 mm, applying higher temperature, using for synthesis of TCP SG LiChrosorb Si 100 with particle size of 5 µm or synthesis of polymeric TCP SG (what allows more TCP groups to be connected onto silica) were tested to find better separation. No better results are obtained than these above.

Using standard compounds it was further investigated how alkyl substituents influence the retention time (Table 8). It is found that for the TCP phase, addition of alkyl substituents to the aromatic rings can affect the π electron system. The alkyl chains are known to be electron donors, so the substituted PASHs would be retained more strongly. If the alkyl chain is long, we have to consider an interaction with the mobile phase and a steric hindrance. A decrease in retention time is observed then [77]. Without an earlier separation on β-cyclodextrin column, it is not possible to obtain a good separation of aromatic compounds on TCP silica gel. This stationary phase separates according to the number of fused aromatic rings, but an alkyl substituent has a huge influence on the retention time and this makes the separation difficult.

Table 8 Alkyl substituent influence on retention time (2 x TCP columns 150 mm × 4 mm, mobile phase - cyclohexane, a flow rate of 1 mL/min, room temperature)

Standard	**Retention time, min**
2-Eicosylbenzothiophene	4.21
2-Decylbenzothiophene	4.46
Benzothiophene (2 rings)	**4.75**
2-Dodecylbenzothiophene	4.74
3-Methylbenzothiophene	5.20
5-Methylbenzothiophene	5.38
Tetrahydrodibenzothiophene	6.46
2,3-Dimethylbenzothiophene	6.75
2,3,7-Trimethylbenzothiophene	10.21
4-Decyldibenzothiophene	6.32
4-Octyldibenzothiophene	7.04
Dibenzothiophene (3 rings)	**7.12**
4-Ethyldibenzothiophene	8.12
2-Methyldibenzothiophene	9.13
4-Methyldibenzothiophene	10.34
2,6-Dimethyldibenzothiophene	16.10
2,4-Dimethyldibenzothiophene	16.78
2,4,6,8-Tetramethyldibenzothiophene	30.10
Phenanthro[4,5-*bcd*]thiophene (4 rings)	10.95
Benzo[*b*]naphtho[2,1-*d*]thiophene	14.24
Benzo[*b*]naphtho[1,2-*d*]thiophene	16.53
Benzo[*b*]phenanthro[9,10-*d*]thiophene (5 rings)	32.40

5.2.2 CD Fractions Analysis

Fractions CD-1, CD-2 and CD-3 were investigated using different analytical techniques, which can give more information regarding the structures of the PASHs in the complex mixture.

UV spectroscopy

The diode array detector used for the monitoring of the separations made it possible to obtain UV spectra for every CD fraction (Figure 26).

The absorption maxima of the UV spectra are shifted to longer wavelengths with the number of CD fraction, as the number of the condensed aromatic rings increases. There is also a difference visible in the UV spectrum appearance for every CD fraction (Figure 26).

The absorption maxima of the fractions are also shifted a few nm to longer wavelengths in comparison with the parent structures, as presented in the example of fraction CD-1, benzothiophene and 3-methylbenzothiophene (Figure 27). These effects are caused by the higher electron density of the aromatic rings derived from multiple alkyl substitution and the concomitant lower energy needed for the excitation. The shape of the UV spectrum for the fractions shows a good agreement with those of the standards.

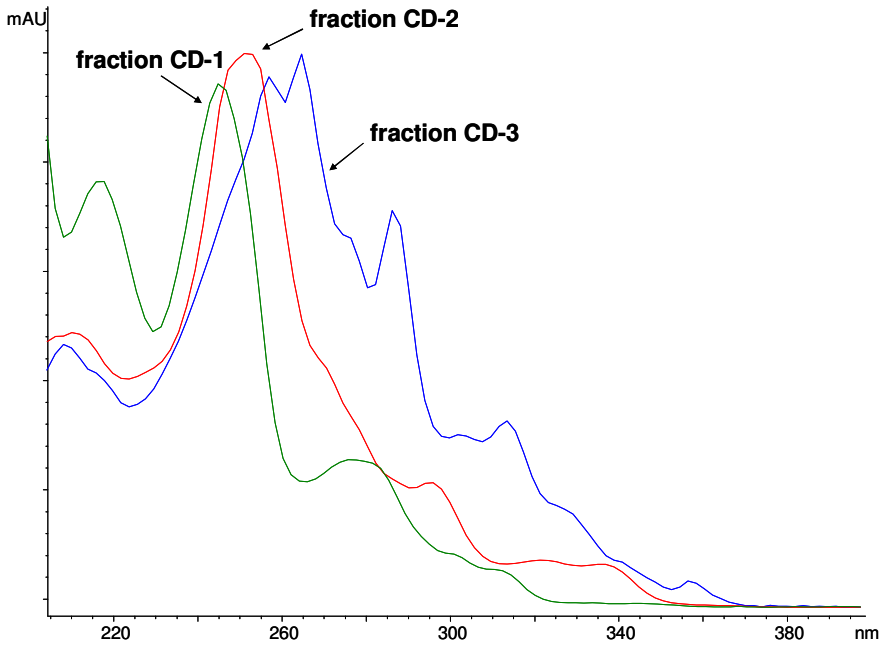

Figure 26 UV spectra for fractions CD-1, CD-2 and CD-3

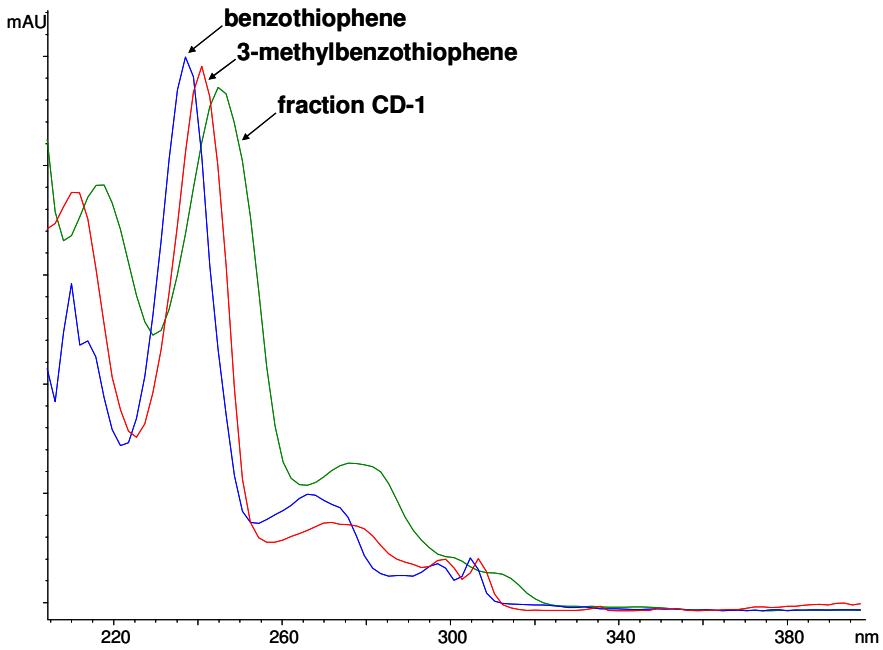

Figure 27 UV spectra for fraction CD-1 and the standards (benzothiophene, 3-methylbenzothiophene)

The number or the shape of the alkyl substituents on the aromatic system cannot be deduced from the UV spectra, but these can give information related to the aromatic system and separation efficiency.

Fluorescence spectroscopy

The fluorescence spectra were recorded in cyclohexane with the emission wavelength selected to correspond to the maximum UV absorption (Figures 28, 29, 30). Similarly to the UV spectra, more aromatic rings in a condensed system cause a shift of the emission and excitation spectrum to longer wavelengths. The maxima of excitation are found to be 337.4 nm, 363.6 nm and 368.6 nm for fraction CD-1, CD-2 and CD-3 respectively. The maximum of emission are found to be 389.6 nm for fraction CD-1, 385.8 nm for fraction CD-2 and 401.2 nm for fraction CD-3. This technique was not used further in this work, but as presented here, it can be applied in future investigation of PASHs.

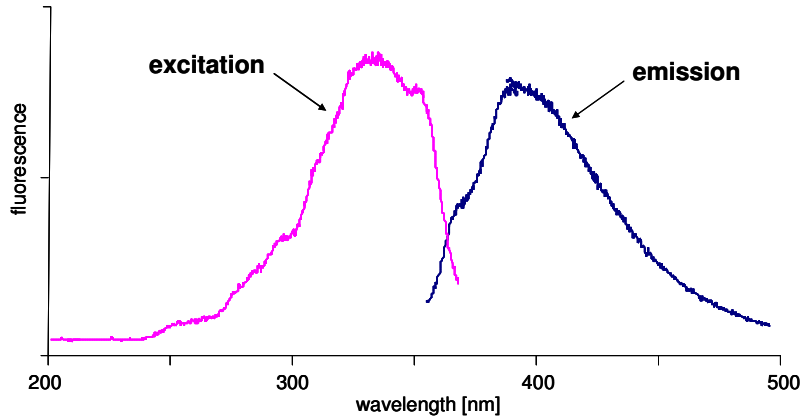

Figure 28 Fluorescence spectrum for fraction CD-1

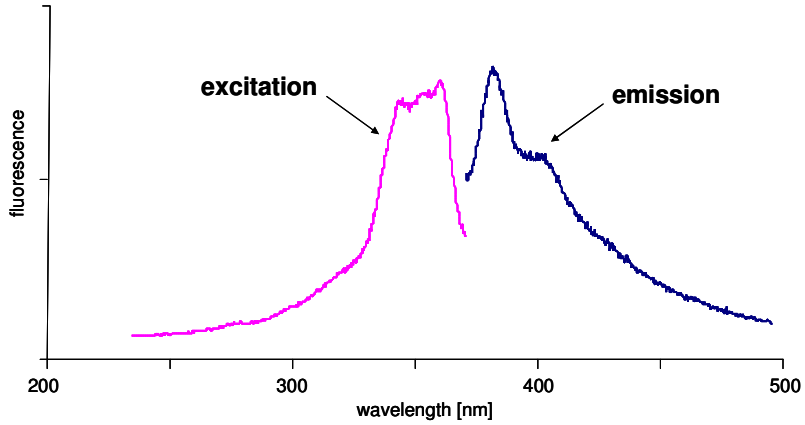

Figure 29 Fluorescence spectrum for fraction CD-2

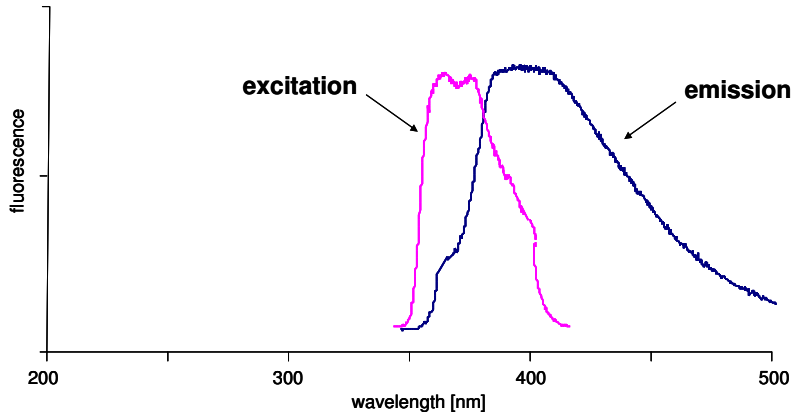

Figure 30 Fluorescence spectrum for fraction CD-3

^{1}H NMR

^{1}H NMR data can be used to measure the ratio of aromatic to aliphatic hydrogens in the fractions. The amount of the aliphatic hydrogens decreases with the CD fraction number, as the number of aromatic rings increases. The ratio of aromatic to aliphatic hydrogens for fraction CD-1 is 1:6.2. The theoretical value calculated for the average mass in the fraction (around 380 amu) and two aromatic rings (benzothiophenes) is around 1:7. This ratio is true only for singly substituted benzothiophene. When two alkyl chains are connected to the aromatic system, the ratio changes to 1:9, as the number of the aromatic and aliphatic hydrogens changes. The theoretical ratio of aromatic to aliphatic hydrogens calculated for fraction CD-2 is around 1:3 (average mass of 320 amu, three rings of dibenzothiophene, singly substituted system) and fraction CD-3 around 1:1 (average mass of 300 amu, four rings, singly substituted system). The measured data for the ratios are presented in Table 9. All these data cannot be taken for the exact calculations of the ratios of the aromatic and aliphatic hydrogens in the fractions, as many different substitutions are possible and the fractions are not separated thoroughly. These data can show only the general trend of changes. As later will be shown after the oxidation of CD fractions, NMR data indicate the increase of the aromatic to aliphatic ratio caused by aromatization. The data can be used to check, if the oxidation succeed and to what extent.

Table 9 ^{1}H NMR data

^{1}H aromatic to aliphatic ratio	
Fraction CD-1	1:6.2
Fraction CD-2	1:3.4
Fraction CD-3	1:2.9

Gas chromatography

Gas chromatography is not suitable for CD fractions investigation because of the low volatility of the compounds in the VGO mixture and an insufficient resolution of such highly complex mixtures. An example of the gas chromatogram (GC-MS,

prepared in the mode of TIC, see appendix) is presented in Figure 31 for fraction CD-1. There is no possibility to carry out an analysis of individual components. Applying the SIM mode for the expected mass range or using an other detector, like the AED, does not simplify the chromatogram appearance much. It is worth noticing that the chromatogram presented shows the already extensively separated fraction CD-1 where mainly benzothiophenes are present.

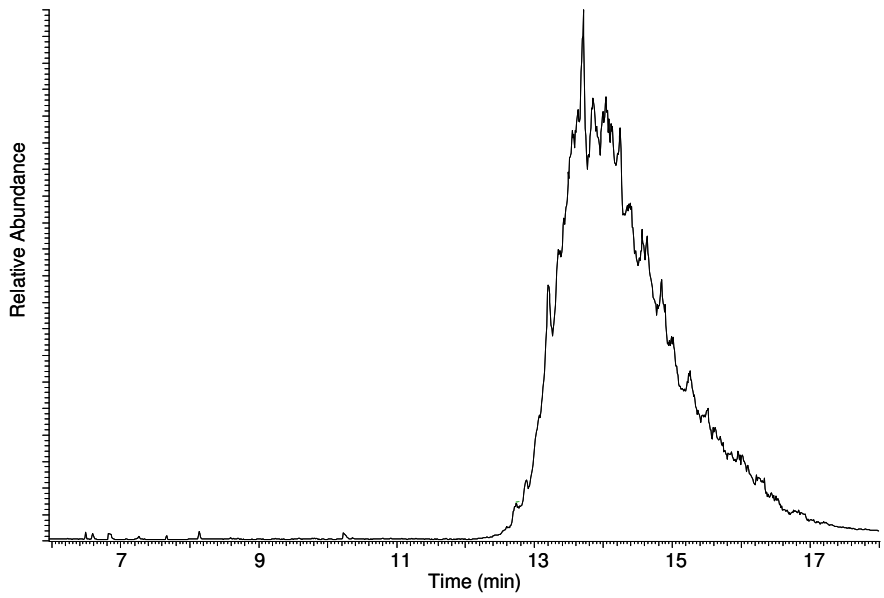

Figure 31 Gas chromatogram (GC-MS) of CD-1 fraction

FT-ICR MS

To overcome the problems of low resolution and low volatility, an FT-ICR MS analysis was performed for the CD fractions. All the compounds of the S1 class together with DBE and KNM are presented in Figures 32, 33, 34. A standard was chosen for every fraction, which later will be used as the reference after the oxidation process. For every fraction it is the most abundant PASH, with the DBE value typical for the specific fraction. The intensity for these compounds is assigned by the value 1 and all the other compounds have a relative intensity to that magnitude. For fraction CD-1 the standard is the component with DBE of 6 and mass of 358 amu, corresponding to a benzothiophene with 16 carbon atoms in the side chain(s). For fraction CD-2, the compound chosen is PASH with DBE of 9 and

mass of 310 amu, a dibenzothiophene with 9 carbon atoms in the side chain(s). The CD-3 fraction has as the standard the component with DBE of 12 and mass of 276 amu, a benzonaphthothiophene with 3 carbon atoms in the side chain(s).

There is no signal with DBE 0 (mercaptans, sulfides), 1 (thiophanes) and 2 (dihydrothiophenes) in fraction CD-1 (Figure 32). These compounds are retained on Pd(II) MP SG. A low concentration of thiophenes (DBE 3), napthenothiophenes (DBE 4) and cyclopentenothiophenes or cyclohexenothiophenes (DBE 5) is found. These compounds should elute in the Pd-1 fraction and it is still not clear why they elute in fraction Pd-2. It can be explained by a strong influence of the alkyl substituents. For the DBE 3 series, molecules with 20 to 22 carbon atoms in the side chains are present. For DBE 4, carbon atoms number in the side chain(s) varies from 16 to 18 (for cyclohexathiophenes), and for DBE 5 from 17 to 21 (for cyclopentenothiophenes). DBE 6 is the most abundant series and corresponds to benzothiophenes. Compounds with 10 to 29 aliphatic carbon atoms are found. Further series with DBE of 7 is represented by napthenobenzothiophenes and the number of carbons in the aliphatic chains varies from 7 (with one quite intensive signal for a compound with 2 aliphatic carbons attached to the aromatic system) to 25 (for 1,2,3,4-tetrahydrodibenzothiophene for example). The compounds with DBE 8 can be represented by dinaphthenobenzothiophenes, indenothiophenes, indanylthiophenes. The masses for this series range from 270 amu to 522 amu. The next series of compounds, that is with DBE 9, as well as DBE 10 and 11, should be present only in fraction CD-2, but unfortunately some overlapping is still observed, the separation is not complete, and some of the compounds representative of fraction CD-2 may be present in fraction CD-1.

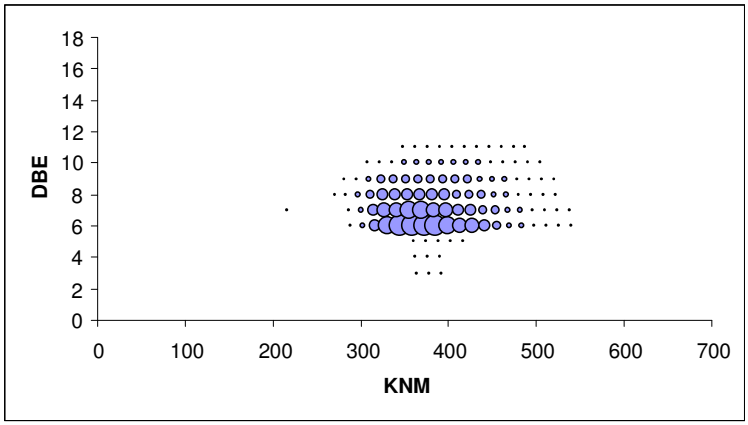

Figure 32 Kendrick plot for fraction CD-1

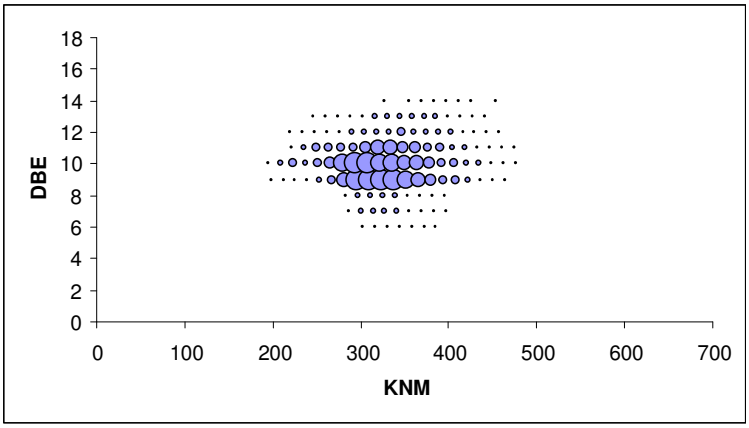

Figure 33 Kendrick plot for fraction CD-2

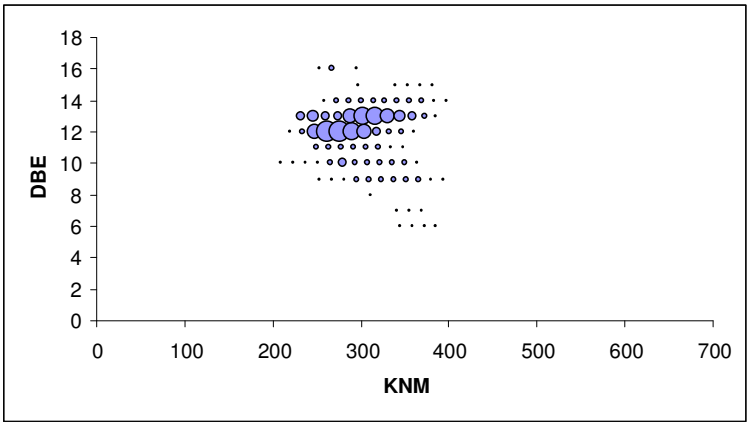

Figure 34 Kendrick plot for fraction CD-3

Figure 33 presents the Kendrick plot for fraction CD-2. For this fraction, the main series of the compounds are those with DBE of 9. There are still some signals from the series of DBE 6 and more intensive series of DBE 7 and 8. Series DBE 9 is mainly represented by dibenzothiophenes, but trinaphthenobenzothiophenes are possible as well. For dibenzothiophenes, 1 to 21 carbon atoms in the side chains are observed. The next higher series with DBE 10 is represented by acenaphthothiophenes, or dibenzothiophene with one naphtheno ring, or benzothiophene with a phenyl group. The mass reaches from 196 amu till 476 amu. The next series, DBE 11, can be represented by acenaphthylthiophenes and has masses in the range of 222 - 474 amu, which means that 1 to 19 carbon atoms in the side chains are possible. The series of DBE 12 as well as 13 and 14 should be present already in fraction CD-3, but again, the lack of perfect separation causes that all fractions overlap one another.

Fraction CD-3 (Figure 34) contains, as expected, signals of very low intensity with lower DBE starting from 6 and more intense by DBE 9, 10, 11. The main series of the compounds for fraction CD-3 is that of DBE 12. The main representatives are benzonaphthothiophenes. The mass range for this series is 220 - 360 amu. The next series of DBE 13 can be represented by naphthenophenanthrothiophenes, or benzonaphthothiophenes with one naphtheno ring, or dibenzothiophenes with one phenyl group. Masses are in the range of 232 - 386 amu. The series of DBE 14, 15 and 16 are also present, but of lower intensity.

There are some signals in fraction CD-2 and CD-3 with high DBE and quite small masses, like for DBE 10 with mass of 196 u for example. A structure for this kind of molecules has to contain highly condensed aromatic system to reach this high DBE with very low mass.

The Kendrick plots give a clear view on the separation efficiency and the sample content, although not all structural information can be gathered at this step. Despite the extensive separation on silica and alumina column, the Pd(II) MP

column, and the β-cyclodextrin columns, there is still some overlap between different compounds types as evidenced in the Kendrick plots.

The use of the Kendrick plots for visualization of the data obtained from ultra-high resolution FT-ICR MS technique is a superior method. The initial separation is essential for reducing the amount of obtained signals and the simplification of the analysis.

5.3 Summary

Despite the intensive separation of the VGO complex mixture on a silica/alumina bed, Pd(II)-MP SG and β-cyclodextrin, a still better separation is needed. In such a complex mixtures, the number of the parent structures goes up with the distillation temperature. DBEs up to 16 were found in VGO and each DBE can be represented by several parent systems. A perfect phase for HPLC separation should be able to separate each parent system. A heavy alkylation influences the retention times and makes the separation even more difficult.

Many different analytical approaches can be applied for the PASHs analysis. FT-ICR MS seems to be the most appropriate for such a high boiling, complex mixture. UV and fluorescence spectra can distinguish between the CD fractions, but further interpretation is difficult and time consuming. NMR data presented here are used only for the ratio between the aromatic and aliphatic hydrocarbons measurement. Even all these analytical methods cannot give a complete answer regarding the structures of the compounds present in a VGO. Especially troublesome is the identification of the (poly) naphtheno structures. To achieve more information, chemical transformations will be investigated.

6 Oxidation

New information about the PASHs is sought, like: the parent structure of an aromatic system, if there are naphtheno rings present in the molecule, the position of the alkyl groups in the aromatic system, the length of the chains and the structure of these chains (linear or branched). To answer some of these questions, the investigation with commonly used techniques described earlier is not enough. The chance to obtain deeper knowledge may be given by chemical transformations and the analysis of the products. Oxidation is such a chemical transformation, which can be applied to the PASHs.

With Cr(VI) in form of chromic acid or sodium dichromate for example, the alkyl group of an alkyl benzene, regardless of its length, is oxidized to a carboxyl group and forms an aromatic carboxylic acid (and an aliphatic carboxylic acid, with one carbon atom less than the original side chain). That gives the desired simplification in the product distribution and provides a general method for the determination of the orientation and number of the alkyl groups in the substituted aromatic system. An exemplary compound oxidation with Cr(VI) is presented in Figure 35.

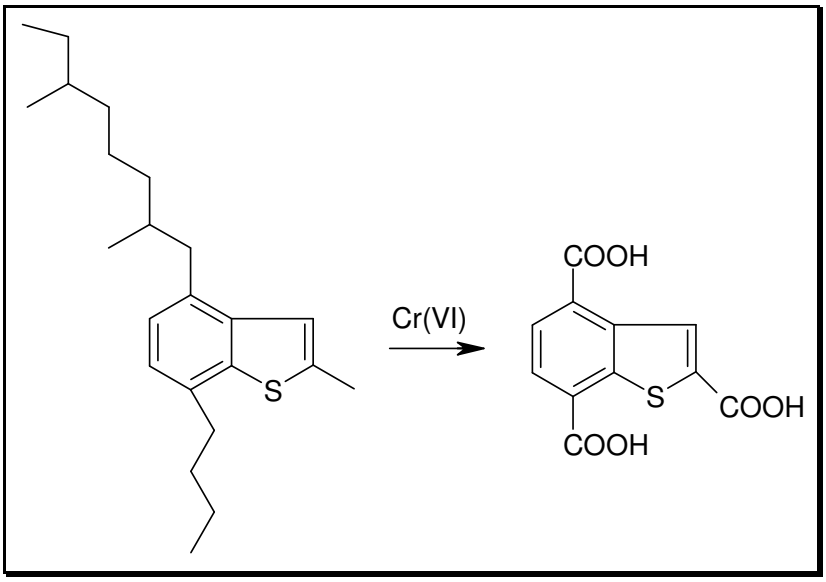

Figure 35 Cr(VI) oxidation

The acid-catalyzed Cr(VI) oxidation of methyl arenes to the corresponding aryl carboxylic acids was investigated by Granzow and Wilson [177]. Yamazaki reported that CrO_3/H_5IO_6 acts as efficient catalytic system for the oxidation of toluenes to the corresponding benzoic acids [178]. Reitsema and Allphin [179] investigated the oxidation of different alkylaromatic hydrocarbons. They found that ethylbenzene was oxidized to phenylacetic or benzoic acid depending on the conditions. *n*-Propylbenzene, iso-propylbenzene, *n*-butylbenzene and styrene could be all oxidized to benzoic acids. *tert*-Butylbenzene was not affected, which can indicate that the initial reaction in the chromate oxidation may be on the α-methylene group of the side chain [179, 180]. Duty *et al.* obtained a 99 % yield by oxidizing 2,6-dimethylnaphthalene to the corresponding dicarboxylic acid using $Na_2Cr_2O_7$. The satisfactory oxidation of the alkylated PAHs to the corresponding aromatic acids and 3-methylthiophene to 3-thiophenecarbocylic acid was achieved also by Friedman *et al.* [181]. A large excess of sodium dichromate can lead to ring destruction [182].

It can be thus expected, that the alkylated PASHs would give appropriate carboxylic acids derivatives [183].

Ruthenium tetroxide oxidation, on the other hand, could answer the question about the length and the structure of the alkyl chains connected to an aromatic system. RuO_4 oxidizes the alkylaromatic species, resulting in the formation of a carboxylic acid from the alkyl part of the molecule. An aromatic system is converted into carbon dioxide and sulfur oxides (Figure 36). Ruthenium tetroxide is typically prepared in situ by the oxidation of a precursor such as ruthenium dioxide or ruthenium trichloride, with a co-oxidant such as sodium periodate [184]. The catalytic oxidation with ruthenium tetroxide has been extensively studied [185-200].

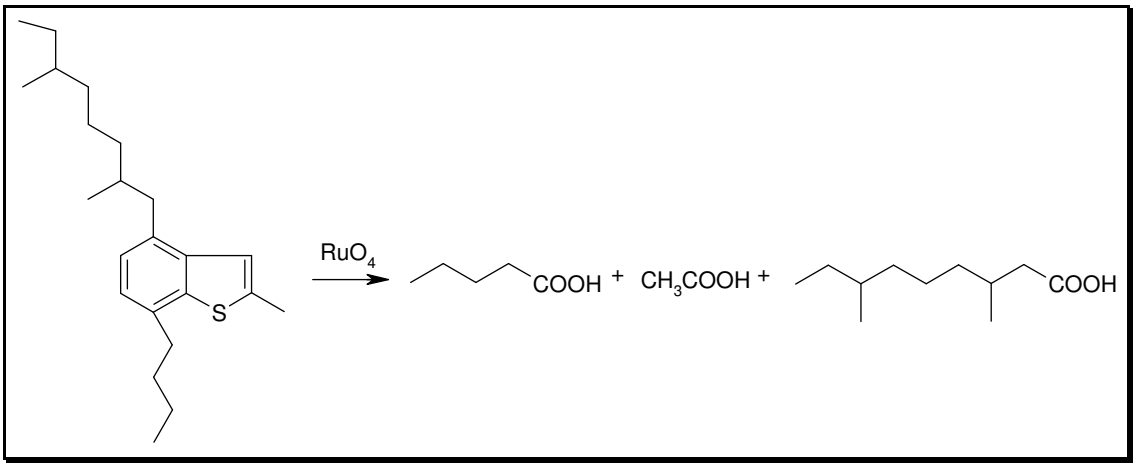

Figure 36 RuO_4 oxidation

The acids received after oxidation would contain the alkyl chains as attached earlier to the aromatic system. That would simplify the analysis of the chains connected to the aromatic rings.

Another type of oxidation, which can give important information about the type of connection of the non-aromatic rings to an aromatic system is dehydrogenation.

6.1 Dehydrogenation

Oxidation understood as the elimination of hydrogen (aromatization) can reveal some information according to the structure of the PASHs, exactly how a six-membered non-aromatic ring (only six-membered rings are investigated in this work) is connected to an aromatic system. A ring can be annealed to an aromatic system, as presented in the literature [8], but also connected by the binding in a non-condensed way, as can be assumed by taking into consideration that cyclohexanecarboxylic acid and cyclohexylacetic acid were found in the products after crude oil photo-oxidation [201]. The dehydrogenation can be achieved with a series of

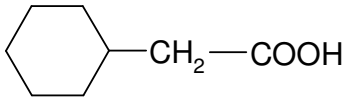

cyclohexanecarboxylic acid

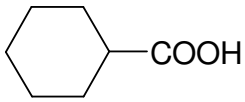

cyclohexylacetic acid

different reagents, but the most important prerequisite is that only a naphtheno ring condensed to an aromatic system is oxidized. A non-condensed saturated ring should remain untouched (Figure 37).

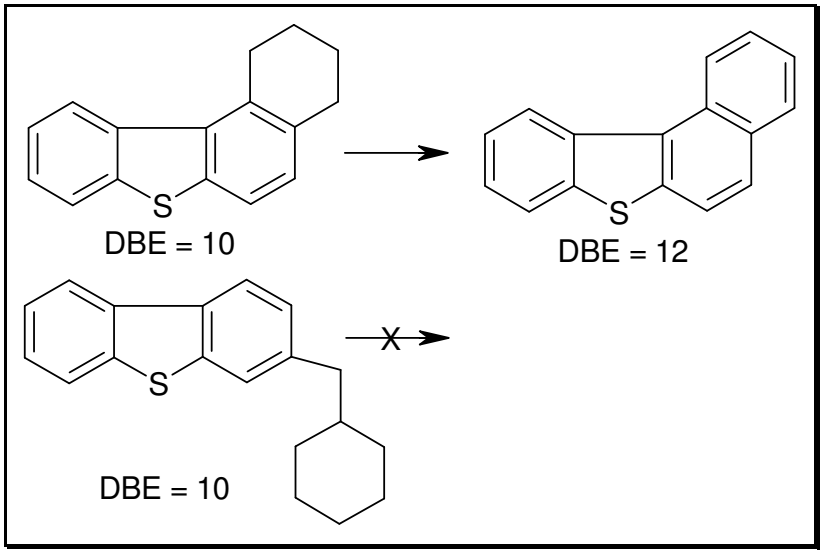

Figure 37 Aromatization example scheme

In this reaction new double bonds would be created in naphtheno rings condensed to an aromatic part of the molecule and a shift to higher DBE would be observed after MS analysis. Figure 37 presents an example where both substrates have DBE of 10, but aromatization should affect only the first of the substrates and give an increase of its DBE from 10 to 12. Nothing should change in the second case. The increase in DBE (observed by a change in peak intensity e.g. in MS) would give us statistical information on how many percent of the molecules possess this kind of structure with a condensed naphtheno ring.

There are three main types of reagents most frequently used to effect aromatization: quinones (which become reduced during oxidation to the corresponding hydroquinones), hydrogenation catalysts (such as palladium, platinum, nickel) and elemental sulfur and selenium (which give H_2S and H_2Se, respectively) [202-204]. They were tested in this work and the results will be reported here.

6.1.1 DDQ

As already mentioned, quinones become reduced to hydroquinones (benzene-1,4-diols) during the aromatization process. Two important quinones are often used for the dehydrogenation, that is DDQ (2,3-dichloro-5,6-dicyano-1,4-benzoquinone) and chloranil (2,3,5,6-tetrachloro-1,4-benzoquinone). DDQ is much more reactive than chloranil (the relative rate of the dehydrogenation of 1,2-dihydronaphthalene at 100 °C is 1 for chloranil, and 5500 for DDQ). *o*-Benzoquinones should not be used as dehydrogenating agents, because the product of this oxidation is a dienophile, which would cause of the formation of benzodioxanes by the Diels-Alder addition [205]. *p*-Benzoquinones can be used with more advantage. Many different reactions can be performed using quinones, but saturated hydrocarbons should be inert to quinones. Some activation of a substrate, such as the presence of a double bond, is necessary for a reaction to occur. The presence of electron-donating groups results in an enhancement of the dehydrogenation process. The aromatization of hydrocarbons by quinines may involve the formation of intermediate hydrocarbon : quinine adducts which should decompose thermally into a dehydrogenated product and a hydroquinone [205, 206]. Different solvents can be used for dehydrogenation purposes, like toluene, chlorobenzene and dioxane [205, 207-217], although oxidation of hydrocarbons with DDQ in dioxane can give also ketones [218].

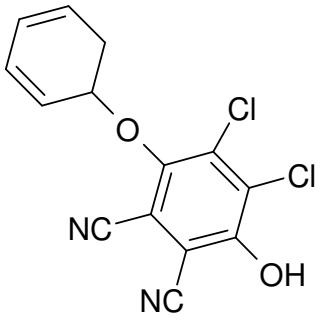

hydrocarbon : quinone adduct (cyclohexadiene and DDQ)

The mechanism possibly involves a transfer of hydride to the quinone oxygen, followed by transfer of a proton to the phenolate ion (Figure 38) [203].

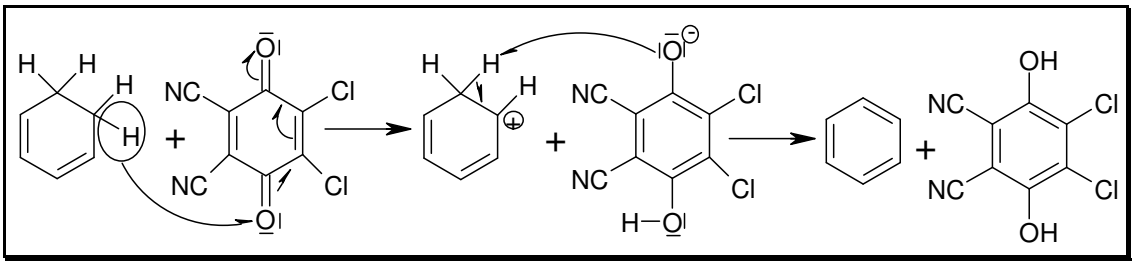

Figure 38 Aromatization with DDQ [203]

6.1.1.1 Experimental Procedure

Around 5 mg of the standard mixture (and in an analogous way the CD fractions) was refluxed for 5 h (or 30 min) in 1 mL of toluene with around three equivalents of DDQ (an excess). The products were purified on silica gel using cyclohexane, and afterwards a small amount of toluene and evaporated [219].

The real-world samples were then investigated using an HPLC system with two TCP columns (150 mm x 4 mm) with cyclohexane as eluent, at room temperature and a flow of 1 mL/min. Afterwards the solvent was evaporated and the remains dissolved in CD_2Cl_2 and ^1H NMR analysis was performed. Finally, after evaporation, the samples were methylated (see chapter 5.1.3) and ESI FT-ICR MS analysis was applied.

6.1.1.2 Results and Discussion (Standard Mixture)

The standard mixture was prepared in order to check the oxidation efficiency of DDQ. Different types of PASHs were used, like an aromatic system with a condensed and a non-condensed non-aromatic ring, a fully aromatic system and an aromatic system with an aliphatic chain. Thus the mixture was composed of:

- 2-cyclohexylmethanobenzothiophene
- tetrahydrobenzo[*b*]naphtho[1,2-*d*]thiophene
- phenanthro[2,1-*b*]thiophene
- 4-decyldibenzothiophene

GC-MS as well as GC-AED and GC-FID were applied to record the chromatograms of the mixture before and after oxidation. The sample was dissolved in cyclohexane and the chromatograms were recorded (Figure 39).

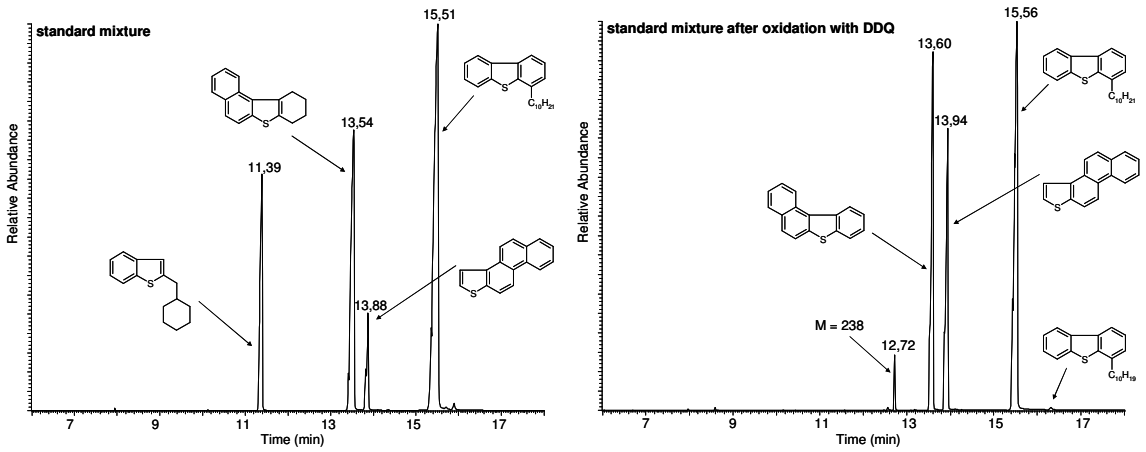

Figure 39 GC chromatograms (GC-MS) of the standard mixture before and after oxidation with DDQ

The standard mixture before oxidation:
2-cyclohexylmethanobenzothiophene
tetrahydrobenzo[*b*]naphtho[1,2-*d*]thiophene
phenanthro[2,1-*b*]thiophene
4-decyldibenzothiophene

The standard mixture after oxidation:
M = 238
benzo[*b*]naphtha[1,2-*d*]thiophene
phenanthro[2,1-*b*]thiophene
4-decyldibenzothiophene
traces of (4-dec-1-enyl)-dibenzothiophene

After the oxidation, the complete loss of 2-cyclohexylmethanobenzothiophene is observed, and the appearance of a new compound with the mass of 238 amu (molecular ion, mass spectrum explained in the next chapter) is detected. Tetrahydrobenzo[*b*]naphtho[1,2-*d*]thiophene is completely oxidized to benzo[*b*]naphtho[1,2-*d*]thiophene. Phenanthro[2,1-*b*]thiophene is not affected by DDQ. The peak for 4-decyldibenzothiophene loses its intensity after the process of oxidation in some not fully understood way. The formation of an adduct with DDQ could be an explanation, because it would not be possible to detect it using described above experimental procedure. An adduct would not elute from silica and

the GC column. Traces of (4-decyl-1-enyl)-dibenzothiophene with the molecular ion at 322 m/z, formed from 4-decyldibenzothiophene, are found.

The results are supported by the analysis of the received mass spectra of the standard mixture components from before and after dehydrogenation (see chapter 6.1.1.3).

The products of 2-cyclohexylmethanobenzothiophene dehydrogenation could not be extensively investigated in the standard mixture. Further experiments were applied afterwards. For this purpose the standard mixture composed of only two components was prepared:

• tetrahydrobenzo[*b*]naphtho[1,2-*d*]thiophene
• 2-cyclohexylmethanobenzothiophene

The mixture was oxidized in the same manner as the previous one. The reaction products were investigated using GC-MS and GC-AED. Already after 30 min of reflux is tetrahydrobenzo[*b*]naphtho[1,2-*d*]thiophene completely oxidized to the stable product benzo[*b*]naphtho[1,2-*d*]thiophene. 2-Cyclohexylmethanobenzothiophene gives two products, one of them showing the elimination of one hydrogen molecule, and a less intensive peak with the loss of two hydrogen molecules. After 1 h of reflux, 2-cyclohexylmethanobenzothiophene is completely lost from the standard mixture, and a new product, after loss of three hydrogen molecules, appears. The intensities for products of the 2-cyclohexylmethanobenzothiophene dehydrogenation diminish with time of reflux, and after 5 h only traces of the substances with one or three hydrogen molecules abstracted are present together with a new product with the mass of 238 amu. Thus the substrate gives a lot of compounds, with different numbers of H_2 molecules eliminated, which are decomposed and lost at the end from the reaction mixture (Figure 40).

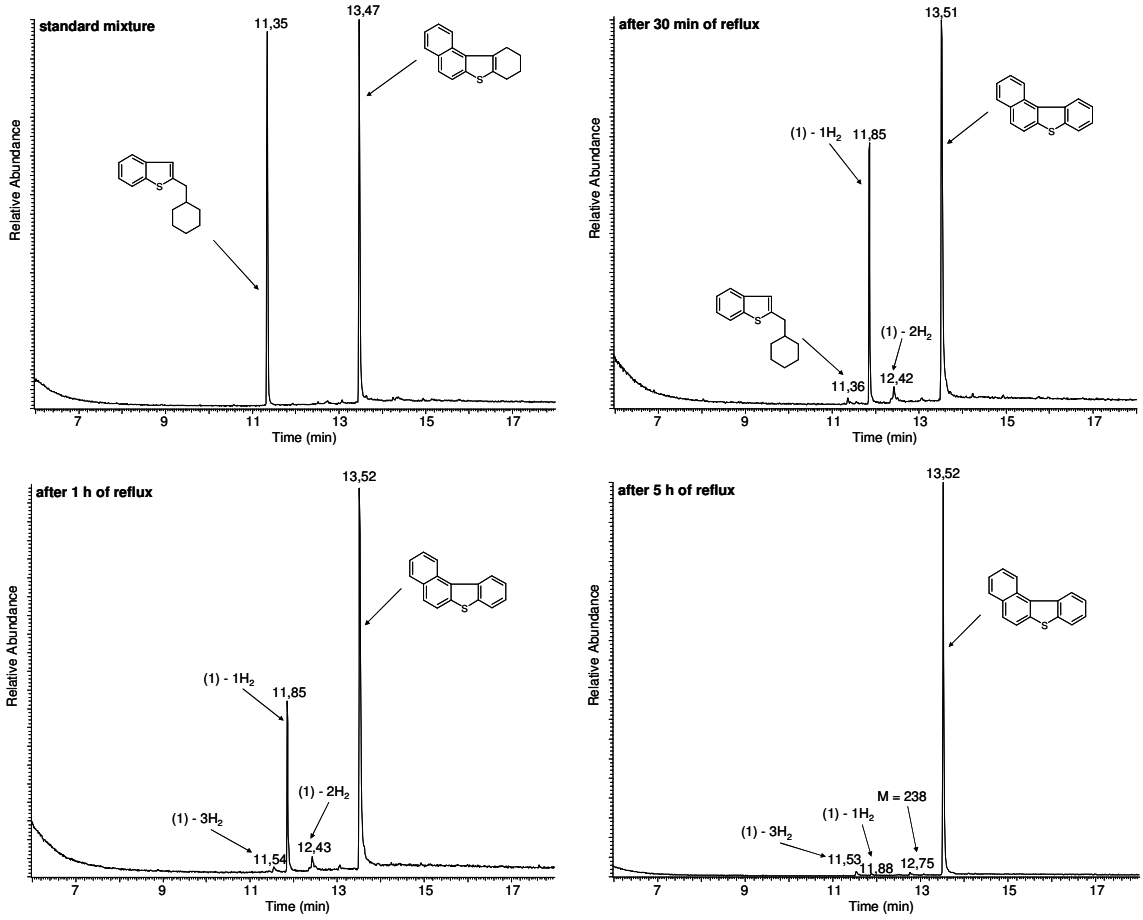

Figure 40 GC chromatograms (GC-MS) of the standard mixture oxidation with DDQ (standard mixture composed of 2-cyclohexylmethanobenzothiophene and tetrahydrobenzo[*b*]naphtho[1,2-*d*]thiophene)

(1) - 2-cyclohexylmethanobenzothiophene

The mass spectra for the products of elimination of one or two hydrogen molecules do not give clear answer about the structure of the compounds. Abstraction of one H_2 gives the base peak of the mass spectrum for the molecular ion at 228 m/z. Loss of two H_2 also gives the base peak for the molecular ion, at 226 m/z. In order to know the hydrogen molecule elimination order in 2-cyclohexylmethanobenzothiophene, the oxidation of the pure compound was applied to obtain the product with abstraction of one hydrogen molecule. For this purpose, a molar amount of DDQ was added to the reaction solution (2-cyclohexylmethanobenzothiophene) and reflux was carried out for 30 min.

^{1}H NMR was applied for structure analysis of the products. ^{1}H NMR results then show that the product of the one H_2 loss is 2-cyclohexylidenemethylbenzothiophene:
^{1}H NMR (600 MHz, CD_2Cl_2) δ = 7.2 - 7.8 ppm (m, 5 H; *Ar*), 6.3 ppm (s, 1 H, *SCCH*), 1.0 - 1.8 ppm (m, 10 H, $(CH_2)_5$)

The elimination of H_2 in the other possible position with creation of 2-cyclohex-1-enylmethyl-benzo[*b*]thiophene would give in theory the ^{1}H NMR spectrum without 6.3 ppm (s, 1 H, *SCCH*), but with other signals instead, that is:
^{1}H NMR (600 MHz, CD_2Cl_2) δ = 7.3 - 7.8 ppm (m, 4 H; *Ar*), 6.95 ppm (s, 1 H; SC*CH*), 5.4 ppm (t, 1 H; C*CH*), 3.22 ppm (s, 2 H, $SCCH_2$), 1.5 - 1.8 ppm (m, 8 H, $(CH_2)_4$)

The second H_2 molecule is then eliminated in the ring and 2-cyclohex-2-en-ylidenemethylbenzothiophene is created. The loss of third H_2 causes the creation of the rearranged 2-benzylbenzothiophene, proven by the mass spectrum analysis and by comparison with the synthesized standard. If oxygen is available, further oxidation is observed with formation of benzo[*b*]thiophen-2-yl-phenyl-methanone.

Table 10. Structures of 2-cyclohexylmethanobenzothiophene oxidation products with DDQ

Structure	Name
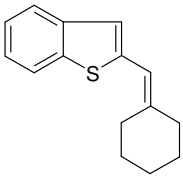	2-cyclohexylidenemethylbenzothiophene
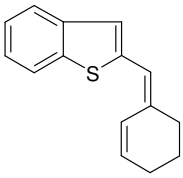	2-cyclohex-2-en-ylidenemethylbenzothiophene
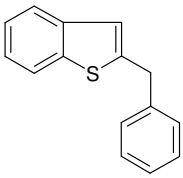	2-benzylbenzothiophene
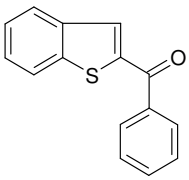	benzo[*b*]thiophen-2-yl-phenyl-methanone

The scheme of 2-cyclohexylmethanobenzothiophene oxidation with DDQ in relation to the reflux time is presented in Figure 41. The products with more H_2 molecules abstraction increase with the time of reflux but are then lost altogether in an unknown reaction. No product peaks are observed by GC.

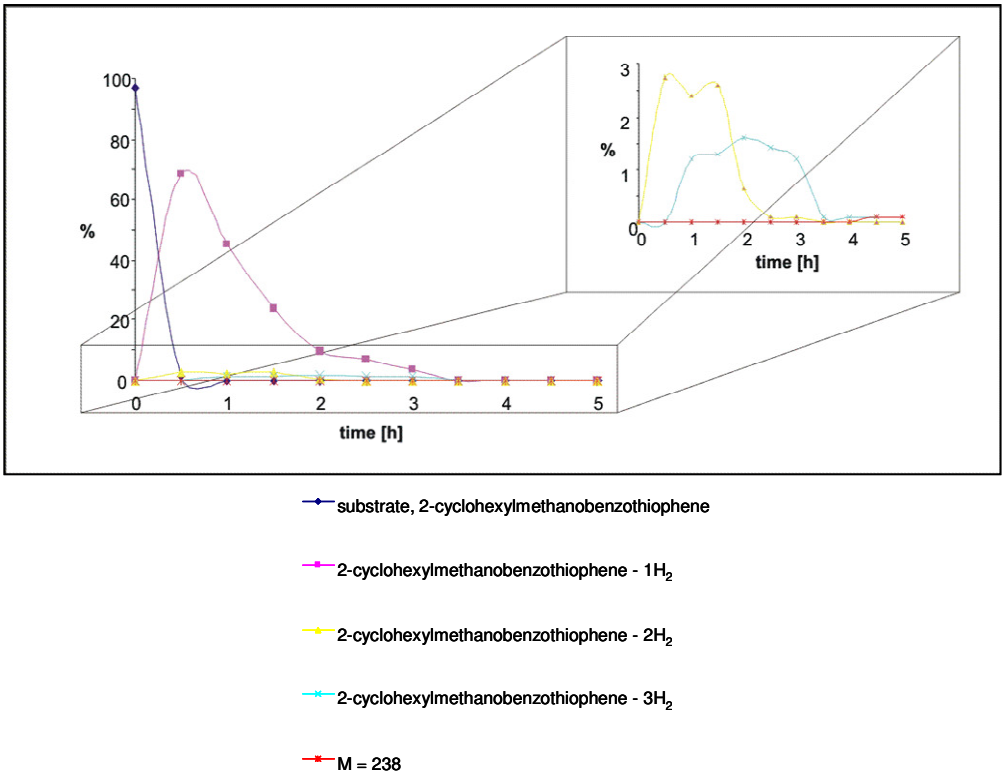

Figure 41 Scheme of 2-cyclohexylmethanobenzothiophene oxidation with DDQ

A similar substrate to 2-cyclohexylmethanobenzothiophene, only with one more methylene group, was synthesized as model compound for the dehydrogenation with DDQ in order to check the difference in oxidation products depending on the length of alkyl chain binding an aromatic system and a saturated ring. The reaction products were investigated as described previously using GC-MS and GC-AED as the reaction was running. Already after 30 min of reflux, the products of elimination of one, two and four H_2 are created. The substrate is still present in the standard mixture though. The mixture content is not affected strongly afterwards. The time of reflux affects only the relative amounts of the products. After 5 h of reflux, 2-cyclohexylethanobenzothiophene with loss of four hydrogen molecules is almost the only one product, with little residual amount of the substrate and the substances with abstraction of one and two H_2 (Figure 42).

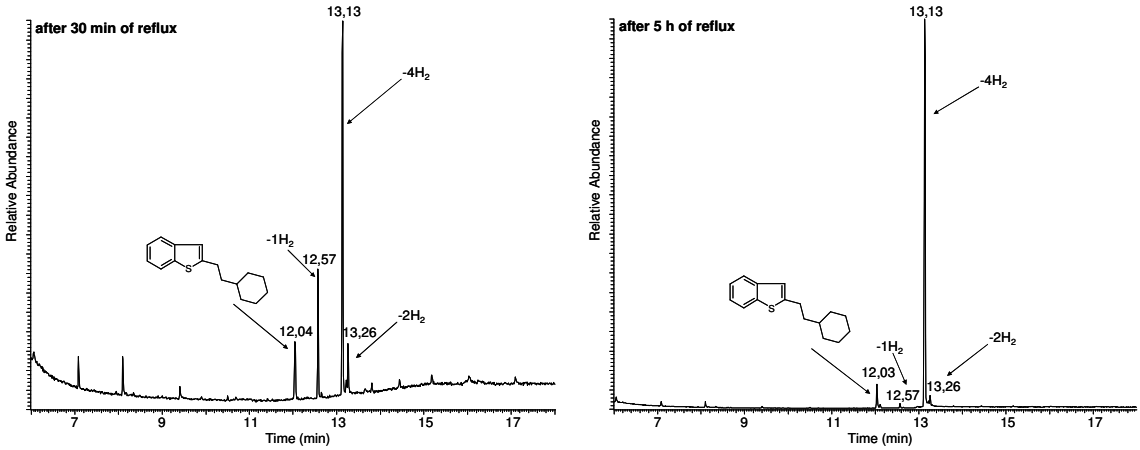

Figure 42 GC chromatograms (GC-MS) of 2-cyclohexylethanobenzothiophene oxidation with DDQ

Elimination of H_2 molecules proceeds analogously to that of 2-cyclohexylmethanobenzothiophene. 2-(2-Cyclohexyl)-vinylbenzo[*b*]thiophene and 2-(2-cyclohex-1-enyl)-vinylbenzo[*b*]thiophene are created by loss of one or two H_2 (with the molecular ions of 242 amu and 240 amu, respectively; the fragmentation pattern in mass spectra is not clear, but analogous to that of 2-cyclohexylmethanobenzothiophene). The stable, main product 2-styrylbenzothiophene is formed by loss of four hydrogen molecules (E or Z).

Table 11. Structures of 2-cyclohexylethanobenzothiophene oxidation products with DDQ

Structure	Name
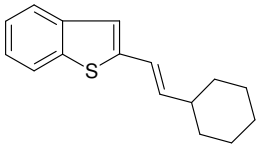	2-(2-cyclohexyl)-vinylbenzo[*b*]thiophene
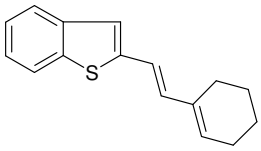	2-(2-cyclohex-1-enyl)-vinylbenzo[*b*]thiophene
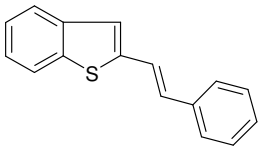	2-styrylbenzothiophene

The mixture of tetrahydrobenzo[*b*]naphtho[1,2-*d*]thiophene and 2-cyclohexylmethanobenzothiophene was also oxidized under milder conditions, at room temperature (for 12 h) and at 70 °C (5 h), to check if it is possible to obtain a product of only the dehydrogenation of condensed naphtheno rings. The samples were taken from the reaction mixture every 20 min and GC-MS was applied to investigate the products. The results show that even at room temperature both types of connection of a non-aromatic ring to an aromatic system are partially oxidized. Tetrahydrobenzo[*b*]naphtho[1,2-*d*]thiophene is partially oxidized to benzo[*b*]naphtho[1,2-*d*]thiophene, and 2-cyclohexylmethanobenzothiophene partially eliminates one hydrogen molecule. The reaction at 70 °C yields, after 5 h, complete oxidation of tetrahydrobenzo[*b*]naphtho[1,2-*d*]thiophene and the main product with loss of one H_2 for 2-cyclohexylmethanobenzothiophene. Traces of the substrate - 2-cyclohexylmethanobenzothiophene and the product with elimination of two H_2 are also detected.

As can be noticed by investigating the standard mixture oxidation (Figure 40), the 30 min reflux with DDQ is sufficient for complete transformation of

tetrahydrobenzo[*b*]naphtho[1,2-*d*]thiophene into benzo[*b*]naphtho[1,2-*d*]thiophene. Phenanthro[2,1-*b*]thiophene is stable even within 5 h of reflux and 4-decyldibenzothiophene eliminates one H_2 (only traces) after 1.5 h of reflux, so this product would not be present in the mixture after 30 min of reflux (the peak height change after aromatization process for 4-decyldibenzothiophene is not fully understood). After 30 min 2-cyclohexylmethanobenzothiophene forms the product with elimination of one H_2, while traces of the substrate remain and the compound with loss of two H_2 is also present. 2-Cyclohexylethanobenzothiophene generally forms the product with elimination of four H_2 (Figure 42), but the peaks from the substrate and the components with loss of one H_2 and two H_2 are also present in smaller quantities. This shows that 30 min of the standard mixture reflux with DDQ generally gives the same oxidation products as after 5 h at 70 °C. Further, the oxidation of the real-world samples under reflux for 30 min was performed as well, as the shorter reflux time should give the opportunity for a less intensive oxidation, and thus possibly a better insight into the real-world sample dehydrogenation results.

6.1.1.3 Mass Spectra (Standard Mixture)

Figure 43 presents the mass spectrum for 2-cyclohexylmethanobenzothiophene with the molecular ion ($M^{+\cdot}$) of 230 amu. The fragment ion at 148 m/z is derived from a McLafferty rearrangement (Figure 44). The fragment ion with an m/z value of 147 amu is created by the cleavage of $C_6H_{11}^{\cdot}$ (Figure 45).

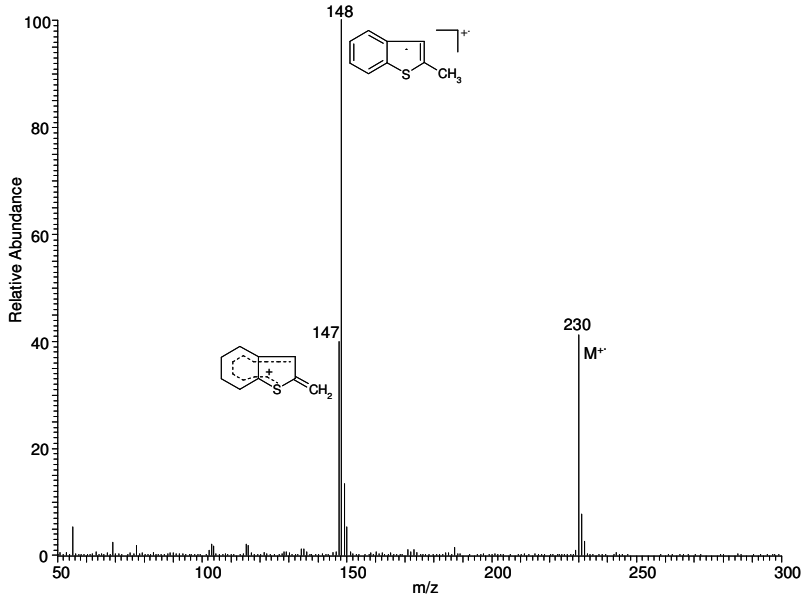

Figure 43 EI mass spectrum of 2-cyclohexylmethanobenzothiophene

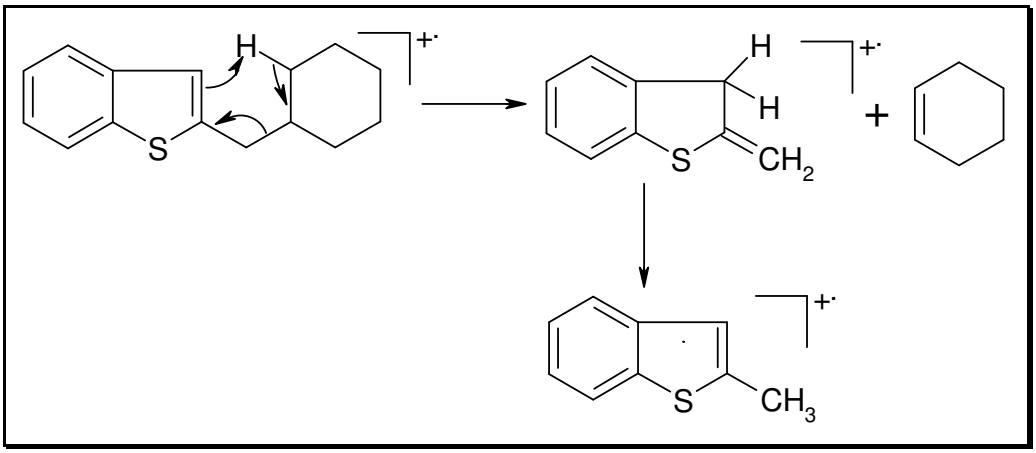

Figure 44 McLafferty rearrangement of 2-cyclohexylmethanobenzothiophene

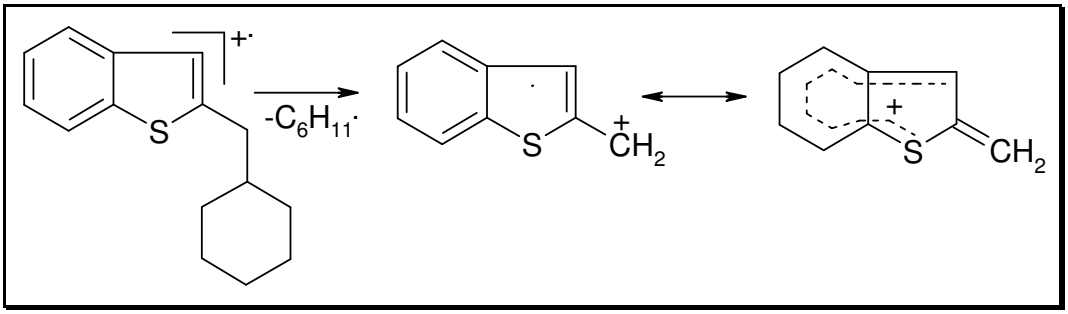

Figure 45 $C_6H_{11}^{\cdot}$ cleavage from 2-cyclohexylmethanobenzothiophene

The mass spectrum for tetrahydrobenzo[*b*]naphtho[1,2-*d*]thiophene is presented in Figure 46. The molecular ion is observed at 238 m/z. The peak at 210 m/z comes from the fragment ion created by the Retro-Diels-Alder reaction (two possible mechanisms, Figure 47).

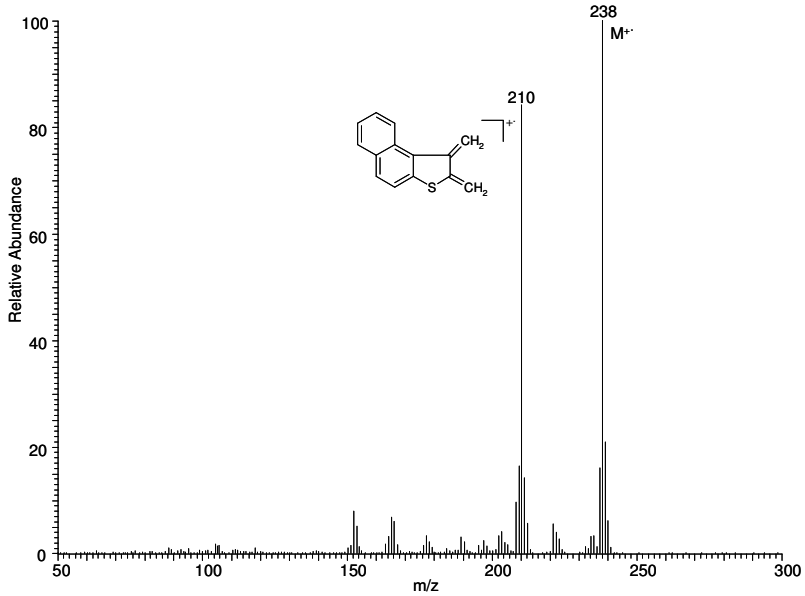

Figure 46 EI mass spectrum of tetrahydrobenzo[*b*]naphtho[1,2-*d*]thiophene

Mechanism I

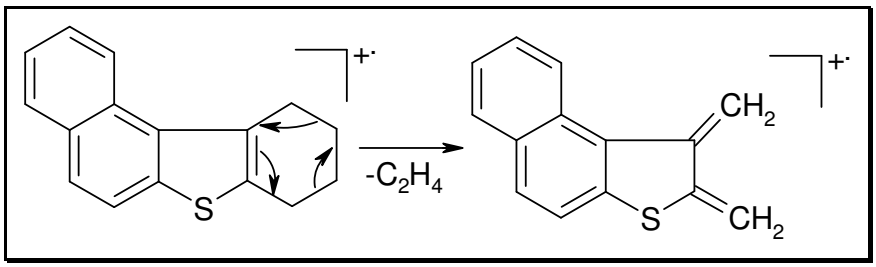

Mechanism II

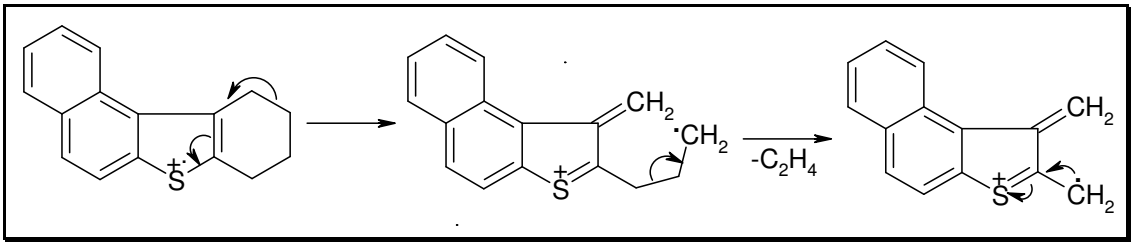

Figure 47 Retro-Diels-Alder reaction for tetrahydrobenzo[*b*]naphtho[1,2-*d*]thiophene

The product of tetrahydrobenzo[*b*]naphtho[1,2-*d*]thiophene oxidation, benzo[*b*]naphtho[1,2-*d*]thiophene, gives a simple mass spectrum with the intensive peak at 234 m/z for the molecular ion (Figure 48).

Also the mass spectrum for phenanthro[2,1-*b*]thiophene contains only one intensive peak for the molecular ion at 234 m/z (Figure 49).

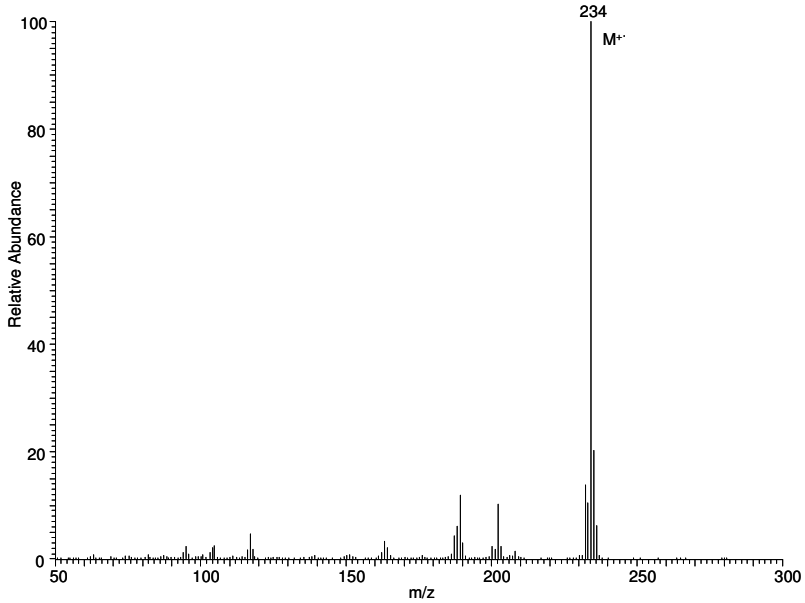

Figure 48 EI mass spectrum of benzo[*b*]naphtho[1,2-*d*]thiophene

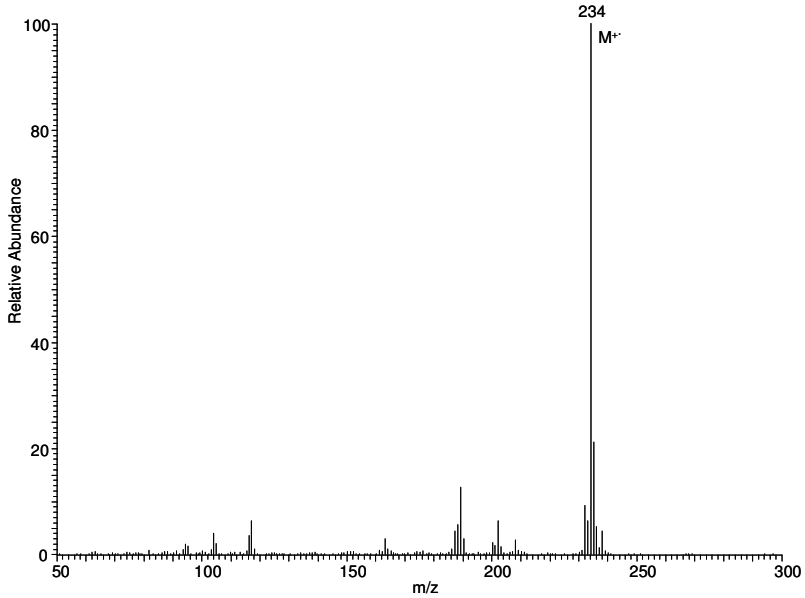

Figure 49 EI mass spectrum of phenanthro[2,1-*b*]thiophene

Figure 50 presents the mass spectrum of 4-decyldibenzothiophene. The signal at 324 m/z comes from the molecular ion. The fragment ion at 198 m/z is derived from a McLafferty rearrangement (Figure 51). The fragment ion with an m/z value of 197 is created by the cleavage of $C_9H_{19}^{\cdot}$ (Figure 52).

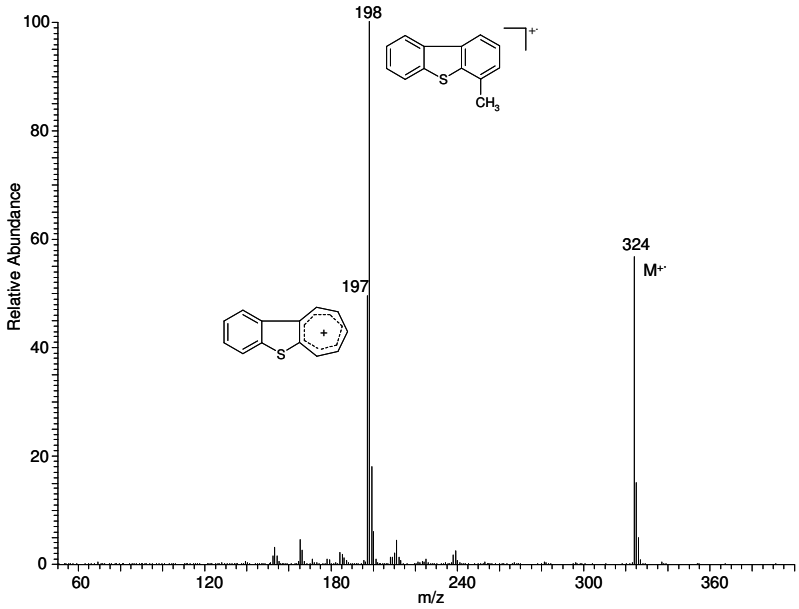

Figure 50 EI mass spectrum of 4-decyldibenzothiophene

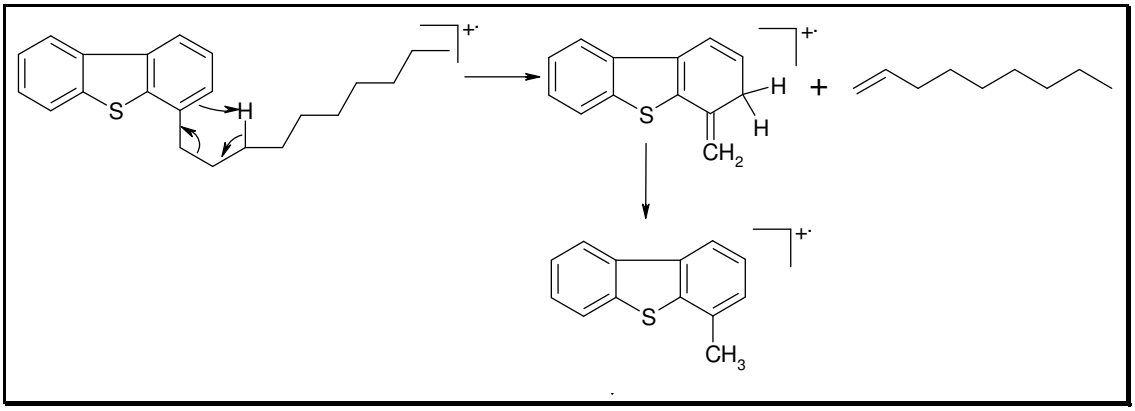

Figure 51 McLafferty rearrangement of 4-decyldibenzothiophene

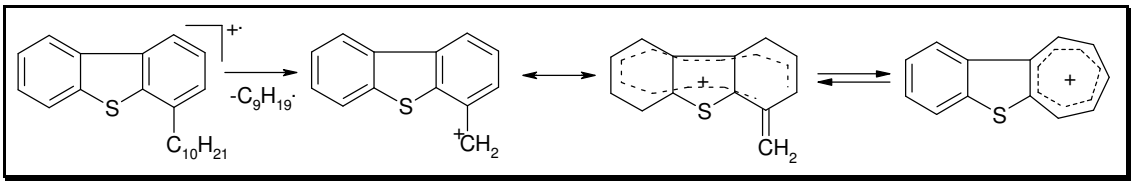

Figure 52 $C_9H_{19}^{\cdot}$ cleavage from 4-decyldibenzothiophene

The mass spectrum of 2-benzylbenzothiophene is presented in Figure 53. The molecular ion ($M^{+\cdot}$) is recorded at 224 m/z. The fragment ion at 223 m/z is derived from the cleavage of $H^{\cdot}$ (Figure 54). The signal at 147 m/z is created by the cleavage of $C_6H_5^{\cdot}$ in an analogous way as for 2-cyclohexylmethanobenzothiophene.

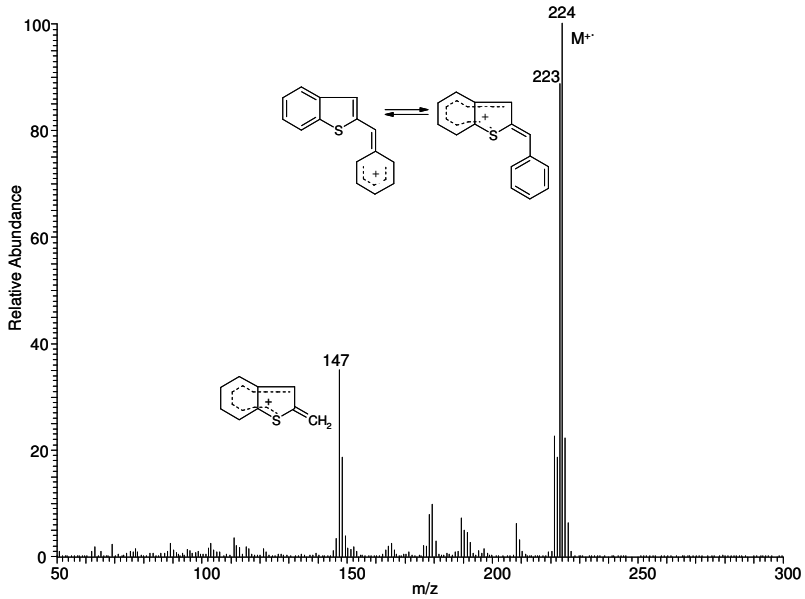

Figure 53 EI mass spectrum of 2-benzylbenzothiophene

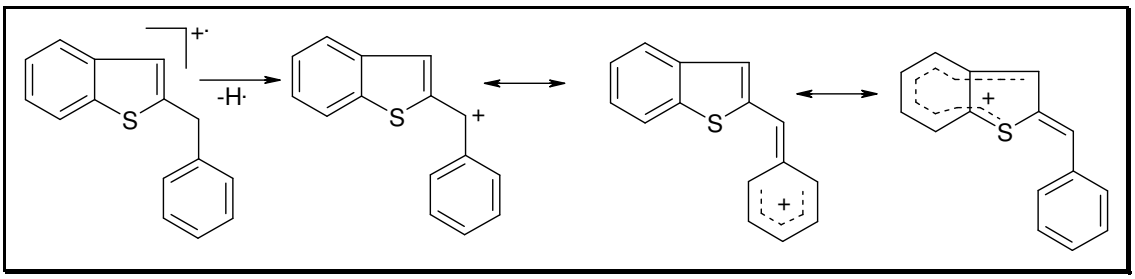

Figure 54 $H^{\cdot}$ cleavage from 2-benzylbenzothiophene

Further oxidation of 2-benzylbenzothiophene leads to the formation of the product with the mass of 238 amu for $M^{+\cdot}$ (mass spectrum, Figure 55), and the base peak at 161 m/z (for the fragment ion, after α-cleavage). A lower intensity for the second fragment ion from the α-cleavage is also visible in the mass spectrum at 105 m/z (Figure 56). That suggests the formation of benzo[*b*]thiophen-2-yl-phenyl-methanone.

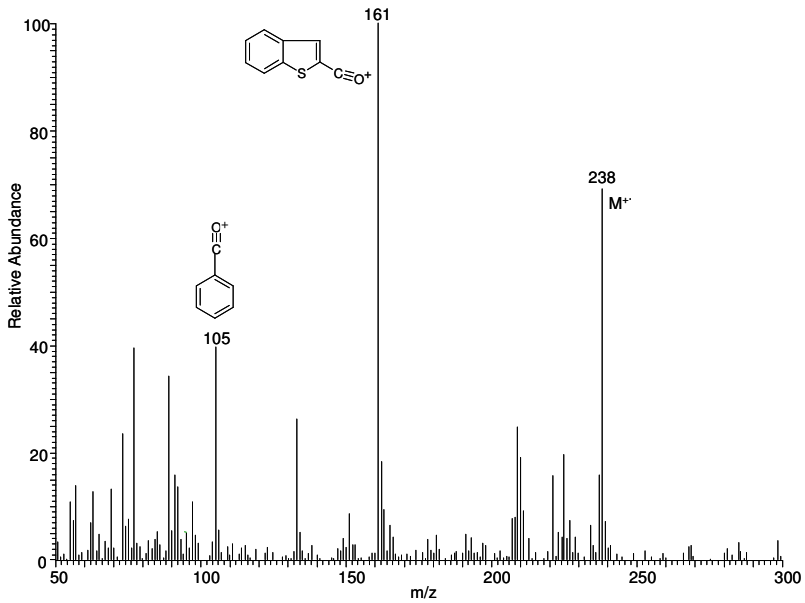

Figure 55 EI mass spectrum of benzo[*b*]thiophen-2-yl-phenyl-methanone

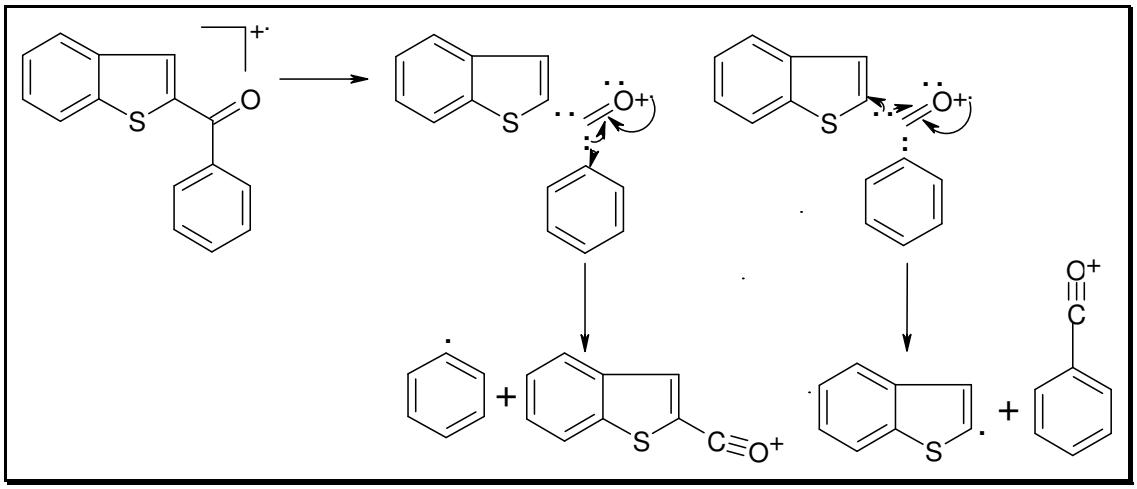

Figure 56 α-Cleavage for benzo[*b*]thiophen-2-yl-phenyl-methanone

The mass spectrum of 2-cyclohexylethanobenzothiophene is presented in Figure 57. The signal at 244 m/z comes from the molecular ion. The signals at 147 amu and 148 amu come from the fragment ions created in the analogous way as for 2-cyclohexylmethanobenzothiophene.

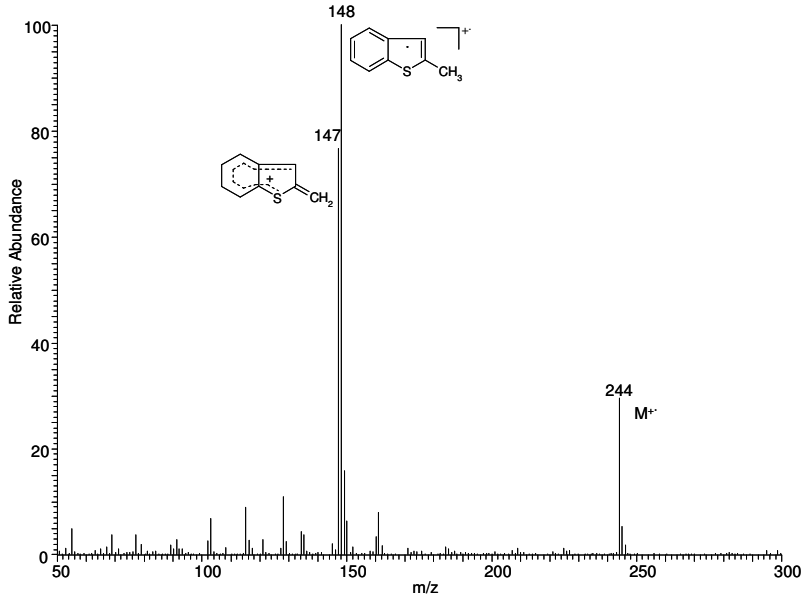

Figure 57 EI mass spectrum of 2-cyclohexylethanobenzothiophene

In the mass spectrum of 2-styrylbenzothiophene (Figure 58), the signal at 236 m/z comes from the molecular ion. The other intensive signals at 235 amu and 234 amu are created by loss of a hydrogen with formation of a possible condensed aromatic system. The exact mechanism is not known.

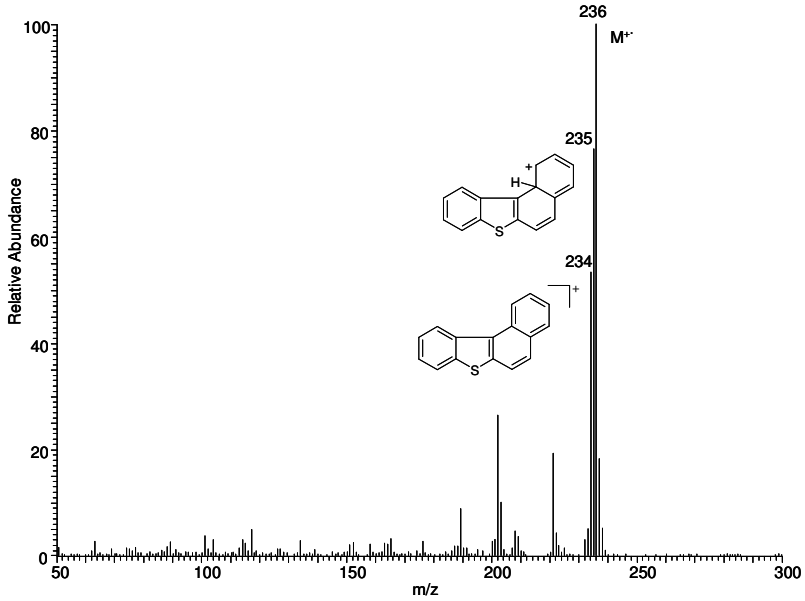

Figure 58 EI mass spectrum of 2-styrylbenzothiophene

6.1.1.4 Results and Discussion (Real-World Sample)

Next the real-world samples (CD-1, CD-2 and CD-3) were oxidized, using DDQ as dehydrogenation agent, for 5 h at reflux. The oxidation was investigated despite the possible decomposition of the non-aromatic rings substituted to an aromatic system, as in the standard mixture. First, the HPLC chromatograms were recorded for the samples before and after the oxidation (Figures 59, 60, 61). In case of a successful oxidation, the signals should shift towards longer retention times, because the oxidized samples should contain more aromatic rings. If aliphatic compounds containing sulfur were created by some unexplained transformations, they would not be visible in the HPLC chromatograms, as UV detection was applied (at 254 nm), where the aliphatic compounds do not show visible absorption.

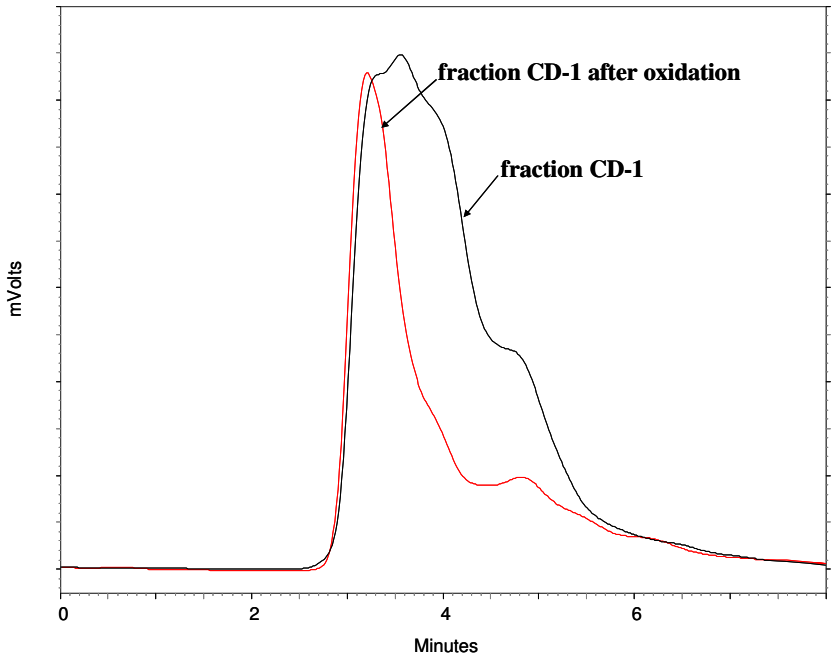

Figure 59 HPLC chromatograms of fraction CD-1 before and after oxidation with DDQ, 5 h reflux (2 x TCP columns 150 mm × 4 mm, mobile phase - cyclohexane, a flow rate of 1 mL/min, room temperature)

The chromatogram for CD-1 after oxidation (Figure 59) shows the partial loss of compounds in the fraction. There is no signal shift to higher retention times, as would be expected after successful oxidation. This kind of change can suggest only the decomposition of some part of the VGO mixture in fraction CD-1.

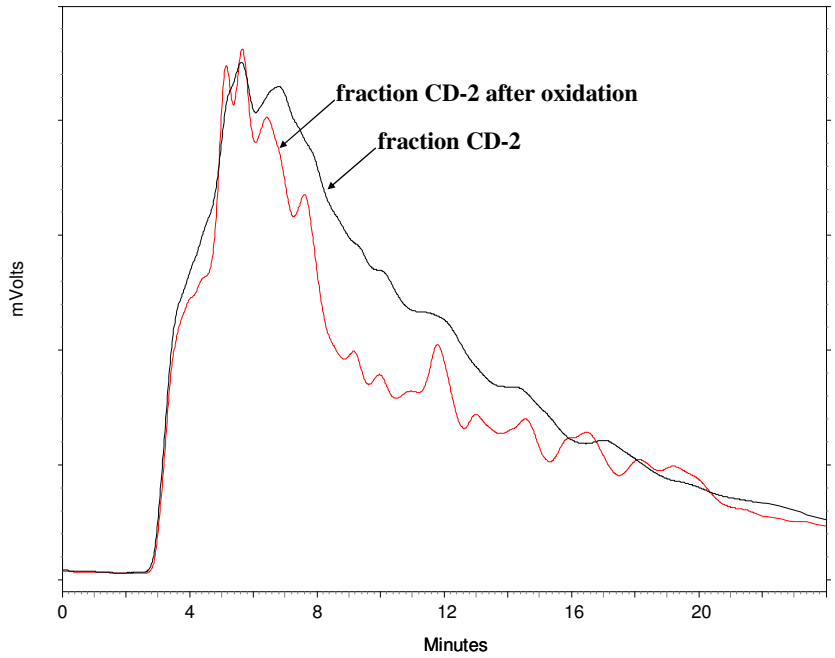

Figure 60 HPLC chromatograms of fraction CD-2 before and after oxidation with DDQ, 5 h reflux (2 x TCP columns 150 mm × 4 mm, mobile phase - cyclohexane, a flow rate of 1 mL/min, room temperature)

Fraction CD-2 after dehydrogenation (Figure 60) has more intensive signals at higher retention times. There are no visible changes for fraction CD-3 after the dehydrogenation (Figure 61), so probably no oxidation takes place. The shifts of retention times, visible for fraction CD-3 after oxidation, can be caused by ambient temperature fluctuations for example.

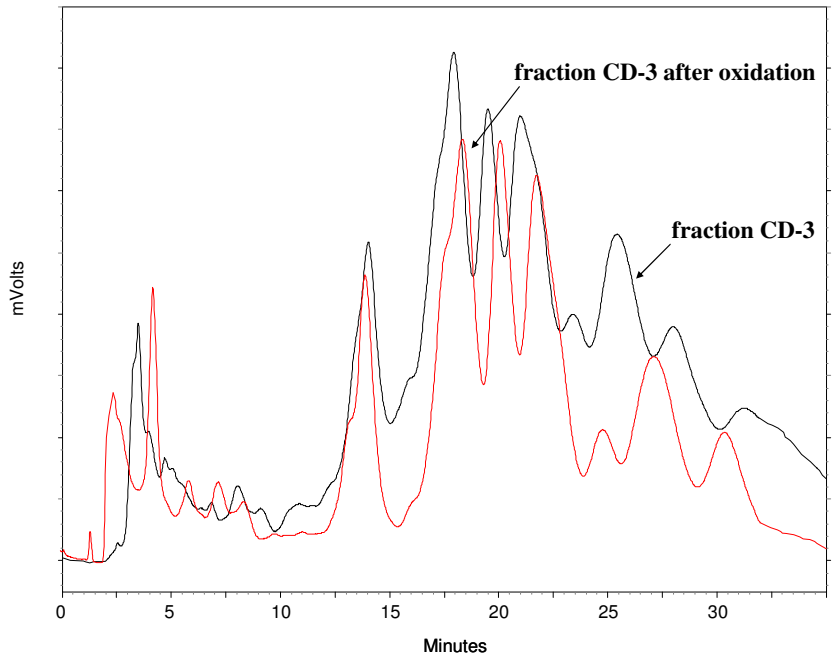

Figure 61 HPLC chromatograms of fraction CD-3 before and after oxidation with DDQ, 5 h reflux (2 x TCP columns 150 mm × 4 mm, mobile phase - cyclohexane, a flow rate of 1 mL/min, room temperature)

The fluorescence spectra were not recorded for the CD fractions before and after oxidation, because the differences between the maxima of excitation and emission for every CD fraction are negligible (see chapter 5.2.2). This method would not give us any remarkable information about the oxidation process.

The CD fractions before and after oxidation were analyzed by ^{1}H NMR in order to compare the ratio of aromatic to aliphatic hydrogens. In case of successful oxidation, an increase of the ratio should be noticed. However, an exact measurement of the degree of oxidation is difficult because of many possible alkyl chain substitution variations on the aromatic systems. As presented in Table 12, the ratio of aromatic to aliphatic hydrocarbons increases after dehydrogenation with DDQ, after a reaction time of 5 h, which may suggest that the observed decomposition of certain compounds does not exclude partial oxidation as well.

Table 12 ^{1}H NMR data for oxidation with DDQ, 5 h

^{1}H aromatic to aliphatic ratio		
Fraction	**before oxidation**	**oxidation with DDQ, 5 h**
CD-1	1:6.2	1:4.7
CD-2	1:3.4	1:2.3
CD-3	1:2.9	1:1.6

The last measurement was preceded by methylation of CD fractions. Afterwards FT-ICR MS analysis was performed. Kendrick plots were prepared for better visualization of the oxidation results (Figures 62, 63, 64). As mentioned in chapter 5.2.2., the component with DBE of 6 and the mass of 358 amu was chosen for fraction CD-1 as the reference components. All changes are compared to the main DBE series of 6 in fraction CD-1. The standard compounds with DBE of 9 and the mass of 310 amu, and DBE of 12 and the mass of 276 amu, were chosen for fractions CD-2 and CD-3, respectively. All the changes are compared to the main DBE series in these fractions: DBE of 9 for fraction CD-2 and DBE of 12 for fraction CD-3.

Compared to the Kendrick plots of fractions CD-1, CD-2 and CD-3 before oxidation (Figures 32, 33, 34), every sample after the dehydrogenation contains a high amount of sulfur compounds with low DBE, such as thiophanes (DBE = 1), dihydrothiophanes (DBE = 2), thiophenes (DBE = 3), naphthenothiopenes (DBE = 4) and cyclopenteno- or cyclohexenothiophenes (DBE = 5). The origin of this kind of compounds is difficult to explain, as the reaction with DDQ should give compounds with a higher DBE than present in the original sample because of the dehydrogenation process. It is also interesting that a lot of signals with higher masses are recorded, much higher than before the oxidation. Decomposition and recombination of the molecules with a high amount of carbon atoms could be an explanation. Possible is also a problem with low intensities. As already observed before the oxidation process, the concentration of the samples is very low, and the oxidation process diminishes the amount of material for the further analysis. The

increased intensities of the signals from compounds with higher DBEs are observed in the sample except for fraction CD-3 (measured and compared with the fractions from before oxidation by the middle masses and higher mass values) after the oxidation, but no reliable calculation is possible, as many not explained processes could take place during reaction with DDQ within 5 h of reflux.

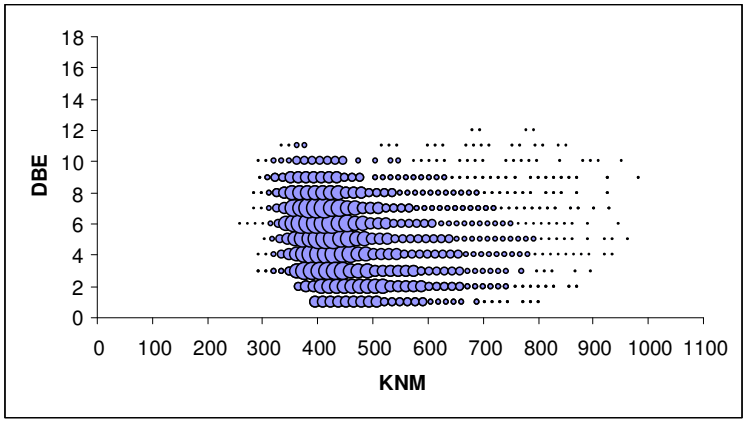

Figure 62 Kendrick plot for fraction CD-1 after oxidation with DDQ, 5 h reflux

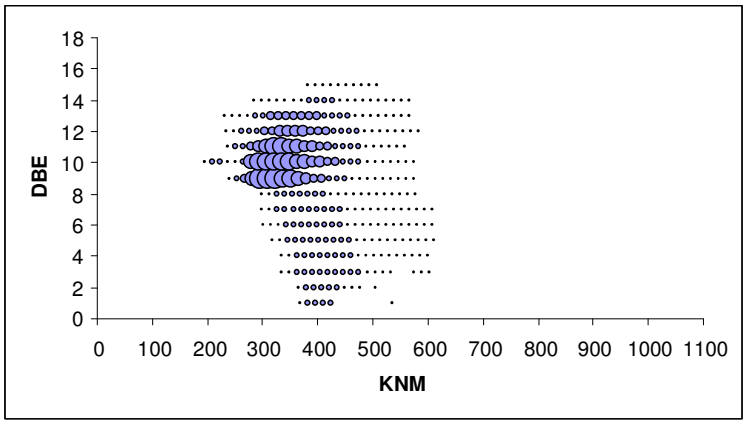

Figure 63 Kendrick plot for fraction CD-2 after oxidation with DDQ, 5 h reflux

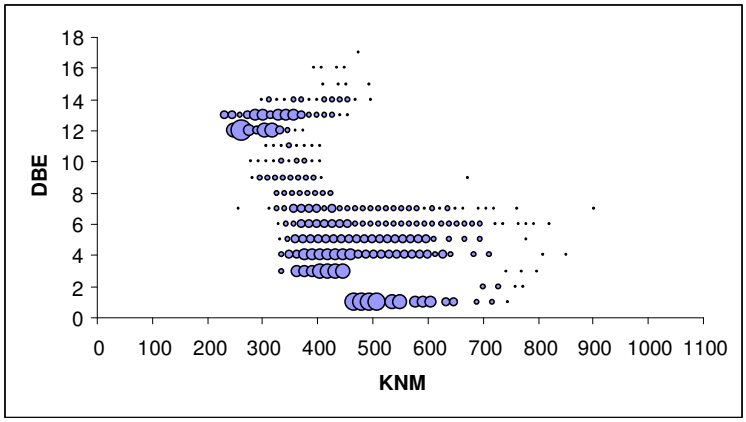

Figure 64 Kendrick plot for fraction CD-3 after oxidation with DDQ, 5 h reflux

In another experiment a shorter reflux time was applied to the real-world sample, as done earlier for the standard mixture. The HPLC chromatograms were recorded for the samples before and after oxidation with 30 min of reflux (Figures 65, 66, 67).

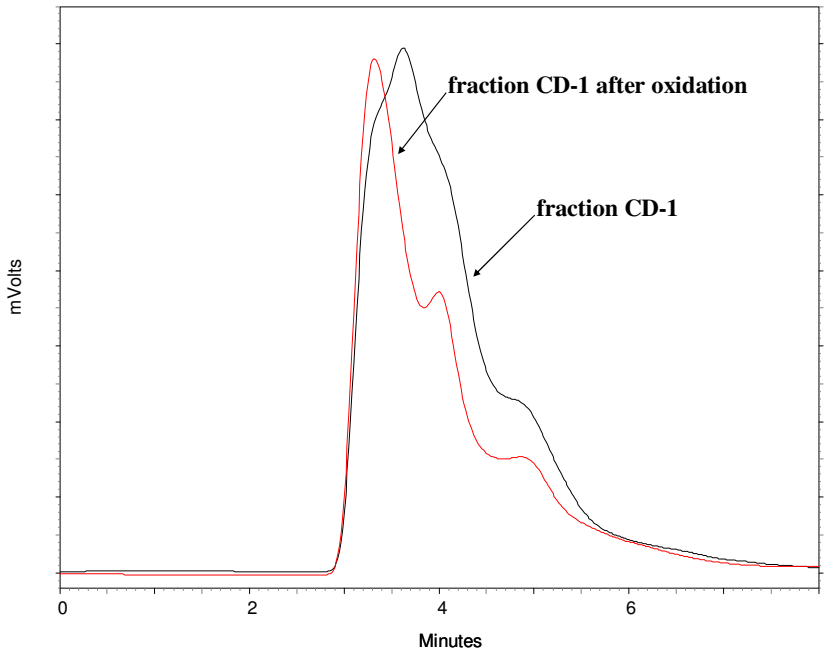

Figure 65 HPLC chromatograms of fraction CD-1 before and after oxidation with DDQ, 30 min reflux (2 x TCP columns 150 mm × 4 mm, mobile phase - cyclohexane, a flow rate of 1 mL/min, room temperature)

Fraction CD-1 after oxidation (Figure 65) shows more intense signal at higher retention time and there is not as harsh degradation observed as in the case of DDQ oxidation within 5 h.

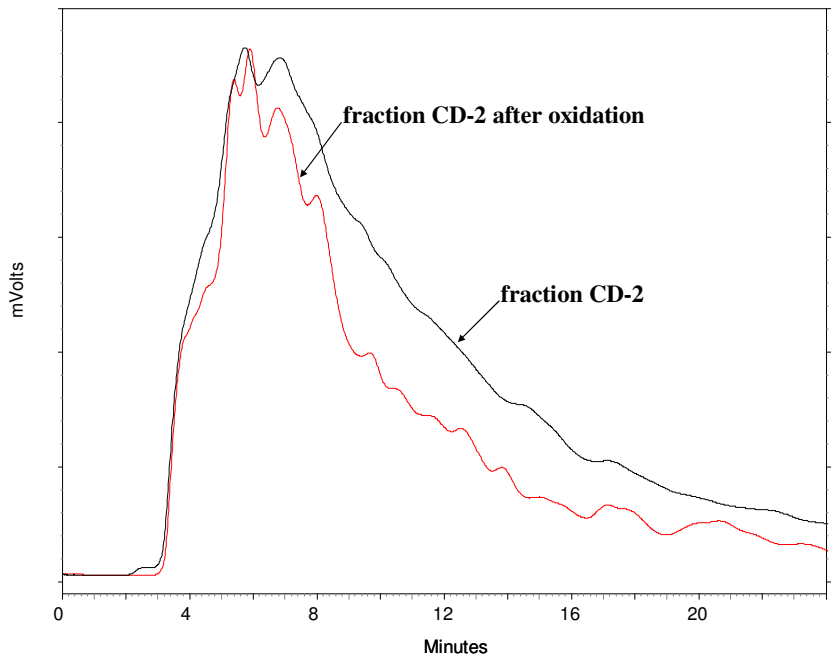

Figure 66 HPLC chromatograms of fraction CD-2 before and after oxidation with DDQ, 30 min reflux (2 x TCP columns 150 mm × 4 mm, mobile phase - cyclohexane, a flow rate of 1 mL/min, room temperature)

Fraction CD-2 after dehydrogenation (Figure 66) has more intensive signals at higher retention times, similarly to the oxidation for 5 h, which can imply partial oxidation. There is again no visible change for fraction CD-3 after the dehydrogenation (Figure 67), so no effective oxidation is expected.

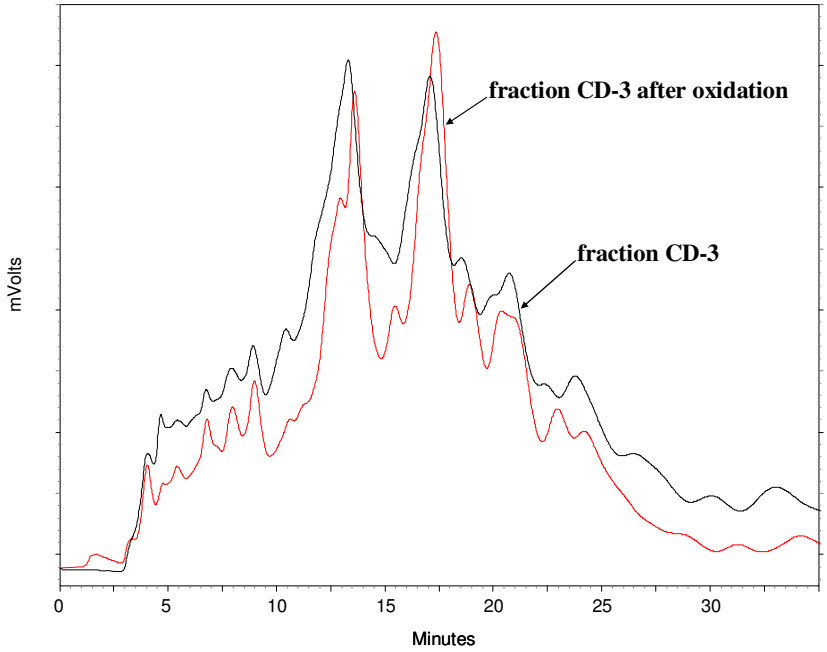

Figure 67 HPLC chromatograms of fraction CD-3 before and after oxidation with DDQ, 30 min reflux (2 x TCP columns 150 mm × 4 mm, mobile phase - cyclohexane, a flow rate of 1 mL/min, room temperature)

^{1}H NMR analysis was applied to the CD fractions before and after oxidation as previously. As presented in Table 13, the ratio of aromatic to aliphatic hydrocarbons increases after dehydrogenation with DDQ for 30 min, which can suggest a successful oxidation. The values are similar to DDQ oxidation for 5 h, but this time no degradation is expected, since the synthesized standard compounds survived this treatment.

Table 13 ^{1}H NMR data for oxidation with DDQ, 30 min

^{1}H aromatic to aliphatic ratio		
Fraction	**before oxidation**	**oxidation with DDQ, 30 min**
CD-1	1:6.2	1:4.3
CD-2	1:3.4	1:2.3
CD-3	1:2.9	1:1.8

The FT-ICR MS measurement was performed after methylation of CD fractions. The Kendrick plots were prepared (Figures 68, 71, 72). The plots look similar to the Kendrick plots of fractions CD-1, CD-2 before dehydrogenation (Figures 32, 33, 34). Only a few signals with lower DBE appear for fraction CD-3 after the oxidation (Figure 72, Figure 34 - before oxidation). The mass range for the CD fractions remains the same as before the oxidation (except for the low DBEs signals of fraction CD-3).

In the Kendrick plot for fraction CD-1 (Figure 68) an increase of the intensities for the signals with higher DBEs is observed (measured and compared with the signals from before oxidation at middle masses of 348 - 358 amu and higher mass series of 416 - 428 amu). The pseudograms were then prepared for better visualizations of the oxidation results.

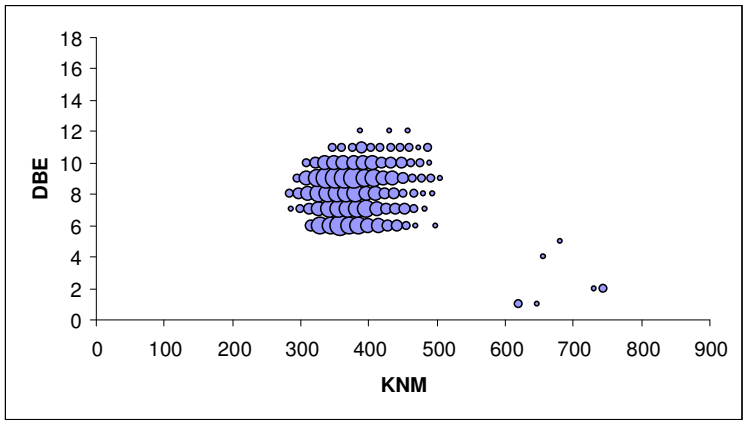

Figure 68 Kendrick plot for fraction CD-1 after oxidation with DDQ, 30 min reflux

The pseudograms for fraction CD-1 before and after dehydrogenation were prepared for the middle mass range (348 - 358 amu), for one series of the compounds, that is with DBE 6, DBE 7, DBE 8 etc. (Figures 69, 70). The changes in the middle mass range are analogous to the changes recorded for the higher mass range. Every signal with a higher DBE will have a mass 2 amu lower, that is one H_2 molecule (one double bond created). DBE for benzothiophenes equals 6. One additional non-aromatic ring makes DBE equal 7. As checked on the standard

mixture, a condensed naphtheno ring should be easily oxidized (two double bonds created in a fused non-aromatic ring), and this would increase the intensity of the signal DBE = 9 and decrease the signal at DBE = 7. Unfortunately compounds with DBE = 7 possessing non-condensed saturated ring can be also oxidized with DDQ (30 min) and give an increase of the signals with DBE of 8, like 2-cyclohexylmethanobenzothiophene, or DBE of 11, DBE of 8 and 9 in smaller quantities, like for 2-cyclohexylethanobenzothiophene. All these possible changes complicate the statistical evaluation of the possible structures in the mixture.

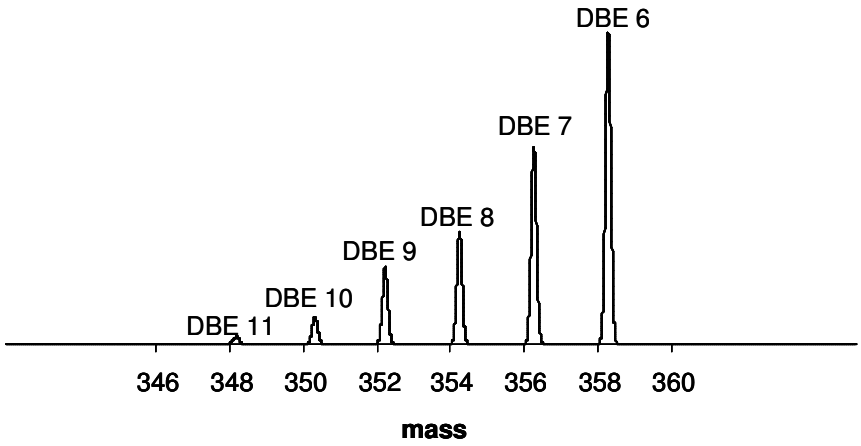

Figure 69 Pseudogram for fraction CD-1 before oxidation (middle mass range 348 - 358 amu)

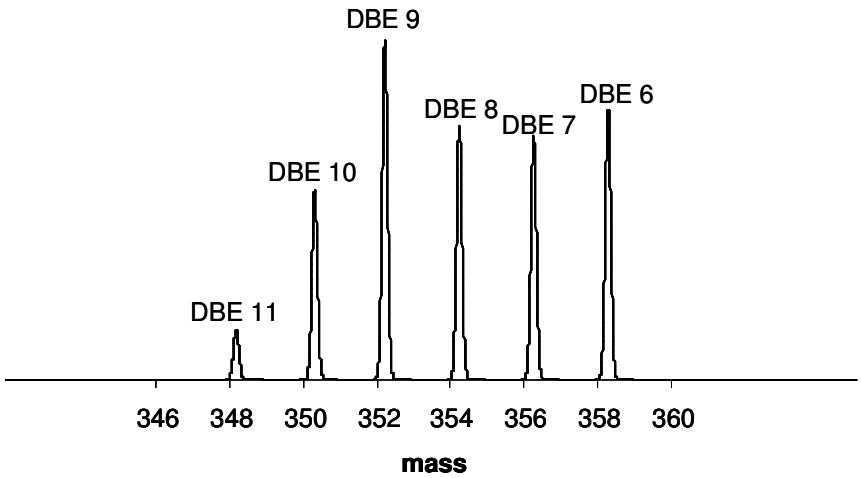

Figure 70 Pseudogram for fraction CD-1 after oxidation with DDQ, 30 min (middle mass range 348 - 358 amu)

The pseudogram for fraction CD-1 after oxidation (Figure 70), compared to the pseudogram for the fraction before oxidation (Figure 69) presents an increase of all the signals with DBE higher than 6, relative to this DBE. This cannot happen without partial loss of the benzothiophene homologous series. It is described already for the standard mixture oxidized with DDQ (Figure 39) that the peak for 4-decyldibenzothiophene loses the intensity in some not fully understood way. Thus in a real-world sample, dibenzothiophene homologous series would supposingly also partially lose the intensity. The same explanation can be applied for benzothiophene series in fraction CD-1. If the signal for DBE 6 remained stable, then by comparison of these two pseudograms, a decrease of DBE 7 would be recorded and an intensity increase of the signals at higher DBEs. The statistical calculations of the possible structures in the mixture in this case would be misleading. It is thus not possible to directly compare these two pseudograms.

The Kendrick plots for fractions CD-2 and CD-3 after oxidation with DDQ for 30 min are presented in Figures 71 and 72. Very low or no increase in the intensities for higher DBEs signals are recorded for these fractions with larger aromatic system when compared to the fractions from before the oxidation (Figures 33, 34). Some low intensity signals at lower and higher masses for fractions CD-2 and CD-3 are lost after the oxiadation with DDQ for 30 min reflux.

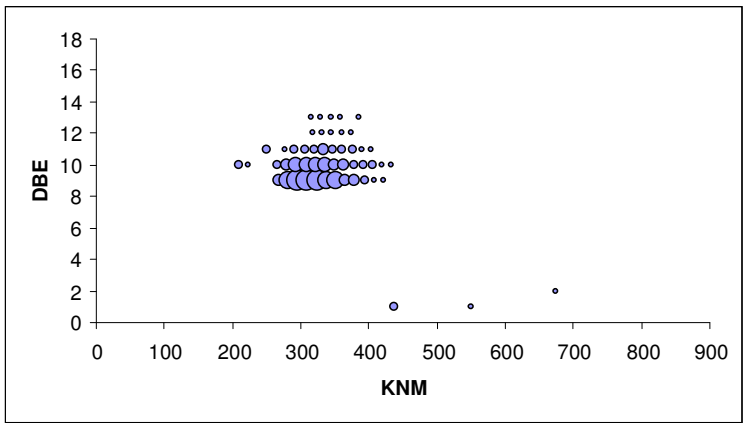

Figure 71 Kendrick plot for fraction CD-2 after oxidation with DDQ, 30 min reflux

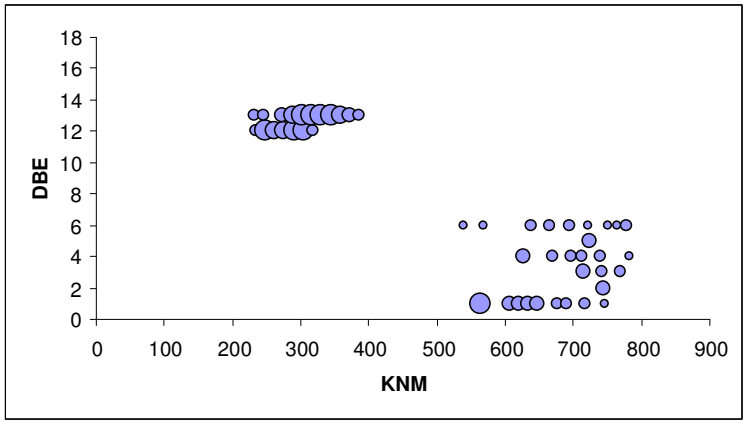

Figure 72 Kendrick plot for fraction CD-3 after oxidation with DDQ, 30 min reflux

6.1.1.5 Results and Discussion (Standard Mixture, Chloranil)

Oxidation with chloranil was also tried, as it is much less destructive than DDQ. Unfortunately, the standard mixture oxidation shows that this oxidant is not strong enough. Phenanthro[2,1-*b*]thiophene and 4-decyldibenzothiophene are not affected by chloranil as with the use of DDQ (also the ratio of peak areas for phenanthro[2,1-*b*]thiophene and 4-decyldibenzothiophene remain comparable before and after oxidation). 2-Cyclohexylmethanobenzothiophene gives only traces of the molecules with loss of one, two and three H_2 (while DDQ decomposed this substrate completely), and tetrahydrobenzo[*b*]naphtho[1,2-*d*]thiophene is oxidized to benzo[b]naphtho[1,2-d]thiophene only to a very small extent (Figure 73). This result excludes chloranil from further investigation.

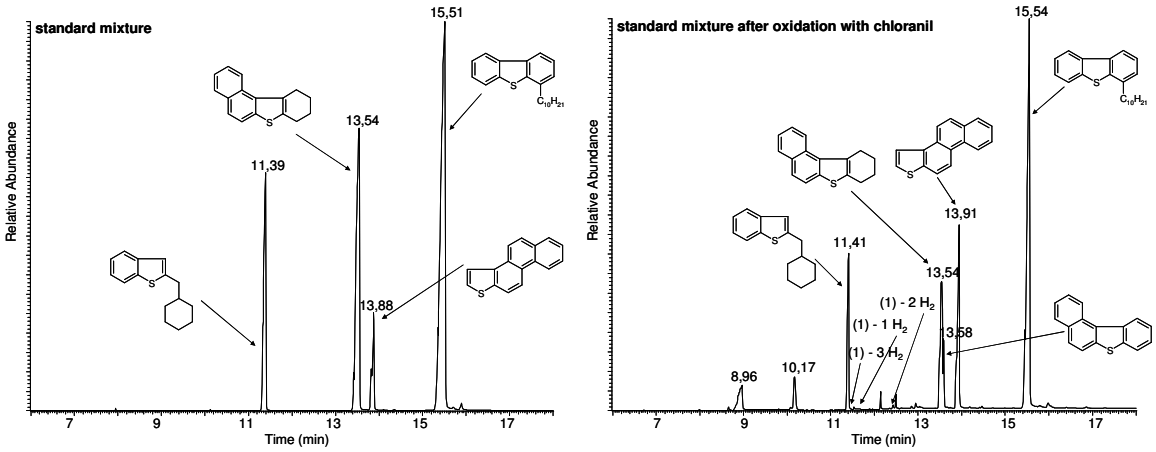

Figure 73 GC chromatograms (GC-MS) of the standard mixture before and after oxidation with chloranil (5 h reflux)

The standard mixture before oxidation:
2-cyclohexylmethanobenzothiophene
tetrahydrobenzo[*b*]naphtho[1,2-*d*]thiophene
phenanthro[2,1-*b*]thiophene
4-decyldibenzothiophene

The standard mixture after oxidation:
2-cyclohexylmethanobenzothiophene
traces of (1) - $1H_2$, (1) - $2H_2$ and (1) - $3H_2$
tetrahydrobenzo[*b*]naphtho[1,2-*d*]thiophene
benzo[b]naphtho[1,2-d]thiophene
phenanthro[2,1-*b*]thiophene
4-decyldibenzothiophene

(1) - 2-cyclohexylmethanobenzothiophene

Peaks with retention time of 8,96 and 10,17 min comes from chloranil and 2,3,5,6-tetrachloro-benzene-1,4-diol respectively.

6.1.1.6 Summary

As presented above, DDQ and chloranil, are not appropriate for the planned investigation. DDQ oxidizes a non-aromatic ring easily, but the oxidation performed is too intense. Chloranil appears to be too weak for the desired oxidation.

For this work it is important that only condensed naphtheno rings are oxidized, leaving a non-condensed ring nonaffected. This kind of distinguishing between two possible connections to an aromatic system would allow for the statistical calculation of the relative amounts of the compounds with a specific connection in the real sample mixture. As DDQ within 5 h of reflux causes extensive sample decomposition to unknown products and within 30 min of reflux possible partial decomposition is observed, as well as the oxidation of both types of connections of the non-aromatic rings, it is not possible to perform any statistical calculations. A gentler, but still effective enough reagent has to be found.

6.1.2 Palladium

In the case of hydrogenation catalysts, like Pd (but also Pt, Ni etc.), the reaction of dehydrogenation is the reverse reaction of the double-bond hydrogenation, and presumably the mechanism is reversed as well (Figure 74). Hydrogenation is an exothermic reaction, while the dehydrogenation is endothermic. The reaction is often carried out under milder conditions if a hydrogen acceptor, such as benzene, is present to remove hydrogen as it is formed [203]. Vigorous boiling helps to dislodge the hydrogen from the active surface of the catalyst. Pd/C was already used for effective dehydrogenation with the result that not only naphtheno rings condensed to aromatic molecule was aromatized, but also rings not directly condensed to an aromatic system. Aliphatic chains remained without changes [210, 214, 215, 220-227].

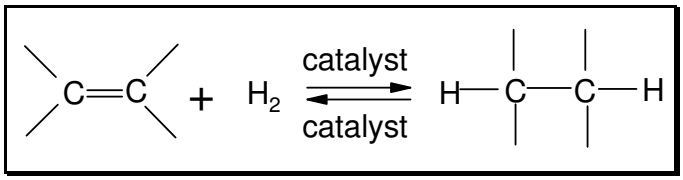

Figure 74 Elimination of hydrogen by a hydrogenation catalyst [203]

6.1.2.1 Experimental Section

Around 5 mg of the standard mixture (and in an analogous way the CD fractions) in decalin (2 mL) and an excess of Pd/C (4 mg, 10 %) was refluxed for 24 h [220]. Afterwards column chromatographic purification was applied using cyclohexane and the sample was evaporated.

The real-world samples were then investigated using a HPLC system with two TCP columns (150 mm x 4 mm), with cyclohexane as eluent at room temperature and a flow of 1 mL/min. Afterwards the solvent was evaporated and the remains dissolved in CD_2Cl_2 for ^1H NMR analysis. Finally, after evaporation, the samples were methylated (see chapter 5.1.3) and ESI FT-ICR MS analysis was applied.

6.1.2.2 Results and Discussion (Standard Mixture)

The standard mixture was prepared to investigate the next dehydrogenation possibility, with Pd as oxidation agent. The mixture was composed of different types of PASHs, as previously used for oxidation with DDQ:

- 2-cyclohexylmethanobenzothiophene
- 2-cyclohexylethanobenzothiophene,
- tetrahydrobenzo[*b*]naphtho[1,2-*d*]thiophene,
- phenanthro[2,1-*b*]thiophene and
- 4-decyldibenzothiophene

GC-MS as well as GC-AED and GC-FID were applied to record the chromatograms before and after oxidation of the standard mixture. Similarly to the oxidation with DDQ, the sample was dissolved in cyclohexane and the chromatograms were recorded. The results are presented in Figure 75. The results are supported by the analysis of the mass spectra of the standard mixture components from before and after dehydrogenation described in chapter 6.1.1.3.

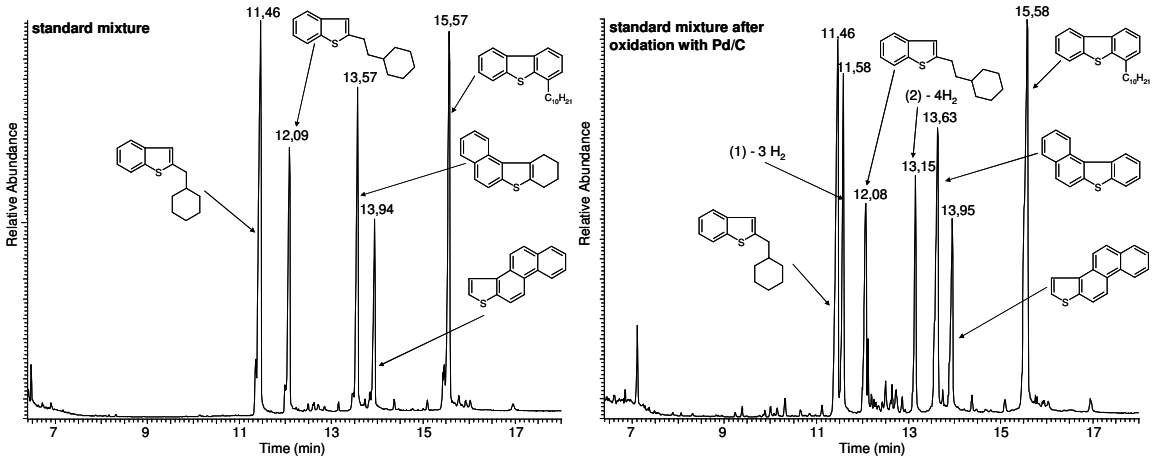

Figure 75 GC chromatograms (GC-MS) of the standard mixture before and after oxidation with Pd/C

The standard mixture before oxidation:
2-cyclohexylmethanobenzothiophene
2-cyclohexylethanobenzothiophene
tetrahydrobenzo[*b*]naphtho[1,2-*d*]thiophene
phenanthro[2,1-*b*]thiophene
4-decyldibenzothiophene

The standard mixture after oxidation:
2-cyclohexylmethanobenzothiophene
(1) - $3H_2$
2-cyclohexylethanobenzothiophene
(2) - $4H_2$
benzo[*b*]naphtho[1,2-*d*]thiophene
phenanthro[2,1-*b*]thiophene
4-decyldibenzothiophene

(1) - 2-cyclohexylmethanobenzothiophene, (2) - 2-cyclohexylethanobenzothiophene

Tetrahydrobenzo[*b*]naphtho[1,2-*d*]thiophene is completely oxidized to benzo[*b*]naphtho[1,2-*d*]thiophene. Phenanthro[2,1-*b*]thiophene and 4-decyldibenzothiophene are not affected, while 2-cyclohexylmethanobenzothiophene and 2-cyclohexylethanobenzothiophene are partially dehydrogenated. In the standard mixture after the oxidation both 2-cyclohexylmethanobenzothiophene and 2-cyclohexylethanobenzothiophene are

present, as well as 2-cyclohexylmethanobenzothiophene with loss of three H_2 and 2-cyclohexylethanobenzothiophene with elimination of four H_2. The results show that this oxidation yields a much simpler product distribution than after oxidation with DDQ and the peak ratio is well preserved after the oxidation. A real-world sample should not give any changes in the homologous series for DBE of 6 in fraction CD-1, DBE of 9 in fraction CD-2 and DBE of 12 in fraction CD-3, because the compounds without any rings are stable during the oxidation with Pd. Thus all changes in the sample after oxidation can be investigated in relation to the main DBE series for every fraction.

6.1.2.3 Results and Discussion (Real-World Sample)

The real-world samples (CD-1, CD-2 and CD-3) were oxidized then, using Pd as a dehydrogenation agent. First the HPLC chromatograms were recorded, for the samples before and after the oxidations (Figures 76, 77, 78). For all CD fractions, the chromatograms from before and after oxidation look the same. No changes are observed. The dehydrogenation is much less harsh than that obtained by DDQ and the differences may thus not be visible in the HPLC chromatograms.

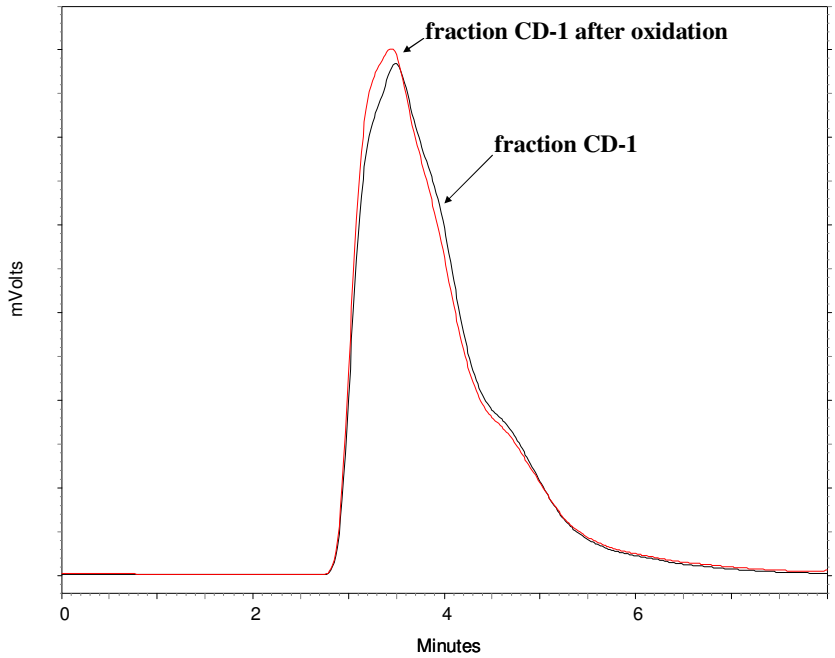

Figure 76 HPLC chromatograms of fraction CD-1 before and after oxidation with Pd (2 x TCP columns 150 mm × 4 mm, mobile phase - cyclohexane, a flow rate of 1 mL/min, room temperature)

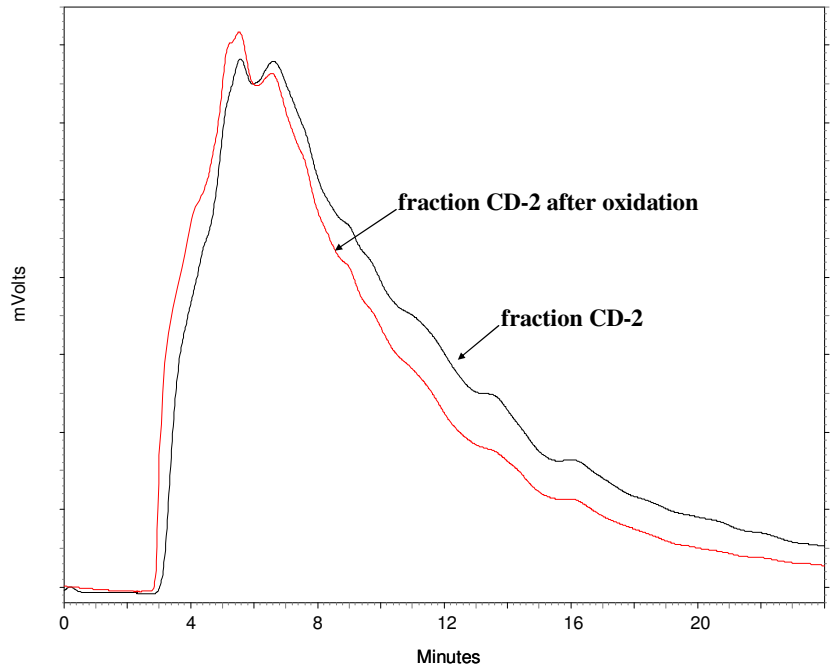

Figure 77 HPLC chromatograms of fraction CD-2 before and after oxidation with Pd (2 x TCP columns 150 mm × 4 mm, mobile phase - cyclohexane, a flow rate of 1 mL/min, room temperature)

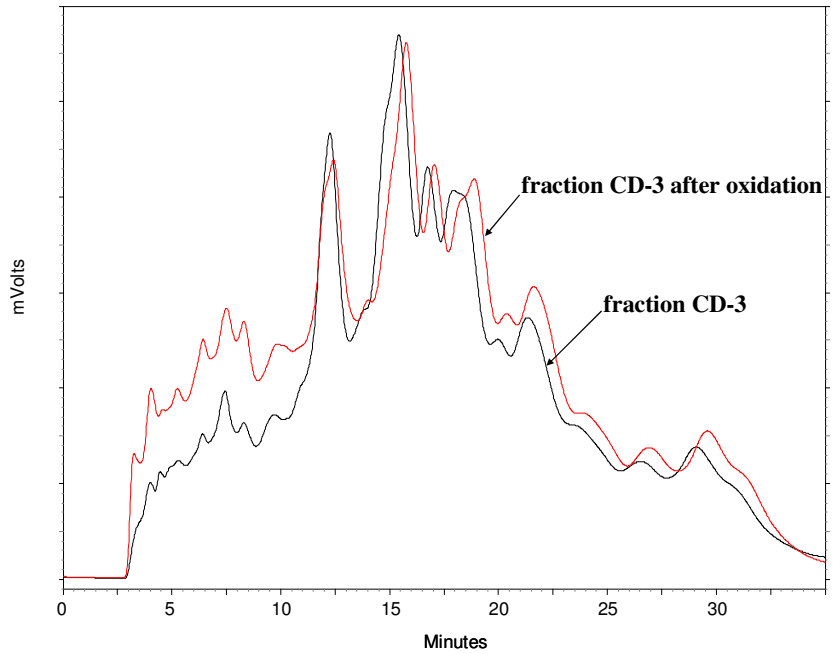

Figure 78 HPLC chromatograms of fraction CD-3 before and after oxidation with Pd (2 x TCP columns 150 mm × 4 mm, mobile phase - cyclohexane, a flow rate of 1 mL/min, room temperature)

The ^{1}H NMR measurement in Table 14 shows that some oxidation takes place, as there is a change in the ratio of aromatic to aliphatic hydrogens. The results present an increase in aromatic hydrogens.

Table 14 ^{1}H NMR data for oxidation with Pd

^{1}H aromatic to aliphatic ratio		
Fraction	**before oxidation**	**oxidation with Pd**
CD-1	1:6.2	1:3.2
CD-2	1:3.4	1:2.1
CD-3	1:2.9	1:1.9

The FT-ICR MS measurement was conducted like before, after methylation of CD fractions. Afterwards the Kendrick plots were prepared (Figures 79, 81, 83). The reference compounds were chosen in the analogous way as for oxidation with DDQ. All the changes are compared to the main DBE series for every fraction.

The plots for fractions CD-1 and CD-2 (Figures 79, 81) look similar to the Kendrick plots of fractions CD-1 and CD-2 from before dehydrogenation, there are no lower DBE signals and the mass range is similar (Figures 32, 33). Fraction CD-3 (Figure 83) shows a different profile than the fraction from before the oxidation (Figure 34). There are intensive signals at lower DBEs and higher masses.

The changes of intensities for the signals at higher DBEs after the oxidation of fraction CD-1 with Pd are more pronounced in the higher mass range, that is 416 - 428 amu (Figure 79). Not many changes are recorded in the middle mass range, 348 - 358 u. As Pd causes an oxidation of the condensed naphtheno rings, as well as partial oxidation of the non-condensed saturated rings, as shown with the standard mixture, the shift to higher DBEs should be recorded for example from DBE = 7 to DBE = 9 (for a condensed naphtheno ring), as well as to DBE = 10 and DBE = 11 (for the non-condensed rings, as for 2-cyclohexylmethanobenzothiophene and 2-cyclohexylethanobenzothiophene).

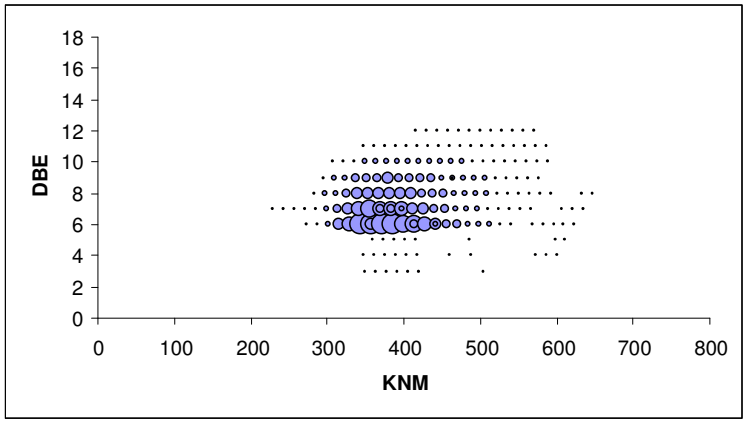

Figure 79 Kendrick plot for fraction CD-1 after oxidation with Pd

The pseudogram for fraction CD-1 before and after oxidation with Pd is presented in Figure 80. The series of DBE 6 (benzothiophenes) is supposed to remain stable, as checked on the standard mixture. As can be seen, the signal for DBE = 7 deceases slightly after the oxidation, and the highest increase is recorded for DBE = 9, which increases around 7 % (Table 15, calculation method explained

under Table 15), which this way suggests the existence of benzothiophenes with one condensed naphtheno ring in the mixture. Unfortunately we cannot be sure how many of the rings connected to aromatic system by methano- or ethano- group are also oxidized. The increase in DBE of 10 and 11 is 5% for both, but as shown with the standard mixture, the oxidation is not complete for these kinds of connections. Therefore an error in the calculation has to be expected. Theoretically it should be expected that the sum of losses will be equal to the sum of gains for all DBE signals in fraction CD-1. Thus the results presented in Table 15, also for further oxidation processes, have to contain an error. It is also important to notice that the reaction of dehydrogenation with Pd is a reversible reaction, so hydrogenation of different structures is also possible, which would lead to misleading results.

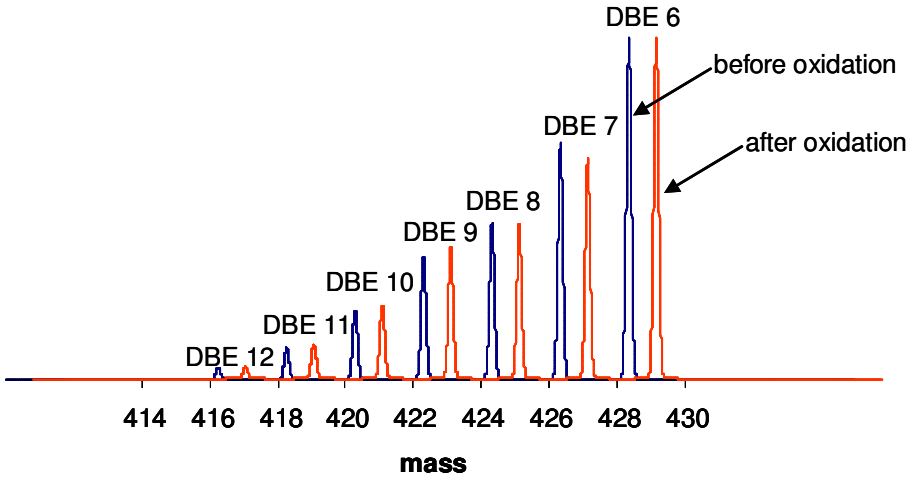

Figure 80 Pseudogram for fraction CD-1 before and after oxidation with Pd (higher mass range 416 - 428 amu)

Peaks for compounds from before and after oxidation occur exactly at the same masses. The pseudogram for the fraction after oxidation is shifted purposely to the right for better visualization.

Table 15 Signal intensity changes after fraction CD-1 oxidation with Pd for higher mass range at 416 - 428 amu

Intensities changes for the signals in fraction CD-1 after oxidation *	
DBE 7	- 7 %
DBE 8	- 1 %
DBE 9	7 %
DBE 10	5 %
DBE 11	5 %
DBE 12	4 %

* The ratio of every peak in % (for specific DBE) was calculated in relation to the signal for DBE = 6 (estimated as 100 %) before and after oxidation, from their intensities. Afterwards the changes were calculated for every DBE after the process of oxidation.

Similarly to fraction CD-1, the increase of the intensities of the signals with higher DBEs values are recorded for fraction CD-2 after oxidation with Pd (Figure 81). The changes are better visible for the higher mass range, that is 370 - 380 amu. Not many changes are recorded in the middle mass range, 302 - 310 amu, even some decreases are observed. The shift to higher DBEs should be recorded for example from DBE = 10 to DBE = 12 (for a condensed naphtheno ring), as well as to DBE = 13 and DBE = 14 (for non-condensed rings).

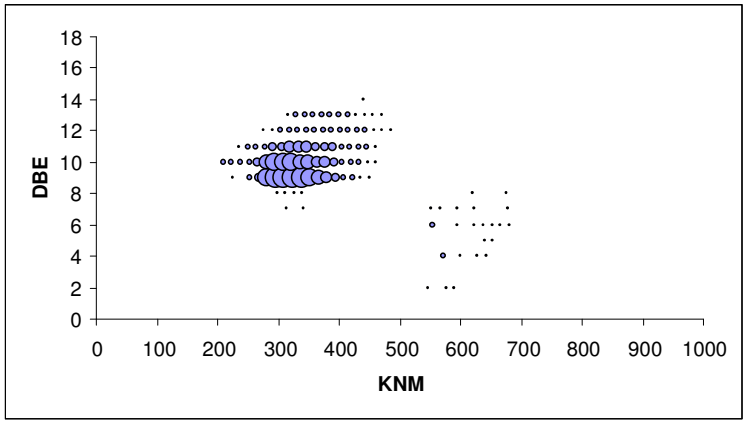

Figure 81 Kendrick plot for fraction CD-2 after oxidation with Pd

The pseudogram for fraction CD-2 before and after oxidation with Pd is presented in Figure 82. As can be seen, the signal for DBE = 10 deceases slightly, and the highest increase is recorded for DBE = 12 (10 %). This could suggest that 10 % of the compounds in the sample with DBE of 10 are dibenzothiophenes with one directly condensed naphtheno ring in this fraction, but the decrease of the signal with DBE of 10 is too low. The error is possible when a structure like for example cyclopentenobenzothiophene with one non-condensed saturated ring (DBE 9) would be oxidized (3 additional double bonds) which would then give an increase in the signal for DBE of 12 without a decrease of DBE 10. This reaction is possible because of still too extensive oxidation with Pd as oxidant. The signals with DBE = 13 and DBE = 14, which would be predictable oxidation products of the rings connected to an aromatic system by methano- or ethano- group, decreases or disappears (Table 16). This unexpected result can be caused by the loss of the higher aromatic compounds during the preparation procedure, for example during the elution from the silica column or methylation.

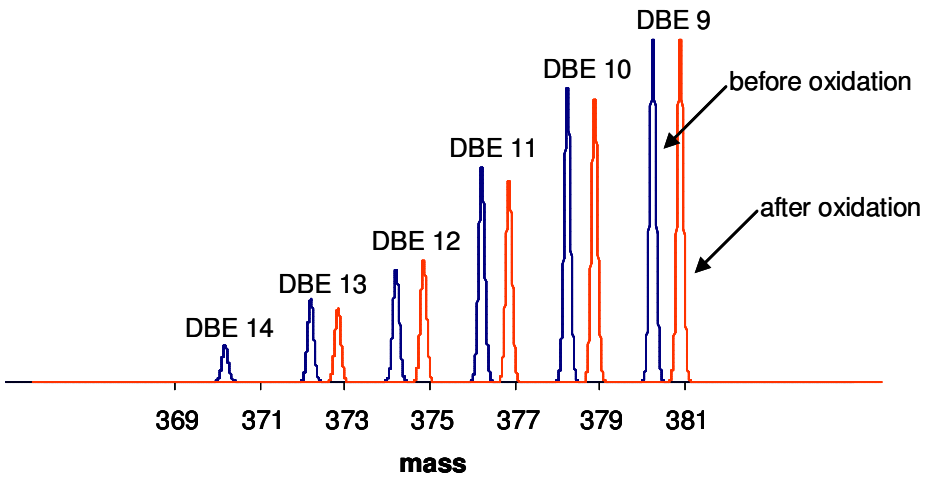

Figure 82 Pseudogram for fraction CD-2 before and after oxidation with Pd (higher mass range 370 - 380 amu)

Peaks for compounds from before and after oxidation occur exactly at the same masses. The pseudogram for the fraction after oxidation is shifted purposely to the right for better visualization.

Table 16 Signal intensity changes after fraction CD-2 oxidation with Pd for higher mass range at 370 - 380 amu

Intensities changes for the signals in fraction CD-2 after oxidation *	
DBE 10	- 3.5 %
DBE 11	- 2 %
DBE 12	10 %
DBE 13	- 10 %
DBE 14	disappeared

* The ratio in % of every peak (for specific DBE) was calculated in relation to the signal for DBE = 9 (estimated as 100 %) before and after oxidation from their intensities. Afterwards the changes were calculated for every DBE after the process of oxidation.

Fraction CD-3 (Figure 83) gives strange results. It is possible that some decomposition takes place, but the existence of signals with low DBEs and higher masses, which are not present in fraction CD-3 before oxidation (Figure 34) can be also connected with very low concentration of this fraction and even lower after the oxidation process. That makes weak signals visible after the reaction. It is also very possible that despite the fact, that all nominal mass series z^* and KMD fit to the sulfur compounds, some other class of compounds is eluted together with fraction CD-3. Aliphatic sulfur compounds can not be present in the sample after extensive separation on silica/alumina bed and Pd(II)-MP SG. It is also doubtful that these signals come from compounds created in the oxidation process, as the profile observed here for low DBE signals with high masses over 500 amu are repeatable not only in the Kendrick plots for fraction CD-3 after oxidation with Se and fraction CD-3 of VGO after HDS, but also in fraction CD-3 of VGO from before HDS (other sample of VGO, IL, was used for the HDS investigation). Also the oxidation results of the standard mixture preclude this idea.

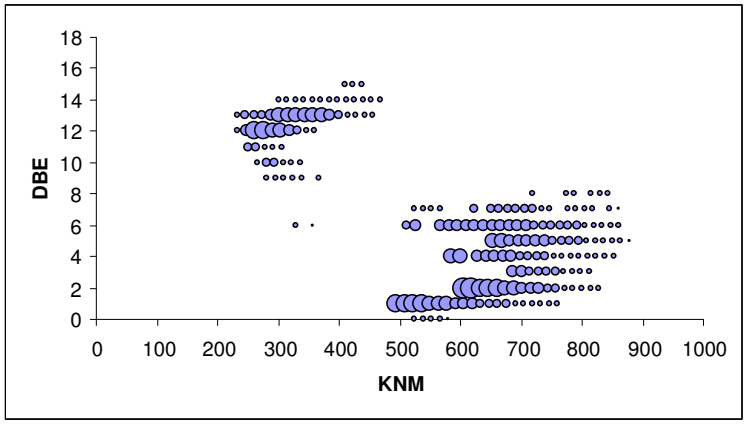

Figure 83 Kendrick plot for fraction CD-3 after oxidation with Pd

6.1.2.4 Summary

Pd appears to be a much better reagent in comparison to DDQ. Condensed non-aromatic rings are oxidized completely, while non-condensed rings are partially oxidized, giving rise to signals of compounds with additional three or four double bonds. Much less changes can be recorded this way allowing better insight into the possible structures in the mixture, exactly into the type of ring connection to an aromatic system. In fraction CD-1, an increase of the signal for DBE of 9 is recorded as high as 7 %, which can suggest that 7 % of the structures are benzothiophenes with one fused naphtheno ring. In fraction CD-2, an increase of the signal for DBE of 12 is estimated to be 10 %, suggesting that 10 % of the structures are dibenzothiophenes with one fused non-aromatic ring, but the decrease of DBE of 10 is only 3.5 %. Shifts to higher DBEs than 9 are recorded for fraction CD-1, which can imply the appearance of saturated rings connected to an aromatic system by alkano groups. Higher signals are not recorded for fraction CD-2. A possible problem can be the loss of the larger aromatic systems, or less sufficient methylation, in comparison to the lower aromatic systems. Still there is a need for an oxidation reagent which would oxidize only the naphtheno rings fused to the aromatic rings.

6.1.3 Selenium

Elemental Se (and S) combines with the hydrogen and gives H_2Se (or H_2S). The use of sulfur is not advisable for the PASHs aromatization as they contain a sulfur atom in the molecules. An effective aromatization was described in the literature, with some migration and possible expulsion of the side chains [203, 204, 214, 228].

Little is known about the oxidation mechanism by Se. A mechanism was suggested by House and Orchin [229]. They proposed that selenium attacks on a double bond in an analogous way to the attack of oxygen, and that reactions involving formation of hydroperselenides and diselenides, with a cleavage to give the radical intermediates, are important steps in the dehydrogenation by Se. A reversible π-complex formation between selenium and an isolated double bond or an aromatic system is known. A rearrangement of this complex is postulated if allylic or benzylic hydrogens are present. Such a rearranged complex can be a hydroperselenide. Using 9,10-dihydrophenanthrene as a model, we can observe a reaction running as presented in Figure 84.

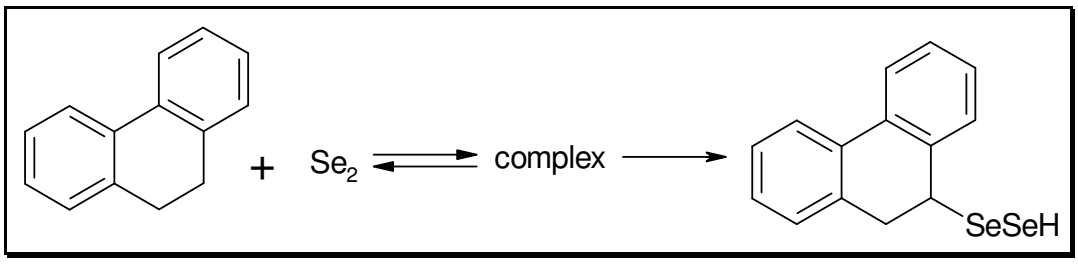

Figure 84 Creation of hydroperselenide [229, 230]

Thermal dissociation of the product could give HSe· and RSe·, each of which is capable of abstracting a hydrogen from another hydroaromatic molecule to give hydrogen selenide and a selenol (Figure 85).

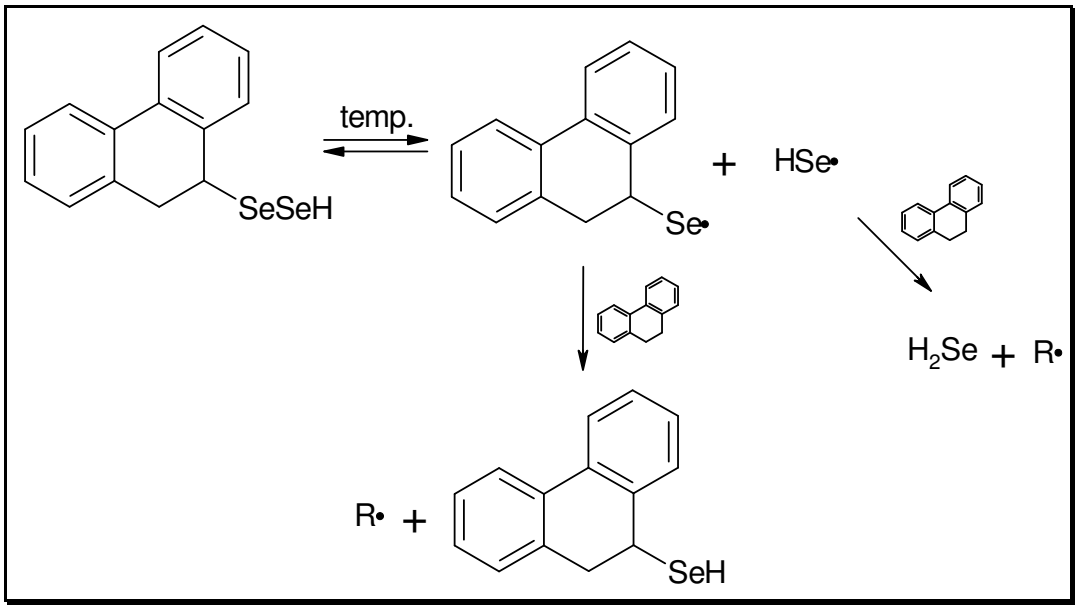

Figure 85 Thermal dissociation of hydroperselenide [229, 230]

Selenol can lead to aromatic products by three routes. There may be a thermal decomposition to hydrogen selenide and an olefin (Figure 86).

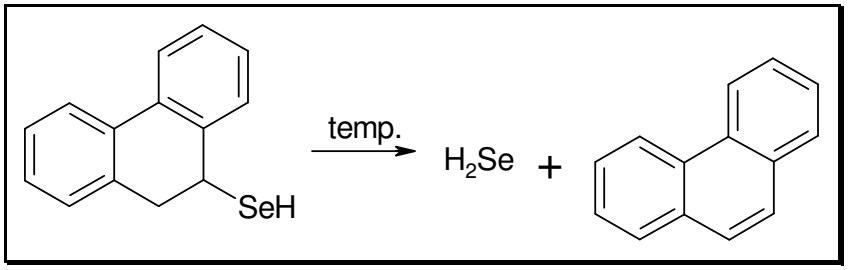

Figure 86 First reaction of selenols [229, 230]

A second reaction of selenols in the absence of air could consist of an oxidation to a diselenide and a reduction of a double bond (Figure 87).

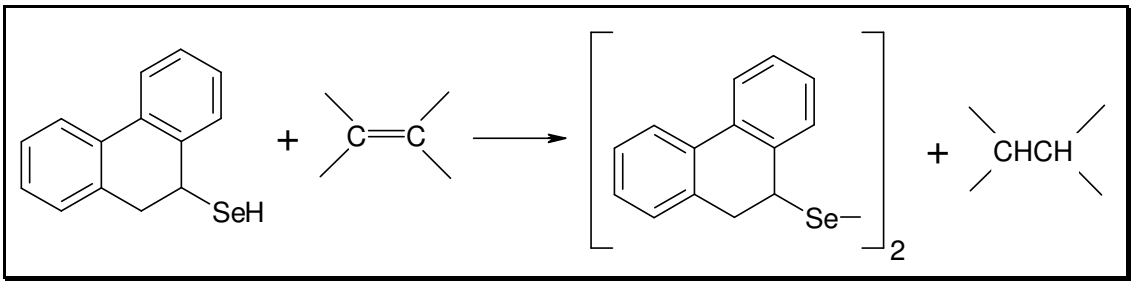

Figure 87 Second reaction of selenols [229, 230]

A third reaction of the selenol could consist of a homolytic cleavage of the C-Se bond followed by a radical disproportionation to form aromatic products (Figure 88) [230].

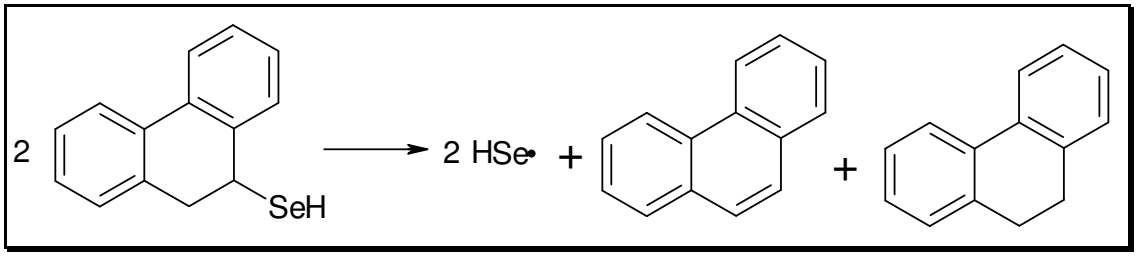

Figure 88 Third reaction of selenols [229, 230]

6.1.3.1 Experimental Section

Around 5 mg of the standard mixture (and in an analogous way the CD fractions) and an excess of powdered selenium (20 mg) were heated to 300 °C in a flask fitted with a condenser. A rubber hose was fitted to the top of the condenser, which led to a series of two traps. The second trap was filled with copper sulfate solution to prevent the hydrogen selenide gas that evolves from the reaction from escaping. The first trap was left empty to prevent any copper sulfate solution from backing up into the reaction mixture. The heating should continue until the evolution of hydrogen selenide gas ceases. The reaction was left for one night. After cooling, 95 % ethanol (1 mL) was added and the mixture refluxed for 30 min. The alcoholic solution was chromatographed on silica gel using cyclohexane and the solvent was evaporated [228].

The real-world samples were investigated using the HPLC system with two TCP columns (150 mm x 4 mm), with cyclohexane as eluent, at room temperature and a flow of 1 mL/min. Afterwards the solvent was evaporated and the remains dissolved in CD_2Cl_2 and ^1H NMR analysis was performed. After evaporation of the solvent, the samples were methylated (see chapter 5.1.3) and ESI FT-ICR MS analysis was applied.

6.1.3.2 Results and Discussion (Standard Mixture)

The standard mixture was prepared in the analogous way as for the oxidation with Pd. The mixture was composed of:

- 2-cyclohexylmethanobenzothiophene
- 2-cyclohexylethanobenzothiophene
- tetrahydrobenzo[*b*]naphtho[1,2-*d*]thiophene
- phenanthro[2,1-*b*]thiophene
- 4-decyldibenzothiophene

GC-MS as well as GC-AED and GC-FID were applied to record the chromatograms from before and after the oxidation of the standard mixture. The results are presented in Figure 89. The results are supported by the analysis of the received mass spectra of the standard mixture components from before and after dehydrogenation described in chapter 6.1.1.3.

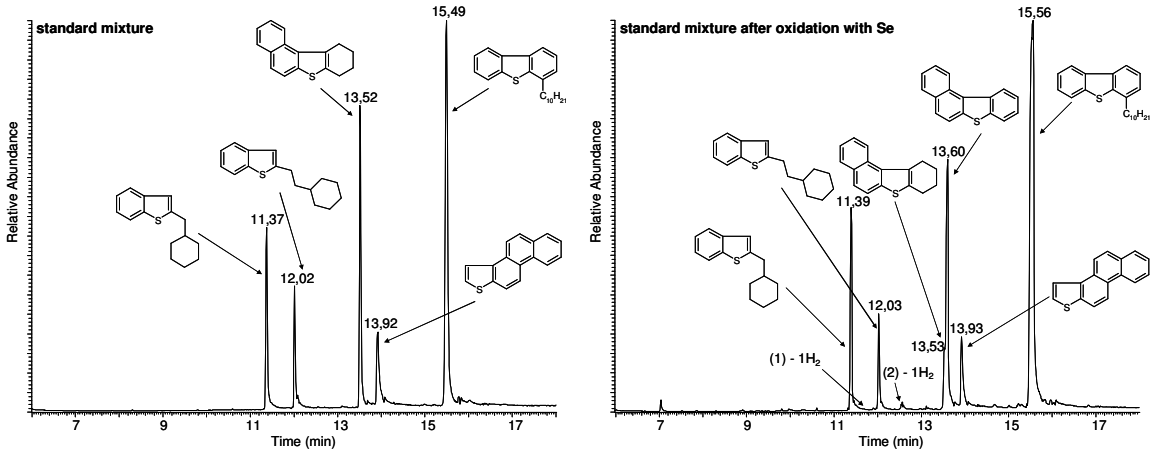

Figure 89 GC (GC-MS) chromatograms of the standard mixture before and after oxidation with Se

The standard mixture before oxidation:
2-cyclohexylmethanobenzothiophene
2-cyclohexylethanobenzothiophene
tetrahydrobenzo[*b*]naphtho[1,2-*d*]thiophene
phenanthro[2,1-*b*]thiophene
4-decyldibenzothiophene

The standard mixture after oxidation:
2-cyclohexylmethanobenzothiophene
traces of (1) - $1H_2$
2-cyclohexylethanobenzothiophene
traces of (2) - $1H_2$
traces of tetrahydrobenzo[*b*]naphtho[1,2-*d*]thiophene
benzo[*b*]naphtho[1,2-*d*]thiophene
phenanthro[2,1-*b*]thiophene
4-decyldibenzothiophene

(1) - 2-cyclohexylmethanobenzothiophene, (2) - 2-cyclohexylethanobenzothiophene

The dehydrogenation with Se does not affect phenanthro[2,1-*b*]thiophene and 4-decyldibenzothiophene. For 2-cyclohexylmethanobenzothiophene and 2-cyclohexylethanobenzothiophene, only traces of products with elimination of one H_2 are found. Tetrahydrobenzo[*b*]naphtho[1,2-*d*]thiophene is oxidized to benzo[*b*]naphtho[1,2-*d*]thiophene, but it is contaminated to a small amount with the substrate. Peak ratio is very well preserved after the oxidation with Se. A real-world

sample should not give any changes for the compounds in the main homologous series for every CD fraction, because the components without fused naphtheno rings are stable during the oxidation with Se.

Unfortunately longer reaction time or a larger excess of Se does not improve the oxidation yield of tetrahydrobenzo[*b*]naphtho[1,2-*d*]thiophene. A less than quantitative oxidation of tetrahydrobenzo[*b*]naphtho[1,2-*d*]thiophene suggests that possibly not all directly condensed non-aromatic rings to aromatic system in the real-world samples will be oxidized, which causes the further statistical evaluation to contain an error.

The other standard mixture, composed of some PAHs (9,10-dihydroanthracene, 2-methylphenanthrene and chrysene) was also tested. 2-Methylphenanthrene and chrysene remain stable in the reaction with Se, as expected, and 9,10-dihydroanthracene is oxidized to anthracene, but also not quantitatively.

6.1.3.3 Results and Discussion (Real-World Sample)

The real-world samples (CD-1, CD-2 and CD-3) were oxidized then, using Se as dehydrogenation agent. The HPLC chromatograms were recorded for the samples before and after the oxidations (Figures 90, 91, 92), but no changes are observed, similar to the Pd case.

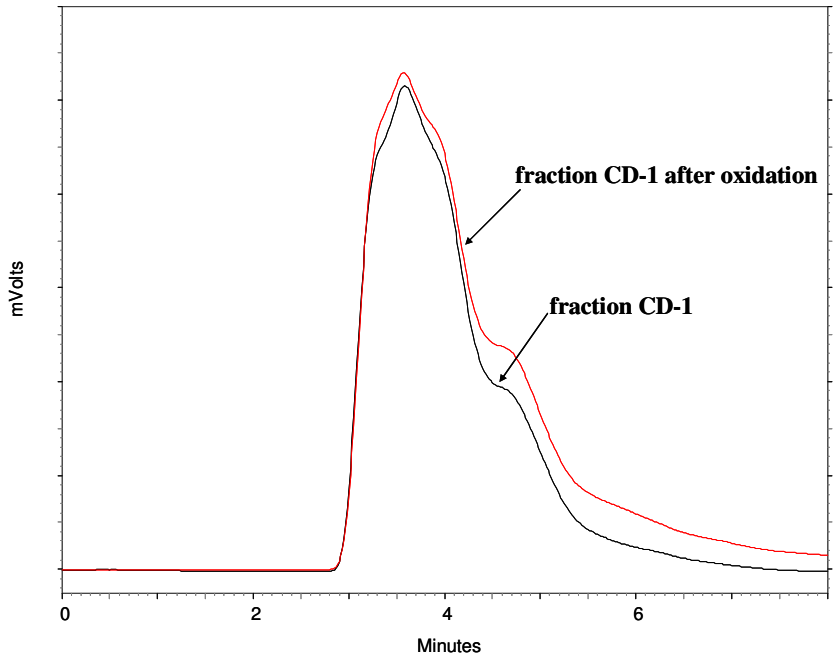

Figure 90 HPLC chromatograms of fraction CD-1 before and after oxidation with Se (2 x TCP columns 150 mm × 4 mm, mobile phase - cyclohexane, a flow rate of 1 mL/min, room temperature)

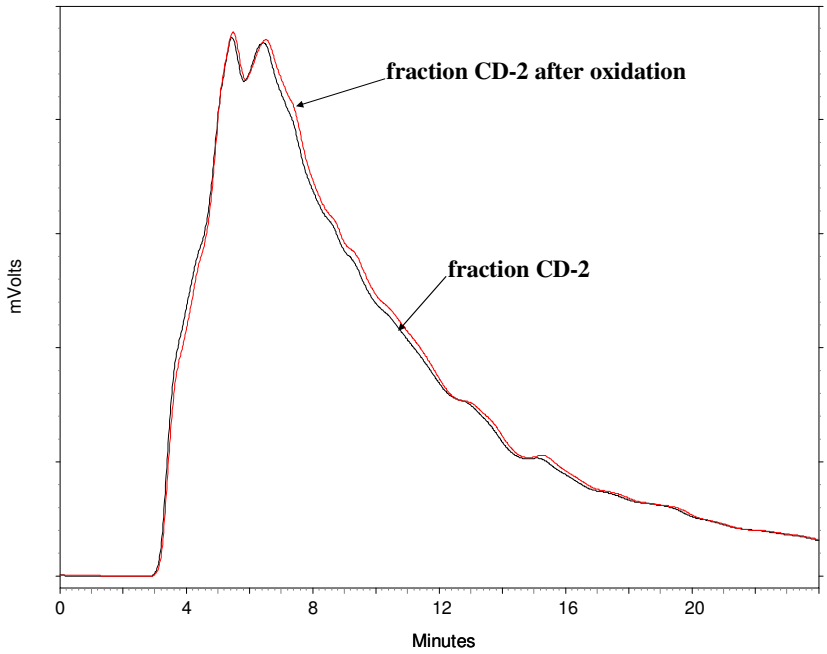

Figure 91 HPLC chromatograms of fraction CD-2 before and after oxidation with Se (2 x TCP columns 150 mm × 4 mm, mobile phase - cyclohexane, a flow rate of 1 mL/min, room temperature)

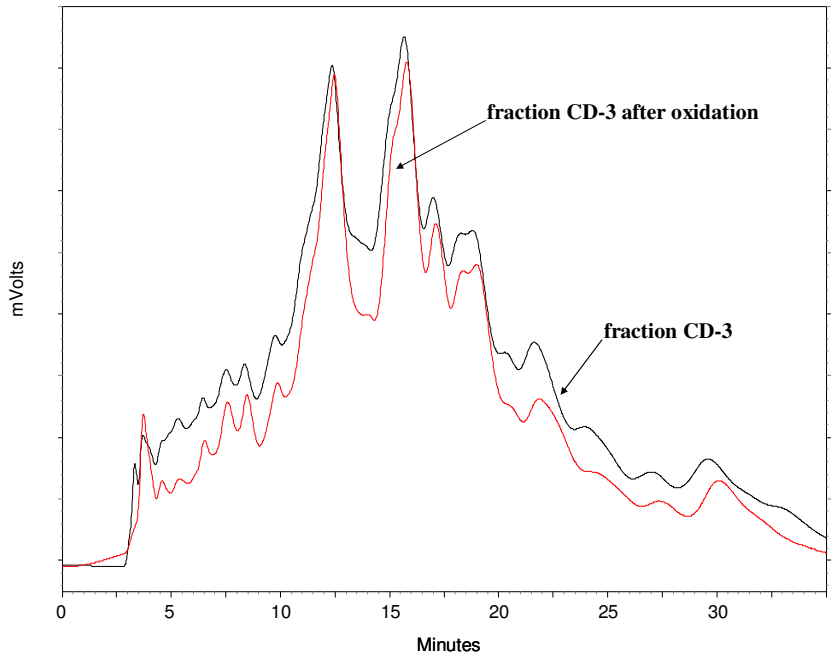

Figure 92 HPLC chromatograms of fraction CD-3 before and after oxidation with Se (2 x TCP columns 150 mm × 4 mm, mobile phase - cyclohexane, a flow rate of 1 mL/min, room temperature)

The ^{1}H NMR measurement in Table 17 shows that the oxidation takes place, as there is a change in the ratio of aromatic to aliphatic hydrogens.

Table 17 ^{1}H NMR data for oxidation with Se

^{1}H aromatic to aliphatic ratio		
Fraction	**before oxidation**	**oxidation with Se**
CD-1	1:6.2	1:3.6
CD-2	1:3.4	1:2.5
CD-3	1:2.9	1:2.2

The FT-ICR MS measurement was carried out like before, after methylation of CD fractions. Afterwards the Kendrick plots were prepared (Figures 93, 95, 97). Again the reference compounds were chosen as before for DDQ and Pd. All changes are compared to the main DBE series for every fraction.

The plot for fraction CD-1 (Figure 93) looks similar to Kendrick plots of fraction CD-1 from before dehydrogenation (Figure 32). There are no lower DBE signals and the mass range is comparable (Figure 93). Fractions CD-2 and CD-3 have a different profile than the fraction before oxidation. There are intensive signals with lower DBEs and higher masses for fraction CD-3 (Figure 97, CD-3 before oxidation - Figure 34), and less intense signals with low DBEs for fraction CD-2 (Figure 95, CD-2 before oxidation - Figure 33).

An increase of the signal intensities with higher DBEs values is recorded for fraction CD-1 (Figure 93) after oxidation with Se. The changes are similar for both mass ranges, for 348 - 358 amu and 416 - 428 amu. As presented for the standard mixture, Se causes oxidation of the condensed non-aromatic rings only. The shift to higher DBEs should be recorded exclusively for this kind of connection of the naphtheno ring. The signal with DBE = 7 should give rise to DBE = 9 for fraction CD-1.

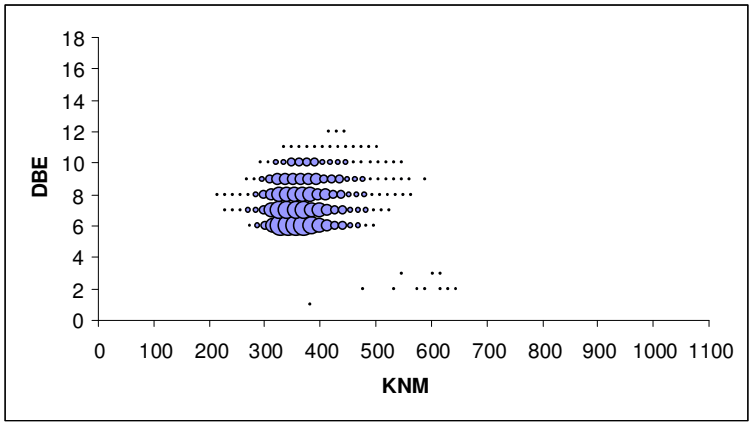

Figure 93 Kendrick plot fraction CD-1 after oxidation with Se

The pseudogram for fraction CD-1 is presented in Figure 94, before and after oxidation. The changes in the middle mass range are analogous to the higher mass range. As indicated in Table 18, the decrease in the signal of DBE = 7 causes an increase in the signal with DBE = 9. The increase is estimated to be 10 %, similar to the oxidation with Pd, where the increase reaches 7 %. We can expect that the

content of benzothiophenes with condensed non-aromatic ring equals around 7 - 10 % in fraction CD-1. The highest increase is recorded for DBE 10, which increases 14.5 %. As only condensed rings are oxidized with Se in the standard mixture, it could be expected, that this increase is caused for example by the oxidation of benzothiophene with two non-aromatic rings, one condensed to aromatic system and one connected by alkano groups, but lack of decrease for the DBE 8 signal makes the assumption doubtful.

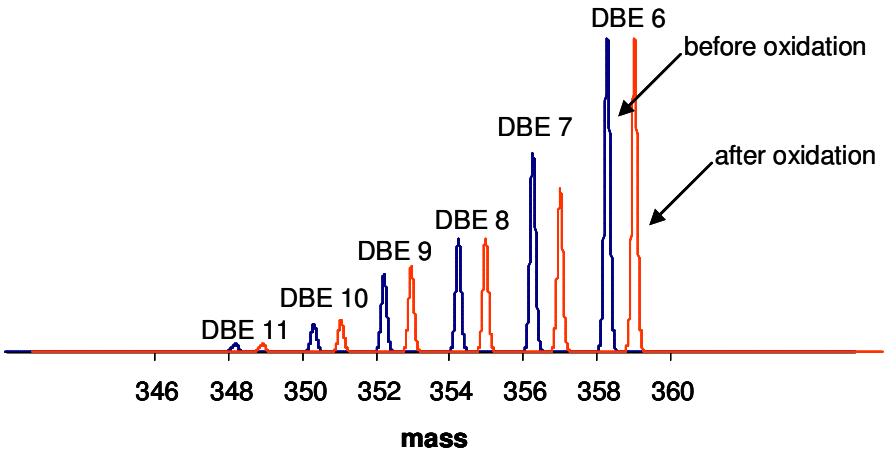

Figure 94 Pseudogram for fraction CD-1 before and after oxidation with Se (middle mass range 348 - 358 amu)

Peaks for compounds from before and after oxidation occur exactly by the same masses. The pseudogram for the fraction after oxidation is shifted purposely to the right for better visualization.

Table 18 Signal intensity changes after fraction CD-1 oxidation with Se for middle mass range at 348 - 358 amu

Intensities changes for the signals in fraction CD-1 after oxidation *	
DBE 7	- 18 %
DBE 8	0.5 %
DBE 9	10 %
DBE 10	14.5 %
DBE 11	4 %

* The ratio in % of every peak (for specific DBE) was calculated in relation to the signal for DBE = 6 (estimated 100 %) before and after oxidation from their intensities. Afterwards the changes were calculated for every DBE after the process of oxidation.

Fraction CD-2 (Figure 95) contains some low DBE signals with higher masses after the oxidation. The same signals appear more intensively in fraction CD-3.

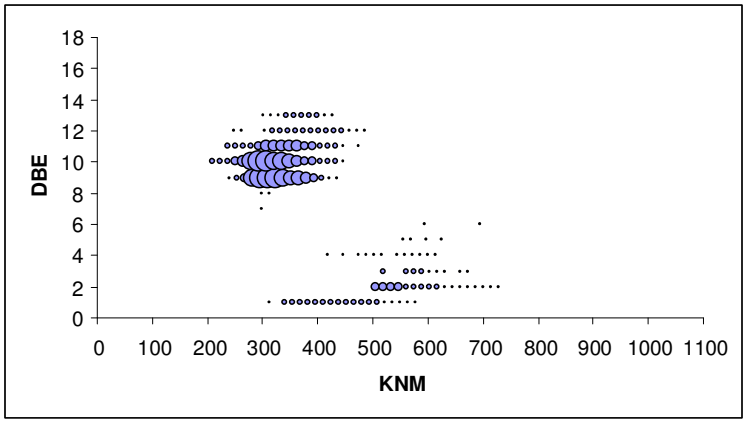

Figure 95 Kendrick plot for fraction CD-2 after oxidation with Se

The pseudogram was prepared for fraction CD-2 using compounds in a higher mass range (Figure 96) where changes were more visible. The decrease in DBE 10 and increase in DBE 12 is recorded as expected (Table 19), but the increase of DBE 12 is lower than for Pd oxidation, only 3 %. The increase for the DBE 11 signal is surprising. An explanation can be an inefficient separation and

contamination of fraction CD-2 with cyclopentenobenzothiophene with one fused non-aromatic ring with DBE = 9. That would give an increase to DBE = 11.

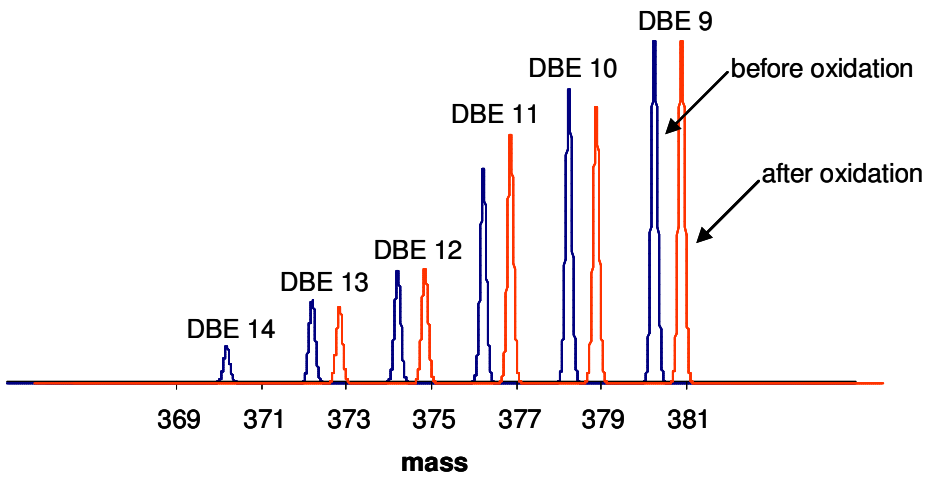

Figure 96 Pseudogram for fraction CD-2 before and after oxidation with Se (higher mass range 370 - 380 amu)

Peaks for compounds from before and after oxidation occur exactly by the same masses. The pseudogram for the fraction after oxidation is shifted purposely to the right for better visualization.

Table 19 Signal intensity changes after fraction CD-2 oxidation with Se for higher mass range at 370 - 380 amu

Intensities changes for the signals in fraction CD-2 after oxidation *	
DBE 10	- 6 %
DBE 11	16 %
DBE 12	3 %
DBE 13	- 7 %
DBE 14	disappears

* The ratio in % of every peak (for specific DBE) was calculated in relation to the signal for DBE = 9 (estimated as 100 %) before and after oxidation from their intensities. Afterwards the changes were calculated for every DBE after the process of oxidation.

Fraction CD-3 does not give any good results (Figure 97). It looks similar to fraction CD-3 after oxidation with Pd and fraction CD-3 of VGO from before and after HDS. The explanation for that is the same as in the case of the oxidation process

with Pd. The existence of signals with low DBEs and higher masses, which are not present in fraction CD-3 before oxidation (Figure 34), can be connected with very low concentration of this fraction and even lower after oxidation. That makes the low intensities of some other signals more visible. It is highly possible that despite the fact that all nominal mass series z^* and KMD fit the sulfur compounds, some other class of compounds is eluted together with fraction CD-3. Extensive separation on silica/alumina bed and Pd(II)-MP SG precludes the appearance of aliphatic sulfur compounds. It is also doubtful if these signals come from the compounds created in the oxidation process, as the profile observed here for low DBE signals is repeatable in the other samples and the oxidation results of the standard mixture do not support this.

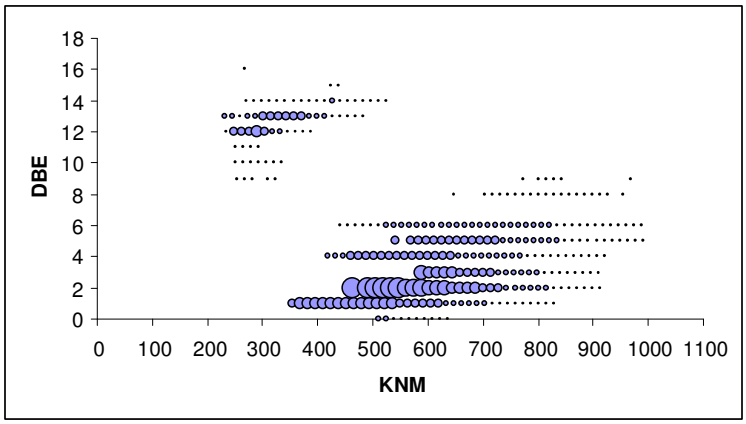

Figure 97 Kendrick plot for fraction CD-3 after oxidation with Se

6.1.3.4 Summary

The oxidation with Se appears to be the most successful one. Only the naphtheno rings fused to an aromatic system are oxidized, but not quantitatively. Traces of the substrate are still detected in the standard mixture. The oxidation of fraction CD-1 suggests 10 % of the structures are benzothiophenes with one condensed non-aromatic ring, similar as with Pd oxidation. The oxidation of fraction CD-2 shows that possibly 3 % of the dibenzothiophenes structure are compounds

with a condensed non-aromatic six-membered ring. Fraction CD-3 does not give any good results, as is the situation for the Pd oxidation.

6.2 Summary

Different oxidation agents were tested for the PASH dehydrogenation. It is important to find an agent which would dehydrogenate only these non-aromatic rings that are fused with aromatic rings.

As presented above, DDQ was investigated first and it appears to be too strong oxidant. 5 h of reflux results not only in the oxidation of the fused rings, but also of the non-condensed rings with decomposition of the obtained products. The real samples reveal some loss of compounds, visible already for example in the HPLC chromatogram for fraction CD-1. The ^{1}H NMR data prove that the oxidation partially succeeded. The Kendrick plots clearly indicate that higher aromatic compounds give rise to the compounds with low DBEs values and larger masses in all the fractions. A statistical evaluation is not possible because of too many not understood changes in the sample. Shortening the time of reflux to 30 min or applying milder temperature conditions does not give much better results, as many oxidation routes are possible making an interpretation impossible. The oxidation investigated for shorter time of reflux is also associated with a partial decomposition.

Pd as an oxidation agent simplifies the oxidation, giving a successful oxidation of rings fused to an aromatic system (giving a DBE shift of 2, by creation of two additional double bonds). It is not free of partial dehydrogenation for the non-condensed saturated rings, giving a shift for DBE signals of 3 or 4. The HPLC chromatograms do not show any changes, possibly suggesting that this method of visualizing the oxidation results is not efficient. The ^{1}H NMR data support the interpretation that an oxidation takes place. The Kendrick plots show that the best results can be noticed in the higher mass range. No good results are obtained for

fraction CD-3, which shows intensive signals with low DBEs caused probably by elution of some other compounds than PASHs.

Se as oxidation agent appears to be the best choice. It oxidizes only rings fused to an aromatic system (although not completely). The HPLC chromatograms, as for Pd, do not imply any changes. The ^{1}H NMR, as for Pd, supports the conclusion that the oxidation takes place. The Kendrick plots show that the best results can be noticed in the higher mass ranges for fraction CD-2. Fraction CD-1 gives reproducible results in the middle and higher mass ranges. No good results are obtained for fraction CD-3 again.

All the results suggest that the oxidation process is not an appropriate method for structural elucidation of fraction CD-3, i.e. for the larger aromatic systems. Maybe the problem lies only in the methylation process followed by ESI FT-ICR MS, as methylation is probably not quantitative. Changing the method of ionization could give a better insight into that problem. Problematic may also be the sample processing after oxidation, that is purification for example. The best results are obtained for fraction CD-1. The reason for that can be that in this fraction only small aromatic systems are present (the mass for benzothiophene is 134 amu). At the same time the masses of the compounds in fraction CD-1 are the highest (average 380 amu). Every extra condensed non-aromatic ring increases the mass by 54 amu. That makes the appearance of more naphtheno rings in the structure more possible than in fraction CD-2, and definitely than in fraction CD-3, where the mass of an aromatic unit reaches minimum 234 amu, and the middle mass of that fraction is around 300 amu.

As mentioned before, the HPLC chromatograms are not helpful for the observation of the oxidation efficiency. They show only the loss of a part of fraction CD-1 and small changes in fraction CD-2 after oxidation with DDQ. They do not change at all for any fraction after dehydrogenation with Pd and Se. The fluorescence spectra were not recorded for the CD fractions before and after

oxidation, because the differences between the maxima of excitation and emission for every CD fraction are negligible and any important information could be obtained. More helpful are ^{1}H NMR analyses (collected in Table 20).

Table 20 ^{1}H NMR data before and after oxidation

^{1}H aromatic to aliphatic ratio					
Fraction	**before oxidation**	**oxidation with DDQ, 5 h**	**oxidation with DDQ, 30 min**	**oxidation with Pd**	**oxidation with Se**
CD-1	1:6.2	1:4.7	1:4.3	1:3.2	1:3.6
CD-2	1:3.4	1:2.3	1:2.3	1:2.1	1:2.5
CD-3	1:2.9	1:1.6	1:1.8	1:1.9	1:2.2

The data for DDQ oxidation can be misleading because of the partial decomposition and thus creation of aliphatic compounds, with aliphatic hydrogens. Despite this fact, the data for DDQ show an increase in the ratio of aromatic to aliphatic hydrogens in comparison to the fractions before oxidation. The dehydrogenation with Pd presents already a higher increase of aromatic hydrogens, higher than for Se, as both types of non-aromatic rings are oxidized with Pd. Se is gentler and oxidizes only the fused rings. The exact interpretation of the NMR data is complicated because of many different possible alkyl substitution patterns at the aromatic rings which influences the hydrogen ratio significantly.

The FT-ICR MS data are the most appropriate for the observation of the oxidation process. As mentioned before, no good results could be collected for fraction CD-3 and DDQ as an oxidation agent should be excluded from the statistical evaluation, because of the misleading results. Thus, for the structural statistical evaluation, Pd and Se can be applied. Calculations are possible for fractions CD-1 and CD-2. The data for signal intensity changes are collected in Table 21.

Table 21 Signal intensity changes after oxidation *

	Pd, masses in the range: 416 - 428 amu for CD-1 370 - 380 amu for CD-2		**Se, masses in the range: 416 - 428 amu for CD-1 370 - 380 amu for CD-2**	
Fraction CD-1	DBE 7	- 7 %	DBE 7	- 18 %
	DBE 8	- 1 %	DBE 8	0.5 %
	DBE 9	**7 %**	DBE 9	**10 %**
	DBE 10	5 %	DBE 10	14.5 %
	DBE 11	5 %	DBE 11	4 %
	DBE 12	4 %	DBE 12	-
Fraction CD-2	DBE 10	- 3.5 %	DBE 10	- 6 %
	DBE 11	- 2 %	DBE 11	16 %
	DBE 12	**10 %**	DBE 12	**3 %**
	DBE 13	- 10 %	DBE 13	- 7 %
	DBE 14	disappeared	DBE 14	disappeared

* The ratio in % of every peak (specific DBE) was calculated in relation to the signal for DBE = 6 (for fraction CD-1) or 9 (for fraction CD-2 (100 %) before and after oxidation from their intensities. Afterwards the changes were estimated for every DBE after the process of oxidation.

The oxidation with Pd suggests 7 % of the benzothiophenes with a fused non-aromatic ring in fraction CD-1 and 10 % of dibenzothiophenes with a fused non-aromatic ring in fraction CD-2. The result for fraction CD-2 is somehow disputable, as not much of a decrease for signals with DBE of 10 is recorded. The oxidation with Se supports the results obtained with Pd, giving 10 % of benzothiophenes with a condensed non-aromatic ring in fraction CD-1, but the value in fraction CD-2 for dibenzothiophenes with condensed naphtheno ring is only 3 %. Many intensity changes are not fully understood and the results can contain a substantial error, caused by possible loss of the compounds during the process and not quantitative methylation before ESI FT-ICR MS.

As mentioned in chapter 5.2.2., the component with DBE of 6 and the mass of 358 amu for fraction CD-1, DBE of 9 and the mass of 310 amu for fraction CD-2, DBE of 12 and the mass of 276 amu for fraction CD-3 were chosen as reference compunds (the same before and after the oxidation, the intensity set to 1). All the changes are compared to the main DBE series in the fractions: DBE of 6 for fraction CD-1, DBE of 9 for fraction CD-2 and DBE of 12 for fraction CD-3. The compounds in these series should not be oxidized (partial loss of these compounds is observed using DDQ), because all changes are measured in relation to these compounds. Possibly the addition (before processing) of an other compound without sulfur as the standard, which is not reactive in the oxidation and with comparable mass to the middle mass of the fractions, would give a more reliable answer regarding the intensity changes which appear during the process of oxidation.

7 Hydrodesulfurization of VGO

The desulfurization process has been described in chapter 1.7. As already mentioned, sulfur removal is dictated by a few important reasons, like: air pollution through release of SO_x [21, 28, 29], poisoning of catalytic converters, as well as the mutagenic or carcinogenic properties of PASHs. Tough environmental legislation has been introduced [20-22, 27, 30-32] in order to lower the amount of sulfur in fuels.

The hydrodesulfurization is a process in which sulfur is removed from the sulfur compounds in a reaction with hydrogen. The HDS is a catalyzed reaction usually involving a metal sulfide catalyst and is usually operated at moderately high temperature and pressure, typically 300 - 350 °C and 50 - 100 atm.

A few aspects about the reactivity towards the HDS of the sulfur compounds are known (see chapter 1.7), like that of a dependence between the local environment of the sulfur in the molecule, the shape of the molecule etc. [21, 27, 29, 30, 33, 35-37]. The polynuclear organic sulfur compounds are among the least reactive sulfur compounds in the HDS reaction.

The same sample of VGO before and after the HDS was investigated here using such analytical tools as HPLC and FT-ICR MS to check the PASHs composition change caused by the process.

7.1 Experimental Section

7.1.1 Sample

The vacuum gas oil (VGO) from Iranian Light crude oil with a boiling range of 390 - 460 °C (other sample than in chapter 5) before (feed) and after HDS (effluent) was supplied by the Institut Français du Pétrole, Vernaison, France. The catalyst used for the HDS was NiMo on alumina from Axens.

7.1.2 Liquid chromatography of PASHs

The SARA fractionation was performed for both samples in the same manner. The aromatics fraction was first isolated from the saturates as described in chapter 5.1.2.1.

Around 200 mg of aromatics were separated on Pd(II)-MP SG into two fractions: Pd-1 and Pd-2, as described in chapter 5.1.2.2.

The Pd-2 fraction was separated on the β-cyclodextrin bonded silica phase into the CD fractions as described in chapter 5.1.2.3.

7.1.3 PASH Methylation

Around 5 mg of every CD fraction was methylated as described in chapter 5.1.3.

7.1.4 Analysis

The HPLC chromatogram presented further was obtained on β-cyclodextrin phase. All the data obtained from FT-ICR MS were further interpreted after the calculations and appropriate sorting in an Excel spreadsheet. The Kendrick plots were prepared for every fraction.

7.2 Results and Discussion

The same VGO before and after the hydrodesulfurization was taken for the investigation. The sulfur content in the sample before HDS was estimated at 2.03 % and after HDS, 0.12 %, indicating that a considerable portion of sulfur was removed from the sample.

Separation was performed exactly in the same way for the two samples. After a first separation on the open tubular column with silica and alumina, around 562 mg

of the saturates and 428 mg of the aromatics were collected for the feed sample. For the effluent sample, around 666 mg of the saturates and 479 mg of the aromatics were collected. Thus after HDS, more saturates were obtained, as the hydrodesulfurization process not only removes a sulfur atom from the molecule but also causes saturation of aromatic molecules to a different extent.

The separation on Pd(II)-MP SG gave around 130 mg of PAHs (Pd-1) and 37 mg of PASHs (Pd-2) for the aromatic fraction of the feed sample. The aromatic fraction of the effluent sample gave around 165 mg of Pd-1 and 7 mg of Pd-2. Much less PASHs were collected from the sample after HDS, explicable by the efficient removed sulfur in the desulfurization process.

Next, the separation on β-cyclodextrin columns is presented in Figure 98.

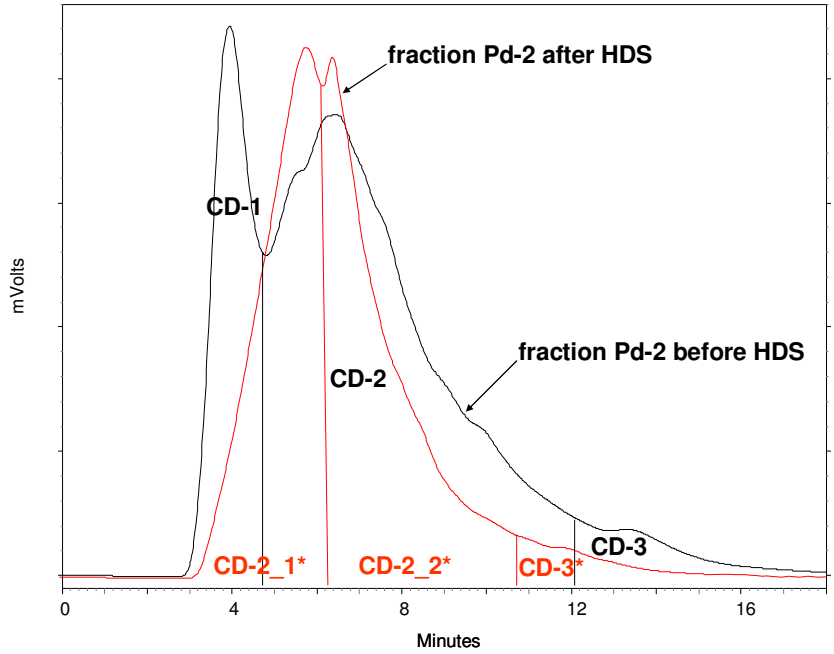

Figure 98 HPLC chromatogram of Pd-2 fraction separation on β-cyclodextrin, before and after HDS (2 x β-cyclodextrin columns 150 mm × 4 mm, mobile phase - cyclohexane with 0.5 % of tert-butyl methyl ether, a flow rate of 1 mL/min, room temperature)

Fraction Pd-2 was separated in a semi-preparative way into three fractions, according to the number of condensed aromatic rings. Around 13.1 mg of fraction CD-1 (two condensed aromatic rings), 13.2 mg of fraction CD-2 (three condensed

aromatic rings) and 3.4 mg of fraction CD-3 (four and more condensed aromatic rings) were collected for the sample before HDS.

Fraction Pd-2 after HDS does not contain fraction CD-1, as these compounds are very reactive towards the desulfurization. Fraction CD-2 looks different than before HDS, and it is divided into two further fractions CD-2_1* and CD-2_2*. Fraction CD-3 is still visible, after HDS. For the fraction after HDS, around 3.2 mg of fraction CD-2_1*, 1.2 mg of fraction CD-2_2* and 1.8 mg of fraction CD-3* were collected.

All CD fractions were methylated and FT-ICR MS analysis was applied to generate the Kendrick plots and reveal the exact changes in the samples from the HDS process.

Figures 99, 100 and 101 present the Kendrick plots for fractions CD-1, CD-2 and CD-3 before HDS.

Similarly to the Kendrick plot for CD-1 in Figure 32, there are no signals with DBE 0 (mercaptans, sulfides), 1 (thiophanes) and 2 (dihydrothiophenes) in fraction CD-1 before HDS (Figure 99). Low concentration of thiophenes (DBE 3), napthenothiophenes (DBE 4) and cyclopentenothiophenes or cyclohexenothiophenes (DBE 5) are found. DBE 6 is the main series containing benzothiophenes. Compounds with 9 to 36 aliphatic carbon atoms are counted. Further series with DBE of 7 is represented by napthenobenzothiophenes and the number of carbons in the aliphatic chains varies from 0 to 34 (for 1,2,3,4-tetrahydrodibenzothiophene for example). The compounds with DBE 8 can be represented by dinaphthenobenzothiophenes, indenothiophenes or indanylthiophenes. The masses for this series range from 242 amu to 662 amu. The next series of the compounds, with DBE 9 (trinaphthenobenzothiophene is present in fraction CD-1), as well as DBE 10, 11, 12 and 13 should be present only in fraction CD-2, but overlapping is still observed, and some of the compounds representative of fraction CD-2 are present in fraction CD-1.

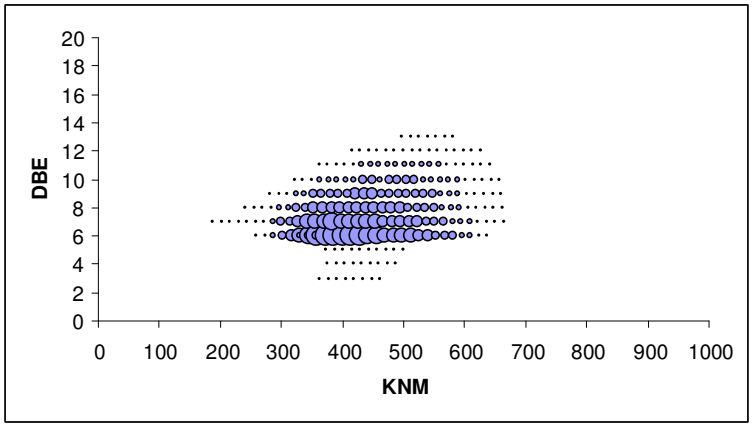

Figure 99 Kendrick plot for fraction CD-1 before HDS

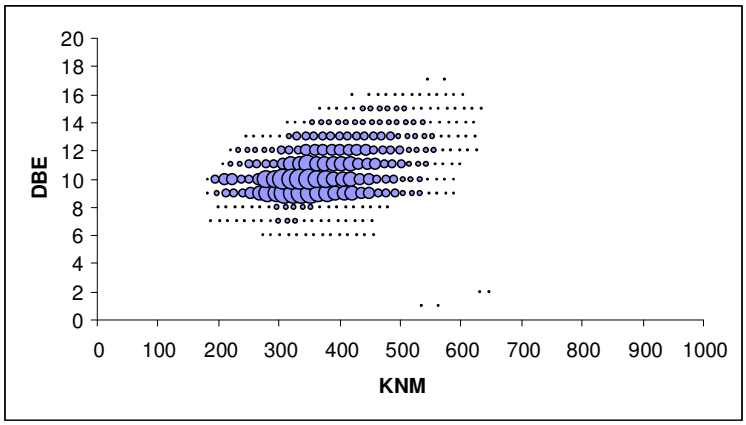

Figure 100 Kendrick plot for fraction CD-2 before HDS

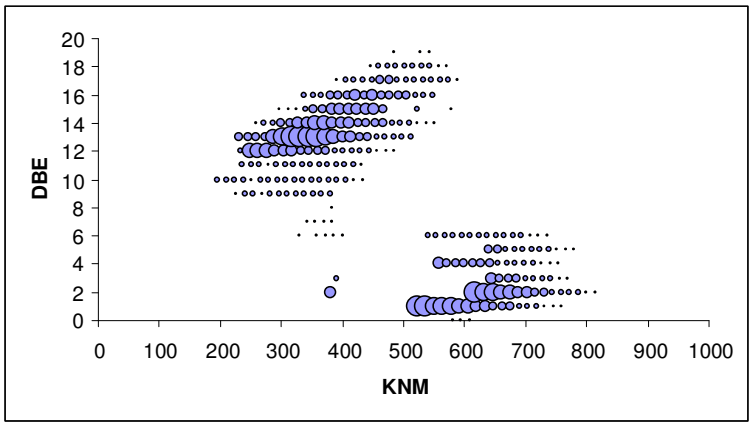

Figure 101 Kendrick plot for fraction CD-3 before HDS

The Kendrick plot for fraction CD-2 before HDS is presented in Figure 100. For this fraction, the main series of the compounds are those with DBE of 9. There are still some signals from the series of DBE 6, more intensive series of DBE 7 and 8 and few with DBE 1 and 2. Series DBE 9 is mainly represented by dibenzothiophenes, but benzothiophenes with three naphtheno rings are possible. For dibenzothiophenes 1 to 29 carbon atoms in the side chains are observed. The next, higher series with DBE 10 is represented by acenaphthothiophenes, or dibenzothiophene with one naphtheno ring, or benzothiophene with a phenyl group. The masses reach from 182 amu till 588 amu. The next series is DBE 11, which can be represented by acenaphthylthiophenes, has masses in the range of 208 - 600 amu, that it has from 0 to 28 carbon atoms in the side chains. The series of DBE 12 as well as 13, 14, 15, 16 and even two signals for DBE = 17 should be present already in fraction CD-3, but again the fractions overlap one another.

Fraction CD-3 (Figure 101) contains very intensive signals at low DBE. Aliphatic sulfur compounds should be removed from the sample after separation on silica/alumina bed and Pd(II)-MP SG. Probably, as mentioned already for the CD-3 fraction after oxidation with Pd and Se, some other compounds are eluted together with PASHs. Signals with DBE 6, 7 and 8 (of low intensity), 9, 10 and 11 are also present. The main series of the compounds for fraction CD-3 should be that of DBE 12. The main representatives are benzonaphthothiophenes. The mass range for this series is 234 - 486 amu. The next series of DBE 13 is even more intense then DBE 12 and can be represented by naphthenophenanthrothiophenes, or benzonapthothiophenes with one naphtheno ring, or dibenzothiophenes with one phenyl group. The masses are in the range of 232 - 512 amu. In the series of DBE 14 the masses are in the range of 258 - 552 amu. This series can be represented by pyrenothiophenes. Series of DBE = 15 is represented by chrysenothiophenes. The masses reach from 298 till 522 amu. For DBE = 16 masses range from 338 till 548 amu. This series is represented by cholanthrenothiophene. Series of DBE 17, 18 and few signals for DBE 19 are also present.

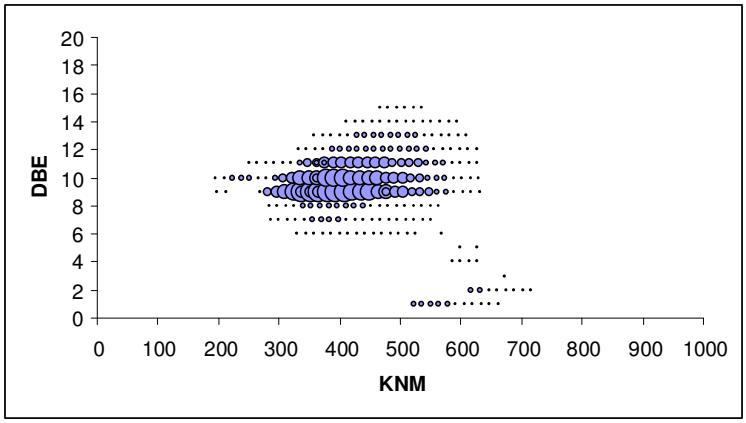

Figure 102 Kendrick plot for fraction CD-2_1* after HDS

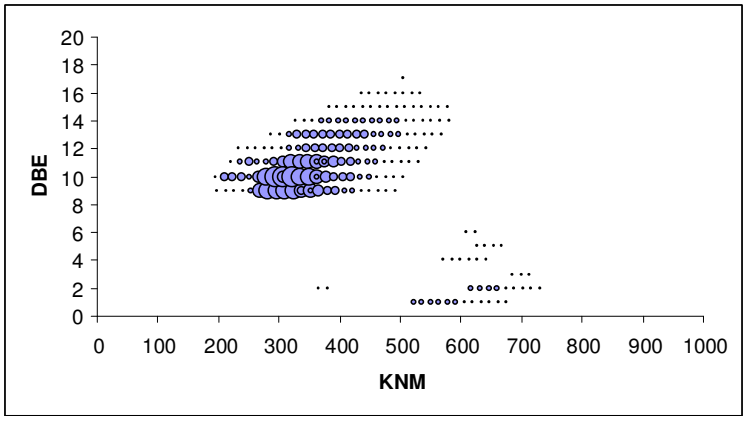

Figure 103 Kendrick plot for fraction CD-2_2* after HDS

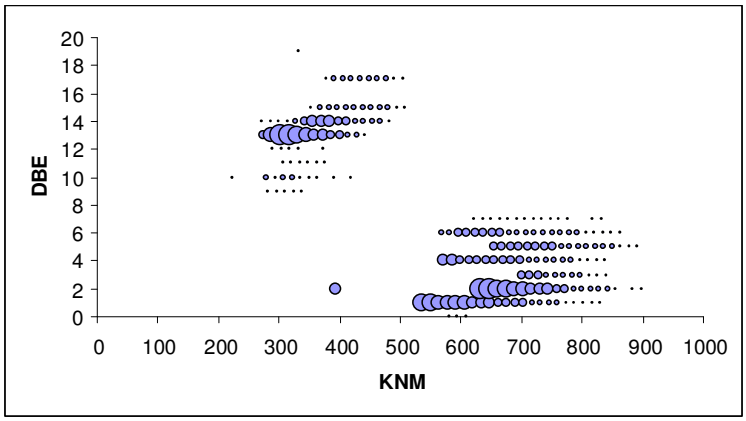

Figure 104 Kendrick plot for fraction CD-3* after HDS

Figures 102, 103 and 104 present the Kendrick plots for fraction CD-2_1*, CD-2_2* and CD-3* obtained after HDS process.

The separation of Pd-2 fraction reveals lack of fraction CD-1 which can be clearly seen in the HPLC chromatogram, Figure 98. FT-ICR MS measurements support these results. There are very low intensity signals for DBE 6 in the first collected fraction after HDS, CD-2_1* (Figure 102). Fraction CD-2_2* (Figure 103) is the continuation of fraction CD-2_1*, more overlaid with fraction CD-3*. Two fractions, CD-2_1* and CD-2_2* are collected with the elution time typical for fraction CD-2 before HDS. As the peak is slightly divided (which was not recorded before HDS), the two fractions are collected separately. More intensive signals are observed starting from DBE 9, the main series for fraction CD-2, before HDS, in both CD-2_1* and CD-2_2*. Lower DBE series are also present in CD-2_1*, and CD-2_2*, but they were also visible in fraction CD-2. In DBE 9 series, for dibenzothiophene 1 to 32 carbon atoms in the side chain are observed. For DBE 10 masses reach from 196 to 630 amu. In DBE 11 series, mass is in the range 222 - 628 amu, so from 1 to 30 carbon atoms in the side chain for acenaphthylthiophenes. Higher representative should be present already in fraction CD-3*, that is series with DBE equal 12 - 16 (even one signal for DBE = 17).

Fraction CD-3* (Figure 104) contains as CD-3 fraction before HDS very intensive signals by low DBE for some compounds of unknown origin. Low intensity signals with DBE 6, 9, 10, 11, even 12 are also present. As mentioned already earlier, the main series of the compounds for fraction CD-3 should be that of DBE 12. But the next series of DBE 13 is much more intense then DBE 12. Masses are in the range of 274 - 442 amu. In the series of DBE 14 masses are in the range 272 - 482 amu. Low intensity series of DBE = 15, 17 and one signal for DBE 19 are also present.

It is known already from the literature that generally alkylbenzonaphthothiophenes and alkylphenanthrothiophenes are more reactive

towards the HDS than alkyldibenzothiophenes where one of the alkyl substituents is located in either 4 or 6 position, but lower than alkylbenzothiophenes [34]. Investigations in this work support this claim. After the HDS process, there was no fraction CD-1 and thus no benzothiophenes, supported by HPLC and FT-ICR MS. They are the most reactive PASHs in the process. The most resistant compounds towards the HDS are those from fraction CD-2 (CD-2_1* and CD-2_2* after HDS), mainly represented by dibenzothiophenes. They are clearly visible in the HPLC chromatogram and in Kendrick plots. Before HDS, CD-2 contained DBE from mainly 6 to 17. After HDS the signals are recorded from DBE 6 till 17 as well. Also mass ranges remain unchanged. The CD-3 fraction, mainly benzonaphthothiophenes, seems to be more reactive in the HDS process than CD-2, but less than CD-1. A lot of signals especially of higher DBE and mass are lost from this fraction after the process.

7.3 Summary

The sulfur removal is an important aspect in environmental chemistry. Environmental legislation stresses the importance of lowering the amount of sulfur in fuels [20-22, 27, 30-32]. The HDS process removes sulfur from the sulfur compounds. A few aspects about the reactivity towards the HDS of the sulfur compounds are known, but still more investigation is needed to make the process more effective.

Here, fraction CD-1, the benzothiophene series, is the most reactive towards the HDS. The most resistant are compounds from fraction CD-2, mainly represented by dibenzothiophenes. The CD-3 fraction, mainly benzonaphthothiophenes, seems to be more reactive in the HDS process than CD-2, but less than CD-1. The HPLC results are supported by FT-ICR MS measurements and the data are presented in forms of the Kendrick plots for better visualization of the results. As fraction CD-2 is quite resistant to the HDS, it can be expected that alkyl substituents in the position 4 and/or 6 are present. It can be also deduced from the results obtained that longer chains can effectively lower the reactivity towards the HDS.

8 Summary

The present demand for energy and diminishing sources of crude oil make it necessary to use the heavier fractions of crudes. Their further processing is hampered, unfortunately, by the large amount of sulfur. The PASHs are the main sulfur-containing compounds in crudes and their concentration goes up with the boiling range. It is essential to get more information about the sulfur compound structures in these fractions, since it would help to increase the efficiency of desulfurization. The environmental regulations in many countries have reduced the maximum allowed sulfur content in fuels, as sulfur oxides produced during fossil fuel combustion are the major air pollutant causing acid rain. The sulfur compounds are also catalyst poisons in processes like fluid catalytic cracking, hydrocracking and catalytic reforming. Many PASHs are suspected to possess mutagenic or carcinogenic effects.

Many different techniques are used for the PASH identification and characterization. GC is one of the techniques, but the weakness of it is that only compounds with the possibility of being volatilized can be analyzed. HPLC can be applied for larger molecules. In recent years FT-ICR MS has taken a significant role in the characterization of complex mixtures of crude oils.

In the present work, the PASHs in VGO (Iranian Light) were investigated. The main goal was to obtain better structural knowledge about the PASHs with one sulfur atom in such a high-boiling fraction, information that can help to retune the desulfurization process to reduce the amount of residual sulfur in fuels.

For VGOs a better separation into fractions of specific structural characteristics is required. Despite the use of three LC steps, namely a silica/alumina bed, Pd(II)-MP SG and β-cyclodextrin, fractions are still overlapping one another. The perfect phase should be able to separate each parent system, but the heavy alkylation influences the retention times and makes the perfect separation difficult.

The first objective of this work thus was developing a better separation of the sulfur containing high-boiling fractions of a crude oil.

The vacuum gas oil was first fractionated on an open tubular column with silica and alumina, to perform a separation of the aromatics and saturates. Further, Pd(II)-MP SG was used, which separates the PAHs from PASHs. The standard separation was earlier carried out on Pd(II)-MP SG using silica with the pore size of 10 nm and the particle size of 10 µm. Here some other silica types were tested, with larger pore size, which allow the collection of compounds with higher masses.

The Pd-2 fraction was separated further on a β-cyclodextrin column into three fractions, according to the number of condensed aromatic rings. The Jordi Gel DVB Polyamino Resin investigated here shows similar behavior to the β-cyclodextrin column. The best conditions have been worked out for both separations.

In the next step of separation, a tetrachlorophthalimide silica gel was used. TCP-modified silica separates the aromatic compounds according to the number of fused aromatic rings, but other effects play an important role. The influence of the substituents connected to an aromatic system on the retention time was investigated, as well as different conditions for the optimal separation.

Different analytical methods were developed for the separated fractions analysis. FT-ICR MS appears as the most informative.

The chemical transformation of the real-world samples can help to develop our knowledge about the structures of the compounds in the complex mixture. Here the extensive chromatographic separation was combined with oxidation in order to get more information about the one-sulfur compounds in the higher-boiling cuts. Different oxidation agents were investigated for the effective dehydrogenation of naphtheno-substituted PASHs. It is important to find an agent which would dehydrogenate only the non-aromatic rings fused directly to the aromatic rings. That could then give information about the content of the specific connection in the mixture. Se as the oxidation agent appears to be the best choice. It oxidizes only rings fused to aromatic rings. The FT-ICR MS data are the most appropriate for the observation of the oxidation process. Thus, after the oxidation with Se it is estimated

that fraction CD-1 contains 10 % of benzothiophenes with condensed non-aromatic ring and fraction CD-2, 3 % of dibenzothiophenes with condensed naphtheno ring. Pd or DDQ show a much higher oxidation potential and thus oxidize also those saturated rings connected in other ways to aromatic rings are oxidized.

As sulfur removal is an important aspect in environmental chemistry, the HDS in which sulfur is removed from the sulfur-containing compounds was also investigated. The polynuclear organic sulfur compounds are known to be the least reactive sulfur compounds in the HDS reaction. Here it is shown that fraction CD-1, containing the benzothiophene series, is the most reactive towards the HDS. The compounds from fraction CD-2, mainly represented by dibenzothiophenes, are the most resistant. The explanation for that can be a large portion of the alkyl substituents in the position 4 and/or 6 in the dibenzothiophenic components. Fraction CD-3, mainly benzonaphthothiophenes, seems to be more reactive in the HDS process than CD-2, but less than CD-1.

Deeper investigation is needed for a better understanding of the behavior of the PASHs in the HDS process. Essential is developing more precise separation techniques to make further analytical work easier. The chemical transformation can give a more extensive knowledge about the structure pattern in the complex mixture, such as the parent structure of an aromatic system, the position and structure of alkyl groups for example. Such efforts can have an important influence on the HDS process and in this way developing new energy resources.

9 Zusammenfassung

Der stetig steigende Bedarf an Energie und die gleichzeitig abnehmenden Ressourcen von Rohöl machen es nötig auch schwerere Fraktionen von Rohöl zu nutzen. Ihre Verarbeitung wird durch den hohen Anteil an Schwefel erschwert. Polyzyklische aromatische Schwefelheterozyklen bilden den Hauptteil der Schwefelverbindungen in Rohöl, deren Konzentration mit höher werdendem Siedepunkt steigt. Es ist von größtem Interesse mehr Informationen über Schwefelverbindungen und ihre Struktur in diesen Fraktionen zu bekommen, da es sehr hilfreich für eine effizientere Entschwefelung wäre. Durch Umweltbestimmungen in vielen Ländern wurde die maximal erlaubte Menge an Schwefel in Treibstoffen reduziert. Schwefeloxide, die während des Verbrennungsprozesses von fossilen Treibstoffen entstehen, werden als eine Hauptursache für Luftverschmutzung und den daraus resultierenden sauren Regen genannt. Zusätzlich sind Schwefelverbindungen Gifte für Katalysatoren, welche für verschiedener Prozesse wie “fluid catalytic cracking“, “hydrocracking“ and “catalytic reforming“ eingesetzt werden. Viele PASHs stehen in Verdacht mutagene und carcinogene Effekte zu haben.

Viele verschiedene Techniken werden benutzt um PASH zu identifizieren und zu charakterisieren. GC ist eine dieser Techniken, aber eine Schwäche ist, dass nur flüchtige Verbindungen analysiert werden können. HPLC kann für größere Moleküle benutzt werden. In jüngster Zeit hat die FT-ICR MS eine wichtige Rolle bei der Charakterisierung komplexer Gemische von Rohölen übernommen.

In dieser Arbeit wurden PASHs in einem VGO (Iranian Light) untersucht. Die Zielsetzung war es, bessere Kenntnisse über die Struktur der PASHs in hochsiedende Fraktionen zu bekommen. Diese Informationen können helfen, den Entschwefelungsprozess dementsprechend zu verändern, dass der Anteil an Schwefel in Treibstoffen reduziert werden kann.

Für VGOs wird eine bessere Trennung in Fraktionen mit spezifischen Strukturcharakteristika benötigt. Trotz des Gebrauchs von drei LC Schritten (Kieselgel/Aluminiumoxid, Pd(II)-MP SG und β-Cyclodextrin) überlappen sich die Fraktionen dennoch. Die perfekte Phase sollte die Eigenschaften besitzen jedes Grundgerüst zu trennen, aber der hohe Einfluss der Alky-Gruppen auf die Retentionszeit gestaltet die Trennung schwierig. Ein erstes Ziel dieser Arbeit war, eine bessere Trennung der schwefelhaltigen hochsiedenden Fraktionen von Rohölen zu entwickeln.

Ein VGO wurde zuerst über eine Schwerkraftsäule mit Kieselgel und Aluminiumoxid fraktioniert, um Aromaten von Aliphaten zu trennen. Weiterhin wurden mittels Pd(II)-MP SG PAHs von PASHs separiert. Die Standard-Trennung wurde zuvor auf Pd(II)-MP SG durchgeführt, wobei Kieselgel mit einer Porengröße von 10 nm und einer Partikelgröße von 10 µm benutzt wurde. Es wurden Kieselgele mit größeren Porendimensionen getestet, um einen Zugang zu größeren Molekülen zu erlangen.

Die Pd-2 Fraktion wurde weiterhin über eine ß-Cyclodextrin Säule in drei Teile getrennt, der Nummer der kondensierten aromatischen Ringe entsprechend. Das Jordi Gel DVB Polyamino Harz, welches hier untersucht wurde, zeigt ein ähnliches Verhalten wie die ß-Cyclodextrin Phase. Die besten Bedingungen wurden für beide Methoden erarbeitet.

Im nächsten Schritt wurde ein Tetrachlorophthalimid Kieselgel zur Trennung genutzt. TCP-modifiziertes Kieselgel trennt die aromatischen Verbindungen entsprechend der Anzahl an kondensierten aromatischen Ringen, wobei auch andere Effekte eine wichtige Rolle einnehmen. Der Einfluss der Substituenten an einem aromatischen System auf die Retentionszeit wurde erforscht wie auch verschiedene Bedingungen für die optimale Trennung.

Verschiedene analytische Methoden wurden für Analyse der getrennten Fraktionen evaluiert. FT-ICR MS scheint die besten Informationen zu liefern.

Die chemische Umwandlung von Realproben kann helfen unser Wissen über die Strukturen von Verbindungen aus einer komplexen Mixtur zu erweitern. Die

intensive chromatographische Trennung wurde mit einer Oxidation kombiniert, um mehr Informationen über die PASHs in den schwerflüchtige Fraktionen zu erhalten. Es wurden verschiedene Oxidationsmittel hinsichtlich einer erfolgreichen Aromatisierung der teilgesättigten PASHs untersucht. Hierbei ist es wichtig, ein Oxidationsmittel zu finden, durch das nur kondensierte Systeme oxidiert werden. Dies kann Informationen über den Inhalt von spezifischen Verbindungen in den Gemischen liefern. Selen als Oxidationsreagenz ist die beste Wahl. Es oxidiert lediglich Ringe, die an Aromaten gebunden sind. Die FT-ICR MS Daten sind am besten geeignet, um den Oxidationsprozess zu überwachen. Nach der Oxidation mittels Selen lässt sich die Menge an Benzothiophen mit einem kondensierten teilgesättigten Ring in Fraktion CD-1 mit etwa 10 % und an Dibenzothiophen mit einem kondensierten Naphtheno-Ring in Fraktion CD-2 mit 3 % abschätzen. Pd und DDQ verfügen über ein zu hohes Oxidationspotential und sind somit in der Lage nicht kondensierte gesättigte Ringe zu aromatisieren.

Weil die Eliminierung von Schwefel ein wichtiger Aspekt in der Umweltchemie ist, wurde die HDS, in welcher Schwefel aus den schwefelhaltigen Molekülen entfernt wird, ebenso untersucht. Bei mehrkernigen organischen Schwefelverbindungen ist bekannt, dass sie die am wenigsten reaktiven Verbindungen in der HDS-Reaktion sind. Es zeigt sich, dass die CD-1 Fraktion, welches die Benzothiophen-Reihe beinhaltet, die höchste Reaktivität gegenüber der HDS hat. Die Verbindungen der CD-2 Fraktion, hauptsächlich repräsentiert durch Dibenzothiophene, zeigen die höchste Resistenz. Die Erklärung kann sein dass ein großer Anteil von Alkylgruppen in Position 4 und/oder 6 in den Dibenzothiophen-Verbindungen sind. Die CD-3 Fraktion, größtenteils Benzonaphthothiophen, scheint reaktiver als CD-2, aber wenig reaktiv als CD-1 im HDS-Prozess zu sein.

Weitergehende Untersuchungen sind dennoch nötig, um ein besseres Verständnis über das Verhalten der PASH im HDS-Prozess zu bekommen. Die Entwicklung effizientere Trennmethoden ist nötig, um die weitere analytische Arbeit

einfacher zu gestalten. Durch chemische Umwandlung kann detaillierteres Wissen über Strukturmodelle in komplexen Gemischen erhalten werden, wie die Grundstrukturen des aromatischen Systems und Position und Struktur von Alkylgruppen. Solche Bestrebungen können einen starken Einfluss auf den HDS-Prozess haben, um den Weg für neue Energieressourcen zu entwickeln.

10 Appendix

10.1 Synthesis of Model Thiophenic Compounds

10.1.1 Synthesis of Tetrahydrodibenzothiophene

10.1.1.1 Synthesis of 2-Bromocyclohexanone

9.38 mL (0.09 mole) of cyclohexanone was added to 24 g of ice water and stirred strongly. The solution was kept at low temperature using an ice-water bath during the following reaction. During 12 h, 4.22 mL (0.08 mole) of bromine was added. Then the mixture was added to 16 mL ice-water and extracted three times with 20 mL chloroform. The combined extracts were washed with saturated sodium carbonate solution and water, and dried with sodium sulfate. After filtration the solvent was removed [219, 231, 232].

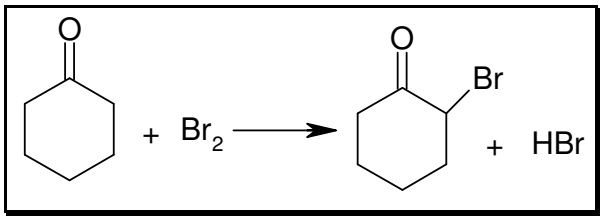

Figure 105 Synthesis of 2-bromocyclohexanone

The yield of the reaction was 84 %, but the product was contaminated as indicated by MS measurement with dibromocyclohexanone and cyclohexanone. The product was used directly for the next step.

10.1.1.2 Sythesis of Tetrahydrodibenzothiophene (One-Pot Synthesis)

10.1.1.2.1 Preparation of Na_2CO_3/SiO_2

Silica gel (16.82 g) was added to a solution of sodium carbonate (30 mmol, 3.18 g) in distilled H_2O, and the mixture was stirred at room temperature for 0.5 h.

Then, H_2O was removed be rotary evaporator under reduced pressure and the resulting reagent was dried in vacuo at 160 °C for 5 h.

10.1.1.2.2 Preparation of PPA/SiO_2

The polyphosphoric acid (PPA, 2 g) and $CHCl_3$ (100 mL) were placed in a round-bottom flask and the mixture was stirred at 50 °C for 1 h. SiO_2 (18 g), which had been dried in vacuo at 160 °C for 2 h, was added to the mixture, and the mixture was stirred for another 1 h. Then the $CHCl_3$ was removed on a rotary evaporator and the resulting solid was dried in vacuo at room temperature for 3 h.

10.1.1.2.3 Procedure

A mixture of α-haloketone (2-bromocyclohexanone, 1 mmol, 0.1 mL), arylthiol (thiophenol, 1 mmol, 0.1 mL), Na_2CO_3/SiO_2 (1 g, 1.5 mmol) and PPA/SiO_2 (3.5 g, 10 wt %) in chlorobenzene (15 mL) was stirred at 135 °C for 6 h, and then the supported reagents were removed by filtration. The filtrate was evaporated to leave crude product, which was purified by flash column chromatography (with cyclohexane) to give desired product [233]. The yield reached 69 %.

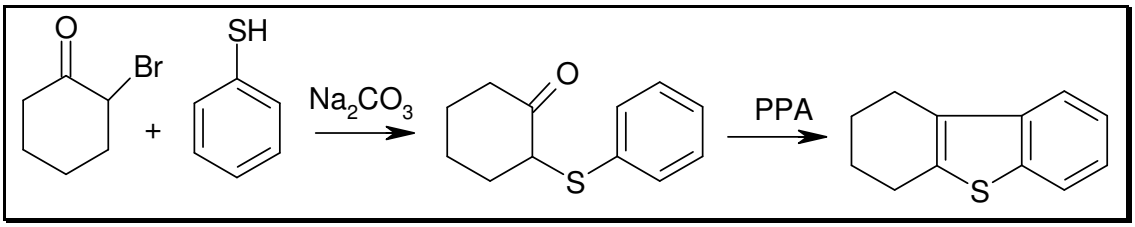

Figure 106 One-pot synthesis

Purity: 96 % (GC)

MS (EI, 70 eV): 188 (100 %, M^+), 160 (94 %, $M^+ - C_2H_4$)

^{1}H NMR (400 MHz, CD_2Cl_2) δ = 7.1 - 7.86 ppm (m, 4 H; *Ar*), 2.7 ppm (t, 4H; CH_2ArCH_2) 1.65 ppm (m, 4 H; CH_2CH_2)

Mp = oil

CH Analyses:

	C (%)	H (%)
Calculated	76.59	6.38
Measurement 1	76.79	6.51
Measurement 2	76.55	6.42

10.1.2 Synthesis of 2-Cyclohexylmethanobenzothiophene

Benzothiophene (2.18 g, 16.3 mmoles) was dissolved in THF (24 mL) under argon atmosphere. 15.2 mL of a 1.6 M solution of *n*-butyllithium in hexanes (24.5 mmoles) were added dropwise to the reaction mixture, which was then refluxed for 1.5 h. After cooling to 0 °C, 3.4 mL of cyclohexylmethyl bromide (24.5 mmoles) were added slowly and the mixture was allowed to stir one night at room temperature. It was then put into a flask with 80 mL of ice-water. The product was extracted with ethyl acetate (2 × 30 mL), the organic phase was washed, dried over sodium sulfate and the solvent was removed [234, 235]. The brown oil was purified on a silica column using cyclohexane as the eluent, and by distillation under reduced pressure. The yield was 45 %.

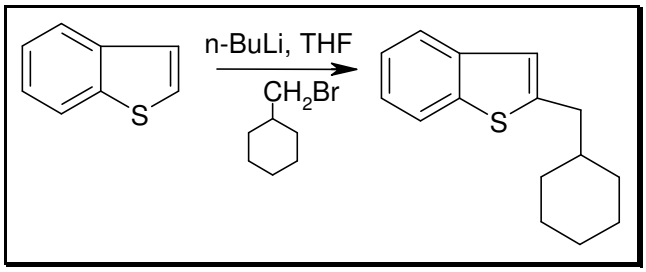

Figure 107 Synthesis of 2-cyclohexylmethanobenzothiophene

Purity: 99.7 % (GC)

MS (EI, 70 eV): 230 (41 %, M^+), 148 (100 %, M^+ - C_6H_{10}), 147 (40 %, M^+ - C_6H_{11})

^{1}H NMR (400 MHz, CD_2Cl_2) δ = 7.1 - 7.9 ppm (m, 4 H; *Ar*), 6.95 ppm (s, 1 H; SC*CH*), 2.75 ppm (d, 2 H; SCCH_2), 1 - 1.8 ppm (m, 11 H, $CH(CH_2)_5$)

Mp = room temp.

CH Analyses:

	C (%)	H (%)
Calculated	78.26	7.83
Measurement 1	78.09	7.87
Measurement 2	78.16	7.82

10.1.3 Synthesis of 2-Cyclohexylethanobenzothiophene

Benzothiophene (2.18 g, 16.3 mmoles) was dissolved in THF (24 mL) under argon atmosphere. 15.2 mL of a 1.6 M solution of *n*-butyllithium in hexanes (24.5 mmoles) were added dropwise to the reaction mixture, which was then refluxed for 1.5 h. After cooling to 0 °C, 3.75 mL of cyclohexylethyl bromide (24.5 mmoles) were added slowly and the mixture was allowed to stir one night at room temperature. It was then put into a flask with 80 mL of ice-water. The product was extracted with ethyl acetate (2 × 30 mL), the organic phase was washed, dried over sodium sulfate and the solvent was removed [234, 235]. The brown oil was purified on a silica column using cyclohexane as the eluent, and by distillation under reduced pressure. The yield was 46 %.

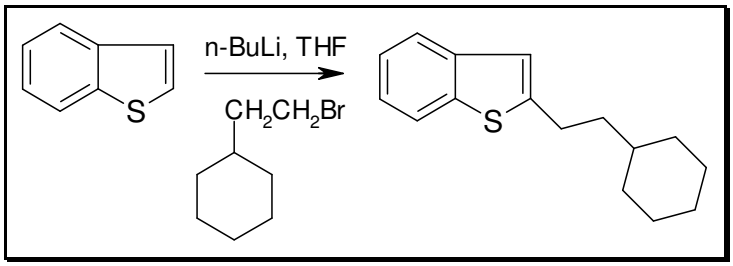

Figure 108 Synthesis of 2-cyclohexylethanobenzothiophene

Purity: 99.8 % (GC)

MS (EI, 70 eV): 244 (30 %, M^+), 148 (100 %, M^+ - C_7H_{12}), 147 (77 %, M^+ - C_7H_{13})

^{1}H NMR (400 MHz, CD_2Cl_2) δ = 7.2 - 7.8 ppm (m, 4 H; *Ar*), 7 ppm (s, 1 H; SC*CH*), 2.9 ppm (t, 2 H; SCCH_2), 1 - 1.8 ppm (m, 13H, $CH_2CH(CH_2)_5$)

Mp = 28 - 30 °C

CH Analyses:

	C (%)	**H (%)**
Calculated	78.69	8.20
Measurement 1	77.16	8.24
Measurement 2	76.39	8.18

10.1.4 Synthesis of 2-Benzylbenzothiophene

Benzothiophene (2.18 g, 16.3 mmoles) was dissolved in THF (24 mL) under argon atmosphere. 15.2 mL of a 1.6 M solution of *n*-butyllithium in hexanes (24.5 mmoles) were added dropwise to the reaction mixture, which was then refluxed for 1.5 h. After cooling to 0 °C, 6 mL of benzyl bromide (24.5 mmoles) were added slowly and the mixture was allowed to stir one night at room temperature. It was then put into a flask with 80 mL of ice-water. The product was extracted with ethyl acetate (2 × 30 mL), the organic phase was washed, dried over sodium sulfate and the solvent was removed [234, 235]. The brown oil was purified on a silica column using cyclohexane as the eluent, and by distillation under reduced pressure. The yield was 78 %.

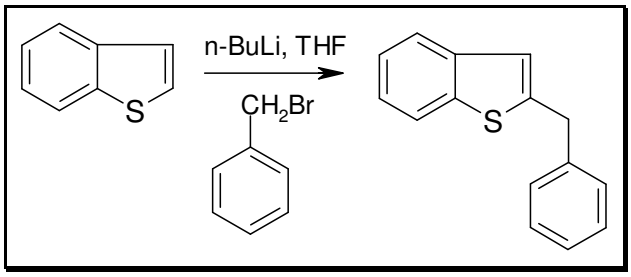

Figure 109 Synthesis of 2-benzylbenzothiophene

Purity: 97.8 % (GC)

MS (EI, 70 eV): 224 (100 %, M^+), 223 (87 %, M^+ - H), 147 (36 %, M^+ - C_6H_5)

^{1}H NMR (400 MHz, CD_2Cl_2) δ = 7.1 - 7.8 ppm (m, 9 H; *Ar*), 6.95 ppm (s, 1 H; SC*CH*), 4.1 ppm (s, 2 H; *CH_2)*

Mp = 78 - 79 °C

CH Analyses:

	C (%)	**H (%)**
Calculated	80.36	5.36
Measurement 1	79.78	5.01
Measurement 2	79.70	5.30

10.1.5 Synthesis of 4-Decyldibenzothiophene

Dibenzothiophene (3 g, 16.3 mmoles) was dissolved in THF (24 mL) under argon atmosphere. 15.2 mL of a 1.6 M solution of *n*-butyllithium in hexanes (24.5 mmoles) were added dropwise to the reaction mixture, which was then refluxed for 1.5 h. After cooling to 0 °C, 5.23 mL of 1-iododecane (24.5 mmoles) were added slowly and the mixture was allowed to stir one night at room temperature. It was then put into a flask with 80 mL of ice-water. The product was extracted with ethyl acetate (2 × 30 mL), the organic phase was washed, dried over sodium sulfate and the solvent was removed [234, 235]. The purification was done by column chromatography on silica and elution with a 1:1 mixture of cyclohexane and pentane. The yield reached 35 %.

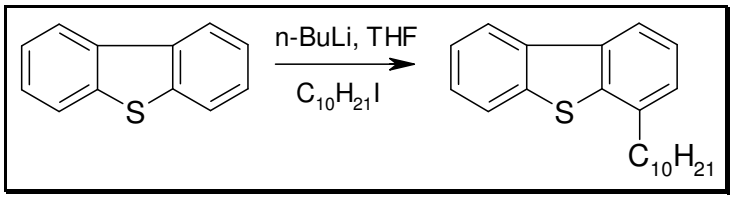

Figure 110 Synthesis of 4-decyldibenzothiophene

Purity: 99.2 % (GC)

MS (EI, 70 eV): 324 (56 %, M^+), 198 (100 %, M^+ - C_9H_{18}), 197 (49 %, M^+ - C_9H_{19})

^{1}H NMR (400 MHz, CD_2Cl_2) δ = 7.2 - 8.2 ppm (m, 7 H; *Ar*), 2.9 ppm (t, 2 H; Ar*CH_2*), 0.9 - 1.9 ppm (m, 19 H; *$(CH_2)_8CH_3$)*

Mp = 40 - 42 °C

CH Analyses:

	C (%)	**H (%)**
Calculated	81.48	8.64
Measurement 1	80.03	8.77
Measurement 2	80.71	8.84

10.1.6 Synthesis of 2-Decylbenzothiophene

Benzothiophene (2.18 g, 16.3 mmoles) was dissolved in THF (24 mL) under argon atmosphere. 15.2 mL of a 1.6 M solution of *n*-butyllithium in hexanes (24.5 mmoles) were added dropwise to the reaction mixture, which was then refluxed for 1.5 h. After cooling to 0 °C, 5.23 mL of 1-iododecane (24.5 mmoles) were added slowly and the mixture was allowed to stir one night at room temperature. It was then put into a flask with 80 mL of ice-water. The product was extracted with ethyl acetate (2 × 30 mL), the organic phase was washed, dried over sodium sulfate and the solvent was removed [234, 235]. The purification was done by column chromatography on silica and elution with pentane. The yield reached 33 %.

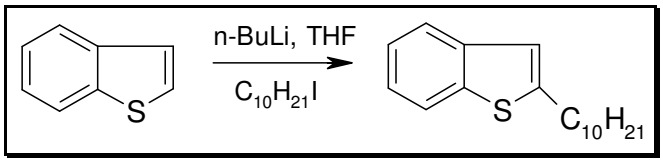

Figure 111 Synthesis of 2-decylbenzothiophene

Purity: 99.9 % (GC)

MS (EI, 70 eV): 274 (20 %, M^+), 148 (100 %, M^+ - C_9H_{18}), 147 (60 %, M^+ - C_9H_{19})

^{1}H NMR (400 MHz, CD_2Cl_2) δ = 7.2 - 8 ppm (m, 4 H; *Ar*), 7.05 ppm (s, 1 H; SC*CH*), 3 ppm (t, 2 H; ArCH_2), 1 - 1.9 ppm (m, 19 H, $(CH_2)_8CH_3$)

Mp = room temp.

CH Analyses:

	C (%)	**H (%)**
Calculated	78.83	9.49
Measurement 1	78.52	9.58
Measurement 2	78.77	9.55

10.1.7 Synthesis of 2-Eicosylbenzothiophene

Benzothiophene (1.1 g, 8.15 mmoles) was dissolved in THF (12 mL) under argon atmosphere. 7.6 mL of a 1.6 M solution of *n*-butyllithium in hexanes (12.25 mmoles) were added dropwise to the reaction mixture, which was then refluxed for 1.5 h. After cooling to 0 °C, 4.42 g of 1-bromoeicosane (12.25 mmoles) were added slowly and the mixture was allowed to stir one night at room temperature. It was then put into a flask with 40 mL of ice-water. The product was extracted with ethyl acetate (2 × 30 mL), the organic phase was washed, dried over sodium sulfate and the solvent was removed [234, 235]. The purification was done by column chromatography on silica and elution with pentane. The yield reached 55 %.

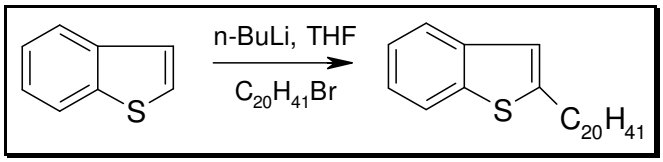

Figure 112 Synthesis of 2-eicosylbenzothiophene

Purity: 99.3 % (GC)

MS (EI, 70 eV): 414 (22 %, M^+), 148 (100 %, M^+ - $C_{19}H_{38}$), 147 (32 %, M^+ - $C_{19}H_{39}$)

^{1}H NMR (400 MHz, CD_2Cl_2) δ = 7.2 - 7.9 ppm (m, 4 H; *Ar*), 7.1 ppm (s, 1 H; SC*CH*), 2.9 ppm (t, 2 H; ArCH_2), 1.1 - 9 ppm (m, 19 H, $(CH_2)_{18}CH_3$)

Mp = 58 - 60 °C

CH Analyses:

	C (%)	**H (%)**
Calculated	81.16	11.11
Measurement 1	80.54	11.20
Measurement 2	81.05	11.18

10.2 Synthesis of Pd(II)-Mercaptopropano Silica Gel

Silica gel (different kinds were used as follows: LiChrosorb Si 100, 10 µm; YMC Gel Silica 12 nm S-5 µm; YMC Gel Silica 20 nm S-5 µm) was dried at 120 °C for 16 h. 10 g of dried silica gel was then refluxed in a solution of 15 mL 3-mercaptopropanotrimethoxysilane in 50 mL of dry toluene for 8 h. The bonded silica gel was filtered off and washed with toluene and methanol (around 30 mL). The obtained mercaptopropano silica gel (MP SG) was dried at 50 °C for 1 day.

2.5 g of MP SG was further treated with 250 mL of aqueous palladium chloride solution (C = 0.01 M) for at least 8 h (on shaker). The palladium bonded silica phase was filtered off, washed with isopropanol, then cyclohexane and dried in vacuo at room temperature for 2 days.

10.3 Synthesis of Tetrachlorophthalimide Silica Gel

10.3.1 Synthesis of Tetrachlorophthalicmonoallylamide-allylammonium Salt

28.6 g of tetrachlorophthalic anhydride was added to 45.6 g of allylamine. The reaction was left till the exotermic process stopped. Then the reaction mixture was refluxed until all of the tetrachlorophthalic anhydride dissolved. The excess of allylamine was removed under vacuum afterwards. The residues were white crystals of the allyl ammonium salt.

10.3.2 Synthesis of Tetrachlorophthalicallylimide

39.8 g of raw allyl ammonium salt was heated at 250 °C under vacuum. After the salt melt, it was heated another 10 min. The solid dark brown product was recrystallized from toluene and taken for the next step of the synthesis.

CHN Analyses:

	C (%)	H (%)	N (%)
Calculated	40.62	1.54	4.31
Measurement 1	40.46	1.70	4.31
Measurement 2	40.48	1.68	4.48

10.3.3 Synthesis of Tetrachlorophthalimidopropanotrichlorosilane

10.5 g of tetrachlorophthalicallylimide, 9.53 mL of freshly distilled trichlorosilane and 30 drops of a 0.1 molar solution of hexachloroplatinic acid in isopropanol were dissolved in 100 mL abs. dichloromethane and refluxed under a dry nitrogen atmosphere for 24 h. Afterwards, the excess of trichlorosilane and solvent were removed under vacuum. The yellow solid residue was washed in the flask with

a small amount of dichloromethane. Dichloromethane was decanted and the product was instantly dissolved in fresh 100 mL abs. dichloromethane.

10.3.4 Synthesis of Tetrachlorophthalimidopropanosilica

10 g of silica gel (LiChrosorb Si 100, 10 µm) was suspended in the above mentioned solution. 15 mL of abs. quinoline was added to it and the mixture was refluxed for 48 h under a nitrogen atmosphere. All the solid particles were removed from the solution afterwards by filtering the mixture trough a glass filter. The modified silica gel was washed with 100 mL toluene, dichloromethane, methanol and acetone and dried at 80 °C for 12 h [75].

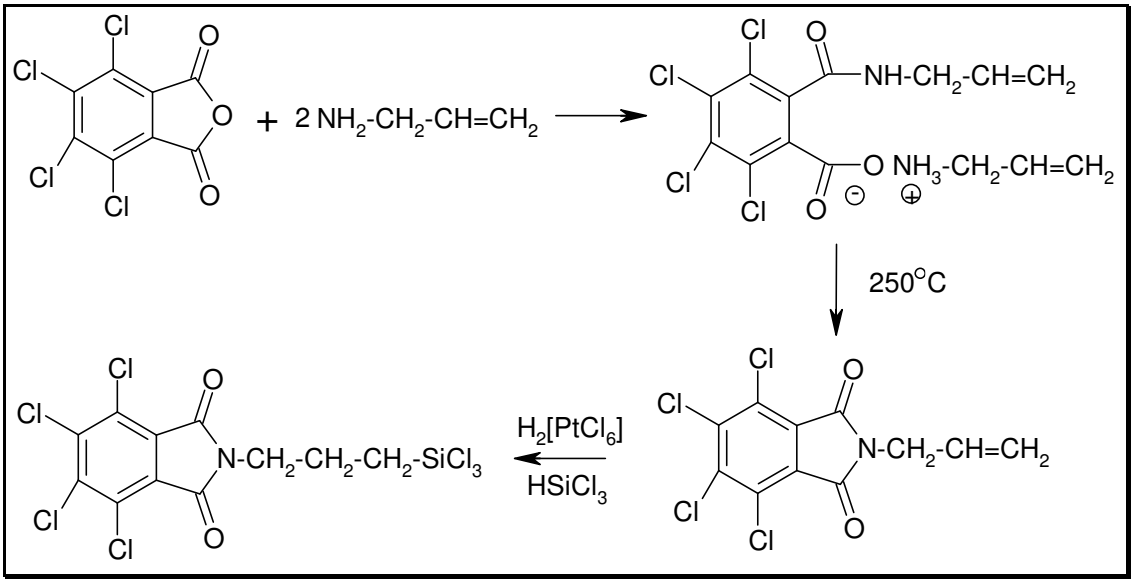

Figure 113 Synthesis of tetrachlorophthalimidopropanotrichlorosilane [75]

CHN Analyses:

	C (%)	H (%)	N (%)
Measurement 1	6.30	1.22	0.55
Measurement 2	6.25	1.18	0.68

10.4 Instrumental Parameters

10.4.1 High-Performance Liquid Chromatography

Knauer Wellchrom

Knauer HPLC system was composed of an interface box, 4 channel solvent degasser, 2 Ministar K 501 analytical pumps, a mixing chamber, an electrical injection valve or basic marathon plus autosampler and a variable wavelength detector (applied at 254 nm). Instrumental control and data collection were done using ChromGate version 2.8.

HP 1050

Hewlett-Packard 1050 HPLC system is composed of a quaternary pump, degasser, manual injection valve and a diode array detector set to record the UV spectra from 200 to 500 nm. Instrumental control and data collection were done using HP ChemStation Rev. A.09.03.

10.4.2 Gas Chromatography

GC-MS

Gas chromatograph:	Finnegan MAT GCQ
Mass spectrometer:	Finnegan MAT GCQ Polaris MS (quadrupole ion trap)
Autosampler:	CTC A200S Liquid Sampler
Injector:	Spli/Splitless (60s)
Injector temperature:	280 °C
Capillary column:	DB-5ms (Agilent), 30 m x 0.25 mm x 0.25 µm
Carrier gas:	Helium 6.0 (BIP), 1.4 mL/min
Temperature program:	60 °C - 1 min - 20 °C/min - 300 °C - 5 min
Injection volume:	1 µL
Transfer line:	275 °C
Ionization condition:	EI, 70 eV, 200 °C
Modus:	Full Scan (50 - 600 amu) and SIM
Instrumental control:	Xcalibur Version 1.3

GC-FID

Gas chromatograph:	Hewlett-Packard 5890 II
Detector temperature:	300 °C
Autosampler:	Gerstel MPS 2L
Injector:	Spli/Splitless (60 s)
Injector temperature:	280 °C
Capillary column:	DB-5ms (Agilent), 30 m x 0.25 mm x 0.25 µm
Carrier gas:	Hydrogen 5.0, 1.4 mL/min
Temperature program:	60 °C - 1 min - 20 °C/min - 300 °C - 5 min
Injection volume:	1 µL
Instrumental control:	HP ChemStation Rev. A.09.03

GC-AED

Gas chromatograph:	Agilent 6890N
Atomic emission detector:	Agilent G2350A
Autosampler:	Gerstel MPS 2L
Injector:	Gerstel cold injection system
Injector temperature:	60 °C - 12 °C/s - 300 °C
Capillary column:	DB-5ms (Agilent), 30 m x 0.25 mm x 0.25 µm
Carrier gas:	Helium 6.0 (BIP), 1.4 mL/min
Temperature program:	60 °C - 1 min - 20 °C/min - 300 °C - 5 min
Injectror:	1 µL
Transfer line:	300 °C
Instrumental control:	HP GC ChemStation Rev. A.07.01

10.4.3 Fourier Transform Ion Cyclotron Resonance Mass Spectrometry

Mass spectra were obtained using APEX III FT-ICR MS (Bruker Daltonics) equipped with 7 T actively shield super conducting magnet and an Agilent ESI source. The samples were introduce in a 1:1 (v/v) solution of dichloromethane/acetonitrile and injected in the infusion mode with a flow rate of 2 µL/min, detecting positive ions. The spray voltage was maintained at 4.5 kV. After vionization process, the ions were accumulated for 0.5 s in the octapol before transferring to the cyclotron cell. At least 64 scans were accumulated for better signal-to noise ratio. Internal and external calibration were done using a mixture of the Agilent electrospray calibration solution of masses 322.04812, 622.02896 and 922.00980 covering the whole range of masses in the sample. All the FT-ICR MS measurements were performed in collaboration with Max-Planck-Institute of Coal Research in Mülheim an der Ruhr (Germany).

10.4.4 Nuclear Magnetic Resonance

Varian 600 unity plus (600 MHz) with 3 channels, pulsed field z-gradients and pulseshaping for all real-word samples and Bruker AV400 for model thiophenic compounds were used (Service Department in the Institute of Organic Chemistry).

10.4.5 Elemental CHN Analyses

Vario EL III CHNOS elemental analysis system was used (Service Department in the Institute of Inorganic and Analytical Chemistry).

10.4.6 Fluorescence spectroscopy

AMINCO Bowman Serie 2 Luminescence Spectrometer (Spectronic Unicam) with software: AB2 Luminescence Spectrometer Ver. 5.00 was applied.

10.5 Materials

Acetone	> 99,5 %	Fluka
Allylamine	98 %	Aldrich
Aluminum oxide, 50 -200 µm	for chromatography	Acros Organics
Argon		in house
Benzo[*b*]naphtho[1,2-*d*]thiophene	> 98 %	in house
Benzo[*b*]naphtho[2,1-*d*]thiophene	> 98 %	in house
Benzo[*b*]phenanthro[9,10-*d*]thiophene	> 98 %	in house
Benzothiophene	95 %	Aldrich
Benzyl bromide	> 98 %	Sigma-Aldrich
Bromine	99.99 %	Sigma-Aldrich
1-Bromoeicosane	97 %	ABCR
n-Butyllithium	1.6 M in hexanes	Acros Organics
tert-Butyl methyl ether	>99.5 %	Merck
p-Chloranil	97 %	Merck
Chlorobenzene	99 %	Acros Organics
Chloroform	99.36 %	Normapur
Copper sulfate		in house
β-Cyclodextrin	for HPLC	Merck
Cyclohexane	99.99 %	Acros Organics
Cyclohexanone	99.8 %	Acros Organics
Cyclohexylethyl bromide	98 %	Acros Organics
Cyclohexylmethyl bromide	96 %	Acros Organics
DDQ	> 95 %	Fluka
Decalin	97 %	ABCR
Dibenzothiophene	99 %	Acros Organics
1,2-Dichloroethane	99.91 %	Fisher
Dichloromethane	99.99 %	Acros Organics
2,3-Dimethylbenzothiophene	> 98 %	in house
2,4-Dimethyldibenzothiophene	> 98 %	in house
2,6-Dimethyldibenzothiophene	> 98 %	in house
2-Dodecylbenzothiophene	> 98 %	in house
Ethanol	95 %	Acros Organics

Ethyl acetate	99.5 %	Acros Organics
4-Ethyldibenzothiophene	> 98 %	in house
n-Heptane	99 %	Grüssing
Hexachloroplatinic acid	> 99.9 %	Acros Organics
1-Iododecane	98 %	ABCR
Isopropanol	99.5 %	Acros Organics
Jordi Gel DVB Polyamino Resin, 100 nm, 5 µm	for HPLC	Jordi
3-Mercaptopropanotrimethoxysilane	95 %	ABCR
Methanol	min. 99.8 %	Normapur
Methyl iodide	99 %	Aldrich
3-Methylbenzothiophene	> 98 %	in house
5-Methylbenzothiophene	> 98 %	in house
2-Methyldibenzothiophene	> 98 %	in house
4-Methyldibenzothiophene	> 98 %	in house
Methylene chloride D2	99.9 %	Euriso-top
Nitrogen		in house
4-Octyldibenzothiophene	> 98 %	in house
Palladium	10 % Pd/C	Fluka
Palladium(II) chloride	min. 59 %	Applichem
n-Pentane	> 99 %	Acros Organics
Phenanthro[4,5-*bcd*]thiophene	> 98 %	in house
Phenanthro[2,1-*b*]thiophene	> 98 %	in house
Polyphosphoric acid	> 83%	Sigma-Aldrich
Quinoline	96 %	Acros Organics
Selenium		in house
Silica gel 60, 63 – 200 µm	for chromatography	Fluka
Silica, LiChrosorb Si 100, 10 nm, 10 µm	for HPLC	Merck
Silica, YMC Gel Silica, 12 nm, 5 µm	for HPLC	YMC
Silica, YMC Gel Silica, 20 nm, 5 µm	for HPLC	YMC
Silver tetrafluoroborate	98 %	Aldrich
Sodium carbonate		in house
Sodium sulfate	98 %	Grüssing
Tetrachlorophthalic anhydride	98 %	Acros Organics
Tetrahydro[*b*]naphtho[1,2-*d*]thiophene	> 98 %	in house

Tetrahydrofuran	> 99 %	Sigma-Aldrich
2,4,6,8-Tetramethyldibenzothiophene	> 98 %	in house
Thiophenol	> 99 %	Acros Organics
Toluene	min. 99.7 %	KMF OptiChem
Trichlorosilane	99 %	Sigma-Aldrich
2,3,7-Trimethylbenzothiophene	> 98 %	in house

10.6 Abbreviations and Symbols

AAS	Atomic absorption spectroscopy
AED	Atomic emission detector
amu	Atomic mass unit
API	Atmospheric pressure ionization
APCI	Atmospheric pressure chemical ionization
APLI	Atmospheric pressure laser ionization
APPI	Atmospheric pressure photoionization
atm	Standard atmosphere (101.325 kPa)
BIP	Built-in-purifier
BT	Benzothiophene
CD (1, 2, 3)	Fractions after separation on β-cyclodextrin
CD (2_1*, 2_2*, 3*)	Fractions after HDS and separation on β-cyclodextrin
CE	Capillary electrophoresis
CI	Chemical ionization
Da	Dalton, unit of mass
DAD	Diode array detector
DBE	Double bond equivalent
DB-5ms	Cross-linked phase composed of 5 % phenyl, 95 % dimethylpolysiloxane
DBT	Dibenzothiophene
DDQ	2,3-Dichloro-5,6-dicyano-1,4-benzoquinone
DNB	3,5-Dinitrobenzoic acid
EI	Electron impact ionization
EPA	Environmental Protection Agency
ESI	Electrospray ionization
e.g.	Exempli gratia, for example
et al.	Et alii, and others
etc.	Et cetera ,and so on
eV	Electron volt
FCC	Fluid catalytic cracking
FD	Field desorption
FI	Field ionization

FPD	Photometric detector
FT-ICR MS	Fourier transform ion cyclotron resonance mass spectrometry
GC	Gas chromatography
GC x GC	Two-dimensional gas chromatography
GPC	Gel permeation chromatography
HDS	Hydrodesulfurization
HPLC	High-performance liquid chromatography
HRMS	High-resolution mass spectrometry
i.e.	Id est, that is
IL	Iranian Light
IR	Infrared spectroscopy
KM	Kendrick mass
KMD	Kendrick mass defect
KNM	Kendrick nominal mass
kWh	Kilowatt hour
LC-MS	Liquid chromatography-mass spectrometry
LEC	Ligand exchange chromatography
$M^{+\cdot}$	Molecular ion
MALDI	Matrix-assisted laser desorption ionization
MS/MS	Tandem mass spectrometry
m/z	Mass-to-charge ratio
NMR	Nuclear magnetic resonance
NP-HPLC	Normal-phase high-performance liquid chromatography
OSC	Organic sulfur compounds
PAHs	Polycyclic aromatic hydrocarbons
PASHs	Polycyclic aromatic sulfur heterocycles
Pd(II)-MP SG	Pd(II)-Mercaptopropanomsilica gel
Pd (1, 2)	Fractions after separation on Pd(II)-MP SG
Pd/C	Palladium on carbon
PDN	4-Aminophthalodinitrile
PPA	Polyphosphoric acid
ppm	Parts per milion
QIT	Quadrupole ion trap
RF	Radio frequency (3 Hz - 300GHz)

RI	Refractive index
RP-HPLC	Reversed-phase high-performance liquid chromatography
S1 class	Compounds with one sulfur atom
SCD	Chemoluminescence detector
SIM	Selected ion monitoring
T	Tesla
TBME	*Tert*-butyl methyl ether
TCP	Tetrachlorophthalimide
TIC	Total ion chromatogram
TOF	Time-of-flight
TSP	Thermospray
UV-vis	Ultraviolet-visible
Ver.	Version
VGO	Vacuum gas oil
vs.	Versus, contra
v/v	Volume per volume
XPS	X-Ray Photoelectron spectroscopy
z	“Hydrogen deficiency”
z*	Nominal mass series

11 References

(1) www.energy.gov/energysources/index.html.
(2) www.darvill.clara.net/altenerg/fossil.html.
(3) www.umich.edu/~ds265/society/fossilfuel.htm.
(4) www.energyquest.ca.gov/story/chapter08.html.
(5) Hayatsu, R.; Winans, R. E.; Scott, R. G.; Moore, L. P. and Studier, M. H. *Fuel* **1978**, *57*, 541-548.
(6) Killops, S. and Killops, V. *Introduction to Organic Geochemistry. Blackwell Publishing, 2005*.
(7) Kropp, K. G. and Fedorak, P. M. *Canadian Journal of Microbiology* **1998**, *44*, 605-622.
(8) Czogalla, C. D. and Boberg, F. *Sulfur Reports* **1983**, *3*, 121-167.
(9) Janssen, A. J. H.; Keizer, A. D. and Kleinjan, W. E. *Elemental Sulfur and Sulfur-rich Compounds I. Springer, 2003; Vol. 230, p 167-188*.
(10) Cyr, T. D.; Payzant, J. D.; Montgomery, D. S. and Strausz, O. P. *Organic Geochemistry* **1986**, *9*, 139-143.
(11) Sinninghe Damsté, J. S.; Rijpstra, W. I. C.; De Leeuw, J. W. and Schenck, P. A. *Advances in Organic Geochemistry* **1987**, *13*, 593-606.
(12) Brassell, S. C.; Lewis, C. A.; Deleeuw, J. W.; Delange, F. and Sinninghe Damsté, J. S. *Nature* **1986**, *320*, 160-162.
(13) Sinninghe Damsté, J. S. and De Leeuw, J. W. *International Journal of Environmental Analytical Chemistry* **1987**, *28*, 1-19.
(14) Sinninghe Damsté, J. S.; De Leeuw, J. W.; Kock-Van Dalen, A. C.; De Zeeuw, M. A.; De Lange, F.; Rijpstra, W. I. C. and Schenck, P. A. *Geochimica et Cosmochimica Acta* **1987**, *51*, 2369-2391.
(15) Vairavamurthy, A. and Mopper, K. *Nature* **1987**, *329*, 623-625.
(16) Sinninghe Damsté, J. S.; Rijpstra, W. I. C.; De Leeuw, J. W. and Schenck, P. A. *Geochimica et Cosmochimica Acta* **1989**, *53*, 1323-1341.
(17) Schmid, J. C.; Connan, J. and Albrecht, P. *Nature* **1987**, *329*, 54-56.
(18) Schade, T. *Analytik von Alkylierten Dibenzothiophenen in Tiefentschwefelten Dieselölen. PhD thesis, Institute of Inorganic and Analytical Chemistry, University of Münster, Münster, 2004*.
(19) www.chevron.com/products/default.aspx.
(20) Bej, S. K.; Maity, S. K. and Turaga, U. T. *Energy & Fuels* **2004**, *18*, 1227-1237.
(21) Babich, I. V. and Moulijn, J. A. *Fuel* **2003**, *82*, 607-631.
(22) Brunet, S.; Mey, D.; Pérot, G.; Bouchy, C. and Diehl, F. *Applied Catalysis A: General* **2005**, *278*, 143-172.
(23) Rudzinski, W. E.; Zhou, K. and Luo, X. M. *Energy & Fuels* **2004**, *18*, 16-21.
(24) www.npra.org/issues/fuels/diesel_sulfur.cfm.
(25) www.dieselnet.com/standards/jp/fuel.php.
(26) Rudzinski, W. E. and Rai, V. *Energy & Fuels* **2005**, *19*, 1611-1618.
(27) Kim, J. H.; Ma, X. L.; Song, C. S.; Lee, Y. K. and Oyama, S. T. *Energy & Fuels* **2005**, *19*, 353-364.
(28) Shiraishi, Y.; Hirai, T. and Komasawa, I. *Industrial & Engineering Chemistry Research* **2001**, *40*, 3398-3405.
(29) Hirai, T.; Ogawa, K. and Komasawa, I. *Industrial & Engineering Chemistry Research* **1996**, *35*, 586-589.

(30) Ma, X. L.; Sakanishi, K. Y. and Mochida, I. *Industrial & Engineering Chemistry Research* **1994**, *33*, 218-222.
(31) Macaud, M.; Sévignon, M.; Favre-Réguillon, A.; Lemaire, M.; Schulz, E. and Vrinat, M. *Industrial & Engineering Chemistry Research* **2004**, *43*, 7843-7849.
(32) Bacaud, R.; Cebolla, V. L.; Membrado, L.; Matt, M.; Pessayre, S. and Galvez, E. M. *Industrial & Engineering Chemistry Research* **2002**, *41*, 6005-6014.
(33) Shafi, R. and Hutchings, G. J. *Catalysis Today* **2000**, *59*, 423-442.
(34) Ma, X. L.; Sakanishi, K. and Mochida, I. *Industrial & Engineering Chemistry Research* **1996**, *35*, 2487-2494.
(35) Landau, M. V.; Berger, D. and Herskowitz, M. *Journal of Catalysis* **1996**, *159*, 236-245.
(36) Nagai, M.; Urimoto, H.; Uetake, K.; Sakikawa, N. and Gonzalez, R. D. *Bulletin of the Chemical Society of Japan* **1989**, *62*, 557-562.
(37) Nag, N. K.; Sapre, A. V.; Broderick, D. H. and Gates, B. C. *Journal of Catalysis* **1979**, *57*, 509-512.
(38) Satterfield, C. N.; Modell, M. and Wilkens, J. A. *Industrial & Engineering Chemistry Process Design and Development* **1980**, *19*, 154-160.
(39) Geneste, P.; Amblard, P.; Bonnet, M. and Graffin, P. *Journal of Catalysis* **1980**, *61*, 115-127.
(40) Houalla, M.; Broderick, D. H.; Sapre, A. V.; Nag, N. K.; Beer, V. H. J. D.; Gates, B. C. and Kwart, H. *Journal of Catalysis* **1980**, *61*, 523-527.
(41) Schulz, H.; Böhringer, W.; Ousmanov, F. and Waller, P. *Fuel Processing Technology* **1999**, *61*, 5-41.
(42) Kilanowski, D. R.; Teeuwen, H.; Debeer, V. H. J.; Gates, B. C.; Schuit, G. C. A. and Kwart, H. *Journal of Catalysis* **1978**, *55*, 129-137.
(43) Kabe, T.; Ishihara, A. and Tajima, H. *Industrial & Engineering Chemistry Research* **1992**, *31*, 1577-1580.
(44) Kabe, T.; Ishihara, A. and Zhang, Q. *Applied Catalysis A: General* **1993**, *97*, L1-L9.
(45) Shiraishi, Y.; Hirai, T. and Komasawa, I. *Industrial & Engineering Chemistry Research* **2001**, *40*, 293-303.
(46) Shiraishi, Y. and Hirai, T. *Energy & Fuels* **2004**, *18*, 37-40.
(47) Milenkovic, A.; Schulz, E.; Meille, V.; Loffreda, D.; Forissier, M.; Vrinat, M.; Sautet, P. and Lemaire, M. *Energy & Fuels* **1999**, *13*, 881-887.
(48) Meille, V.; Schulz, E.; Vrinat, M. and Lemaire, M. *Chemical Communications* **1998**, 305-306.
(49) Hernández-Maldonado, A. J.; Stamatis, S. D.; Yang, R. T.; He, A. Z. and Cannella, W. *Industrial & Engineering Chemistry Research* **2004**, *43*, 769-776.
(50) Ma, X. L.; Sakanishi, K.; Isoda, T. and Mochida, I. *Fuel* **1997**, *76*, 329-339.
(51) Institut Français du Pétrole, D. o. P. a. A. *Petroleum Products; Separation of Saturates, Aromatics, Resins and Asphaltanes Fractions; Liquid Adsorption Chromatography*.
(52) Later, D. W.; Lee, M. L.; Bartle, K. D.; Kong, R. C. and Vassilaros, D. L. *Analytical Chemistry* **1981**, *53*, 1612-1620.
(53) Andersson, J. T. *Separation Methods in the Analysis of Polycyclic Aromatic Sulfur Heterocycles. Elsevier Science B. V., 2001; Vol. 3, p 75-98*.
(54) Frysingèr, G. S.; Gaines, R. B. and Reddy, C. M. *Abstracts of Papers of the American Chemical Society* **2002**, *224*, U519-U520.
(55) Carbognani, L. and Izquierdo, A. *Journal of Chromatography* **1989**, *484*, 399-408.
(56) Bundt, J.; Herbel, W. and Steinhart, H. *Journal of High Resolution Chromatography* **1992**, *15*, 682-685.

(57) Willey, C.; Iwao, M.; Castle, R. N. and Lee, M. L. *Analytical Chemistry* **1981**, *53*, 400-407.
(58) Drushel, H. V. and Sommers, L. *Analytical Chemistry* **1967**, *39*, 1819-1829.
(59) Andersson, J. T. *International Journal of Environmental Analytical Chemistry* **1992**, *48*, 1-15.
(60) Seshadri, T. and Kettrup, A. *Fresenius Zeitschrift für Analytische Chemie* **1982**, *310*, 1-5.
(61) Helfferich, F. *Nature* **1961**, *189*, 1001-1002.
(62) Ghaloun, N.; Michael, G. and Khan, Z. *Journal of Liquid Chromatography & Related Technologies* **2002**, *25*, 1409-1420.
(63) Andersson, J. T. *Analytical Chemistry* **1987**, *59*, 2207-2209.
(64) Andersson, J. T.; Schade, T. and Müller, H. *Abstracts of Papers of the American Chemical Society* **2002**, *224*, U574-U575.
(65) Nishioka, M. *Energy & Fuels* **1988**, *2*, 214-219.
(66) Marvin, C. H.; Li, C. L.; Allan, L. M. and McCarry, B. E. *International Journal of Environmental Analytical Chemistry* **2000**, *77*, 15-28.
(67) Müller, H.; Andersson, J. T. and Schrader, W. *Analytical Chemistry* **2005**, *77*, 2536-2543.
(68) Schade, T.; Roberz, B. and Andersson, J. T. *Polycyclic Aromatic Compounds* **2002**, *22*, 311-320.
(69) Sripada, K. and Andersson, J. T. *Analytical and Bioanalytical Chemistry* **2005**, *382*, 735-741.
(70) Olsson, M.; Sander, L. C. and Wise, S. A. *Journal of Chromatography* **1989**, *477*, 277-290.
(71) Panda, S. K.; Schrader, W. and Andersson, J. T. *Journal of Chromatography A* **2006**, *1122*, 88-96.
(72) Félix, G.; Thienpont, A. and Dentraygues, P. *Chromatographia* **1992**, *34*, 177-181.
(73) Ecknig, W.; Trung, B.; Radeglia, R. and Gross, U. *Chromatographia* **1982**, *16*, 178-182.
(74) Nondek, L. and Malek, J. *Journal of Chromatography* **1978**, *155*, 187-190.
(75) Holstein, W. *Chromatographia* **1981**, *14*, 468-477.
(76) McKinney, D. E.; Clifford, D. J.; Hou, L.; Bogdan, M. R. and Hatcher, P. G. *Energy & Fuels* **1995**, *9*, 90-96.
(77) Jadaud, P.; Caude, M. and Rosset, R. *Journal of Chromatography* **1988**, *439*, 195-211.
(78) Wise, S. A.; Chesler, S. N.; Hertz, H. S.; Hilpert, L. R. and May, W. E. *Analytical Chemistry* **1977**, *49*, 2306-2310.
(79) Mansfield, C. T.; Barman, B. N.; Thomas, J. V.; Mehrotra, A. K. and McCann, J. M. *Analytical Chemistry* **1999**, *71*, 81R-107R.
(80) Al-Zaid, K.; Khan, Z. H.; Hauser, A. and Al-Rabiah, H. *Fuel* **1998**, *77*, 453-458.
(81) Selucky, M. L.; Parker, R. J. and Frakman, Z. G. *Fuel Processing Technology* **1992**, *32*, 77-86.
(82) Hirsch, D. E.; Hopkins, R. L.; Coleman, H. J.; Cotton, F. O. and Thompson, C. J. *Analytical Chemistry* **1972**, *44*, 915-919.
(83) Rodgers, P. A.; Creagh, A. L.; Prange, M. M. and Prausnitz, J. M. *Industrial & Engineering Chemistry Research* **1987**, *26*, 2312-2318.
(84) Alexander, G. L.; Creagh, A. L. and Prausnitz, J. M. *Industrial & Engineering Chemistry Fundamentals* **1985**, *24*, 301-310.
(85) Larsen, B. S.; Fenselau, C. C.; Whitehurst, D. D. and Angelini, M. M. *Analytical Chemistry* **1986**, *58*, 1088-1091.
(86) Boduszynski, M. M. *Energy & Fuels* **1988**, *2*, 597-613.

(87) Woods, J. R.; Kung, J.; Adjaye, J.; Kotlyar, L. S.; Sparks, B. D. and Chung, K. H. *Petroleum Science and Technology* **2004**, *22*, 347-365.
(88) Wingen, L. M.; Low, J. C. and Finlayson-Pitts, B. J. *Journal of Chemical Education* **1998**, *75*, 1599-1603.
(89) Pasadakis, N.; Gaganis, V. and Varotsis, N. *Fuel* **2001**, *80*, 147-153.
(90) Pace, C. M. and Betowski, L. D. *Journal of the American Society for Mass Spectrometry* **1995**, *6*, 597-607.
(91) Davies, I. L.; Bartle, K. D.; Williams, P. T. and Andrews, G. E. *Analytical Chemistry* **1988**, *60*, 204-209.
(92) Mössner, S. G. and Wise, S. A. *Analytical Chemistry* **1999**, *71*, 58-69.
(93) Wise, S. A.; Sander, L. C. and May, W. E. *Journal of Chromatography* **1993**, *642*, 329-349.
(94) Link, D. D.; Baltrus, J. P. and Rothenberger, K. S. *Energy & Fuels* **2003**, *17*, 1292-1302.
(95) Hua, R. X.; Wang, J. H.; Kong, H. W.; Liu, J.; Lu, X. and Xu, G. W. *Journal of Separation Science* **2004**, *27*, 691-698.
(96) Thomas, D.; Crain, S. M.; Sim, P. G. and Benoit, F. M. *Journal of Mass Spectrometry* **1995**, *30*, 1034-1040.
(97) López Garcia, C.; Becchi, M.; Grenier-Loustalot, M. F.; Païsse, O. and Szymanski, R. *Analytical Chemistry* **2002**, *74*, 3849-3857.
(98) Garcia, C. L.; Becchi, M.; Grenier-Loustalot, M. F.; Paisse, O. and Szymanski, R. *Analytical Chemistry* **2002**, *74*, 3849-3857.
(99) Herod, A. A.; Bartle, K. D. and Kandiyoti, R. *Energy & Fuels* **2007**, *21*, 2176-2203.
(100) Benner, R. L. and Stedman, D. H. *Analytical Chemistry* **1989**, *61*, 1268-1271.
(101) Nishioka, M.; Bradshaw, J. S.; Lee, M. L.; Tominaga, Y.; Tedjamulia, M. and Castle, R. N. *Analytical Chemistry* **1985**, *57*, 309-312.
(102) Yin, C. and Xia, D. *Fuel* **2004**, *83*, 433-441.
(103) Andersson, J. T. *Analytical and Bioanalytical Chemistry* **2002**, *373*, 344-355.
(104) Kurata, S. and Nagai, M. *Energy & Fuels* **2004**, *18*, 1220-1225.
(105) Hegazi, A. H.; Andersson, J. T. and El-Gayar, M. S. *Fuel Processing Technology* **2004**, *85*, 1-19.
(106) Stumpf, A.; Tolvaj, K. and Juhász, M. *Journal of Chromatography A* **1998**, *819*, 67-74.
(107) Depauw, G. A. and Froment, G. F. *Journal of Chromatography A* **1997**, *761*, 231-247.
(108) Lumpkin, H. E. *Analytical Chemistry* **1956**, *28*, 1946-1948.
(109) Qian, K. N. and Dechert, G. J. *Analytical Chemistry* **2002**, *74*, 3977-3983.
(110) Hsu, C. S. and Qian, K. *Energy & Fuels* **1993**, *7*, 268-272.
(111) Holmes, S. A. and Raska, K. A. *Fuel* **1986**, *65*, 1539-1545.
(112) Robins, C. and Limbach, P. A. *Rapid Communications in Mass Spectrometry* **2003**, *17*, 2839-2845.
(113) Jackson, S. N. and Murray, K. K. *Rapid Communications in Mass Spectrometry* **2001**, *15*, 1448-1452.
(114) Schaub, T. M.; Hendrickson, C. L.; Qian, K. N.; Quinn, J. P. and Marshall, A. G. *Analytical Chemistry* **2003**, *75*, 2172-2176.
(115) Van Berkel, G. J. and Asano, K. G. *Analytical Chemistry* **1994**, *66*, 2096-2102.
(116) Fenn, J. B.; Mann, M.; Meng, C. K.; Wong, S. F. and Whitehouse, C. M. *Mass Spectrometry Reviews* **1990**, *9*, 37-70.
(117) Stenson, A. C.; Landing, W. M.; Marshall, A. G. and Cooper, W. T. *Analytical Chemistry* **2002**, *74*, 4397-4409.

(118) Lafleur, A. L.; Taghizadeh, K.; Howard, J. B.; Anacleto, J. F. and Quilliam, M. A. *Journal of the American Society for Mass Spectrometry* **1996**, *7*, 276-286.
(119) Marvin, C. H.; Smith, R. W.; Bryant, D. W. and McCarry, B. E. *Journal of Chromatography A* **1999**, *863*, 13-24.
(120) Panda, S. K.; Schrader, W.; al-Hajji, A. and Andersson, J. T. *Energy & Fuels* **2007**, *21*, 1071-1077.
(121) Apicella, B.; Alfè, M.; Barbella, R.; Tregrossi, A. and Ciajolo, A. *Atti del 29th Meeting of the Italian Section of the Combustion Institute, Pisa, June14-17* **2006**, III3.1-III3.6.
(122) Schrader, W.; Panda, S. K.; Brockmann, K. L. and Benter, T. *The Analyst* **2008**.
(123) Gross, J. H. *Mass Spectrometry, A Textbook. Springer, 2004*.
(124) March, R. E. *Journal of Mass Spectrometry* **1997**, *32*, 351-369.
(125) Hughey, C. A.; Rodgers, R. P. and Marshall, A. G. *Analytical Chemistry* **2002**, *74*, 4145-4149.
(126) Wu, Z. G.; Jernstrom, S.; Hughey, C. A.; Rodgers, R. P. and Marshall, A. G. *Energy & Fuels* **2003**, *17*, 946-953.
(127) Kramer, R. W.; Kujawinski, E. B. and Hatcher, P. G. *Environmental Science & Technology* **2004**, *38*, 3387-3395.
(128) Guan, S. H.; Marshall, A. G. and Scheppele, S. E. *Analytical Chemistry* **1996**, *68*, 46-71.
(129) Marshall, A. G. and Rodgers, R. P. *Accounts of Chemical Research* **2004**, *37*, 53-59.
(130) Wu, Z. G.; Rodgers, R. P. and Marshall, A. G. *Analytical Chemistry* **2004**, *76*, 2511-2516.
(131) www.chm.bris.ac.uk/ms/theory/fticr-massspec.html.
(132) Marshall, A. G.; Hendrickson, C. L. and Jackson, G. S. *Mass Spectrometry Reviews* **1998**, *17*, 1-35.
(133) Marshall, A. G. and Grosshans, P. B. *Analytical Chemistry* **1991**, *63*, 215-229.
(134) Marshall, A. G. and Hendrickson, C. L. *Annual Review of Analytical Chemistry* **2008**, *1*, 19.11-19.21.
(135) Schrader, W. and Klein, H. W. *Analytical and Bioanalytical Chemistry* **2004**, *379*, 1013-1024.
(136) Miyabayashi, K.; Naito, Y.; Tsujimoto, K. and Miyake, M. *International Journal of Mass Spectrometry* **2002**, *221*, 93-105.
(137) Fu, J. M.; Kim, S.; Rodgers, R. P.; Hendrickson, C. L.; Marshall, A. G. and Qian, K. N. *Energy & Fuels* **2006**, *20*, 661-667.
(138) Zeller, L. C.; Kennady, J. M.; Kenttämaa, H. and Campana, J. E. *Analytical Chemistry* **1993**, *65*, 2116-2118.
(139) Hughey, C. A.; Rodgers, R. P.; Marshall, A. G.; Qian, K. N. and Robbins, W. K. *Organic Geochemistry* **2002**, *33*, 743-759.
(140) Bruce, J. E.; Anderson, G. A.; Udseth, H. R. and Smith, R. D. *Analytical Chemistry* **1998**, *70*, 519-525.
(141) Wu, Z. G.; Rodgers, R. P. and Marshall, A. G. *Energy & Fuels* **2005**, *19*, 1072-1077.
(142) Rodgers, R. P.; White, F. M.; Hendrickson, C. L.; Marschall, A. G. and Andersen, K. V. *Analytical Chemistry* **1998**, *70*, 4743-4750.
(143) Klein, G. C.; Rodgers, R. P. and Marshall, A. G. *Fuel* **2006**, *85*, 2071-2080.
(144) Müller, H.; Schrader, W. and Andersson, J. T. *Abstracts of Papers of the American Chemical Society* **2004**, *227*, U1092-U1092.
(145) Kim, S.; Stanford, L. A.; Rodgers, R. P.; Marshall, A. G.; Walters, C. C.; Qian, K.; Wenger, L. M. and Mankiewicz, P. *Organic Geochemistry* **2005**, *36*, 1117-1134.
(146) Stanford, L. A.; Rodgers, R. P.; Marshall, A. G.; Czarnecki, J.; Wu, X. A. and Taylor, S. *Energy & Fuels* **2007**, *21*, 973-981.

(147) Schaub, T. M.; Rodgers, R. P. and Marshall, A. G. *Energy & Fuels* **2005**, *19*, 1566-1573.
(148) Stanford, L. A.; Kim, S.; Klein, G. C.; Smith, D. F.; Rodgers, R. P. and Marshall, A. G. *Environmental Science & Technology* **2007**, *41*, 2696-2702.
(149) Purcell, J. M.; Hendrickson, C. L.; Rodgers, R. P. and Marshall, A. G. *Analytical Chemistry* **2006**, *78*, 5906-5912.
(150) Kim, S.; Rodgers, R. P. and Marshall, A. G. *International Journal of Mass Spectrometry* **2006**, *251*, 260-265.
(151) Panda, S. K.; Andersson, J. T. and Schrader, W. *Analytical and Bioanalytical Chemistry* **2007**, *389*, 1329-1339.
(152) Campbell, J. L.; Crawford, K. E. and Kenttämaa, H. I. *Analytical Chemistry* **2004**, *76*, 959-963.
(153) Barrow, M. P.; McDonnell, L. A.; Feng, X. D.; Walker, J. and Derrick, P. J. *Analytical Chemistry* **2003**, *75*, 860-866.
(154) Milgram, K. E.; White, F. M.; Goodner, K. L.; Watson, C. H.; Koppenaal, D. W.; Barinaga, C. J.; Smith, B. H.; Winefordner, J. D.; Marshall, A. G.; Houk, R. S. and Eyler, J. R. *Analytical Chemistry* **1997**, *69*, 3714-3721.
(155) Wang, Z. and Fingas, M. *Journal of Chromatography A* **1997**, *774*, 51-78.
(156) Nolte, T. *Kapillarelektrophoretische Trennung Derivatisierter Polyaromatischer Schwefelheterocyclen. MSc thesis, Institute of Inorganic and Analytical Chemistry, University of Münster, Münster, 2008*.
(157) Künnemeyer, J. *Kapillarelektrophoretische Trennung Derivatisierter Polyaromatischer Schwefelheterocyclen. Institute of Inorganic and Analytical Chemistry, University of Münster, Münster, 2005*.
(158) Singh, H. and Gulati, I. B. *Revue de L'Institut Francais du Pétrole* **1987**, *42*, 587-598.
(159) Semple, K. M.; Cyr, N.; Fedorak, P. M. and Westlake, D. W. S. *Canadian Journal of Chemistry* **1990**, *68*, 1092-1099.
(160) Kapur, G. S.; Chopra, A. and Sarpal, A. S. *Energy & Fuels* **2005**, *19*, 1065-1071.
(161) Kapur, G. S. and Berger, S. *Energy & Fuels* **2005**, *19*, 508-511.
(162) Giraud, J. and Marzin, C. *Organic Magnetic Resonance* **1979**, *12*, 647-651.
(163) Clutter, D. R.; Petrakis, L.; Stenger, R. L. and Jensen, R. K. *Analytical Chemistry* **1972**, *44*, 1395-1405.
(164) Struppe, H. G.; Janke, H.; Deutsch, K. and Grunov, S. *Petroleum Chemistry* **1987**, *27*, 1-11.
(165) Jaramillo, J. C. P.; Velazco, D. R. M. and Baldrich, C. *Fuel* **2004**, *83*, 337-342.
(166) Ali, F.; Khan, Z. H. and Ghaloum, N. *Energy & Fuels* **2004**, *18*, 1798-1805.
(167) Charrié-Duhaut, A.; Schaeffer, C.; Adam, P.; Manuelli, P.; Scherrer, P. and Albrecht, P. *Angewandte Chemie* **2003**, *115*, 4794-4797.
(168) Green, T. K.; Whitley, P.; Wu, K.; Lloyd, W. G. and Zhui Gan, L. Z. *Energy & Fuels* **1994**, *8*, 814-814.
(169) George, G. N.; Gorbaty, M. L.; Kelemen, S. R. and Sansone, M. *Energy & Fuels* **1991**, *5*, 93-97.
(170) Kelemen, S. R.; George, G. N. and Gorbaty, M. L. *Fuel* **1990**, *69*, 939-944.
(171) Kok, W. T. *Chromatographia* **2000**, *51*, S5-S89.
(172) Jorgenson, J. W. and Lukacs, K. D. *Journal of Chromatography* **1981**, *218*, 209-216.
(173) Hsu, C. S.; Qian, K. N. and Chen, Y. N. C. *Analytica Chimica Acta* **1992**, *264*, 79-89.
(174) Kendrick, E. *Analytical Chemistry* **1963**, *35*, 2146-2154.
(175) Chmielowiec, J. and George, A. E. *Analytical Chemistry* **1980**, *52*, 1154-1157.
(176) Hinze, W. L. *Separation and Purification Methods* **1981**, *10*, 159-237.
(177) Granzow, A. and Wilson, A. *Journal of Organic Chemistry* **1972**, *37*, 3063-3066.

(178) Yamazaki, S. *Tetrahedron Letters* **2001**, *42*, 3355-3357.
(179) Reitsema, R. H. and Allphin, N. L. *Journal of Organic Chemistry* **1962**, *27*, 27-28.
(180) Lee, S. and Fuchs, P. L. *Journal of the American Chemical Society* **2002**, *124*, 13978-13979.
(181) Friedman, L.; Fishel, D. L. and Shechter, H. *Journal of Organic Chemistry* **1965**, *30*, 1453-1457.
(182) Duty, R. C.; Hayatsu, R.; Scott, R. G.; Moore, L. P.; Winans, R. E. and Studier, M. H. *Fuel* **1980**, *59*, 97-101.
(183) Winans, R. E.; Scott, R. G.; McBeth, R. L. and Hayatsu, R. *Abstracts of Papers of the American Chemical Society* **1980**, *179*, 262-267.
(184) Warton, B.; Alexander, R. and Kagi, R. I. *Organic Geochemistry* **1999**, *30*, 1255-1272.
(185) Remusat, L.; Derenne, S. and Robert, F. *Geochimica et Cosmochimica Acta* **2005**, *69*, 4377-4386.
(186) Carlsen, P. H. J.; Katsuki, T.; Martin, V. S. and Sharpless, K. B. *Journal of Organic Chemistry* **1981**, *46*, 3936-3938.
(187) Nuñez, M. T. and Martin, V. S. *Journal of Organic Chemistry* **1990**, *55*, 1928-1932.
(188) Chakraborti, A. K. and Ghatak, U. R. *Journal of the Chemical Society-Perkin Transactions 1* **1985**, 2605-2609.
(189) Méndez, A.; Bermejo, J.; Santamaria, R.; Blanco, C. G. and Menéndez, R. *Energy & Fuels* **2000**, *14*, 936-942.
(190) Bakke, J. M. and Frøhaug, A. E. *Journal of Physical Organic Chemistry* **1996**, *9*, 310-318.
(191) Kasai, M. and Ziffer, H. *Journal of Organic Chemistry* **1983**, *48*, 2346-2349.
(192) Bressan, M.; Forti, L. and Morvillo, A. *Journal of Molecular Catalysis* **1993**, *84*, 59-66.
(193) Blokker, P.; Schouten, S.; de Leeuw, J. W.; Sinninghe Damsté, J. S. and van den Ende, H. *Geochimica et Cosmochimica Acta* **2000**, *64*, 2055-2065.
(194) Nomura, M.; Artok, L.; Murata, S.; Yamamoto, A.; Hama, H.; Gao, H. and Kidena, K. *Energy & Fuels* **1998**, *12*, 512-523.
(195) Obeng, M. and Stock, L. M. *Energy & Fuels* **1996**, *10*, 988-995.
(196) Kidena, K.; Matsumoto, K.; Murata, S. and Nomura, M. *Energy & Fuels* **2004**, *18*, 1709-1715.
(197) Yoshioka, H. and Ishiwatari, R. *Organic Geochemistry* **2005**, *36*, 83-94.
(198) Dragojlović, V.; Bajc, S.; Amblès, A. and Voitorović, D. *Organic Geochemistry* **2005**, *36*, 1-12.
(199) Griffith, W. P. and Kwong, E. *Synthetic Communications* **2003**, *33*, 2945-2951.
(200) Murahashi, S. I.; Komiya, N.; Oda, Y.; Kuwabara, T. and Naota, T. *Journal of Organic Chemistry* **2000**, *65*, 9186-9193.
(201) Fathalla, E. M. *Degradation of Crude Oil in the Environment: Toxicity Arising Through Photochemical Oxidation in the Aqueous Phase. PhD thesis, Institute of Inorganic and Analytical Chemistry, University of Münster, Münster, 2007*.
(202) Nakamichi, N.; Kawabata, H. and Hayashi, M. *Journal of Organic Chemistry* **2003**, *68*, 8272-8273.
(203) March, J. and Smitch, M. B. *March's Advanced Organic Chemistry. Reactions, Mechanisms, and Structure. Wiley & Sons, 2007*.
(204) Rabindran, K. and Tilak, B. D. *Proceedings of the Indian Academy of Science, Section A* **1952**, *37*, 557-563.
(205) Patai, S. and Rappoport, Z. *The Chemistry of the Quinonoid Compounds. Chapter 23. Quinones as Oxidants and Dehydrogenating Agents. Wiley, 1988; p. 1351-1384*.

(206) Dwivedi, P. C.; Banga, A. K. and Agarwal, R. *Indian Journal of Chemistry, Section A: Inorganic, Bio-inorganic, Physical, Theoretical & Analytical* **1985**, *24*, 459-462.
(207) Bushman, D.; Grossman, S. J.; Jerina, D. M. and Lehr, R. E. *Journal of Organic Chemistry* **1989**, *54*, 3533-3544.
(208) Radtke, R.; Hintze, H.; Rösler, K. and Heesing, A. *Chemische Berichte* **1990**, *123*, 627-633.
(209) Brock, M.; Hintze, H. and Hessing, A. *Chemische Berichte* **1986**, *119*, 3727-3736.
(210) Young, T. E.; Heitz, L. J. and Steklenski, D. J. *Journal of Organic Chemistry* **1973**, *38*, 1567-1569.
(211) Horn, T.; Wegener, S. and Müllen, K. *Macromolecular Chemistry and Physics* **1995**, *196*, 2463-2474.
(212) Müller, P.; Joly, D. and mermoud, F. *Helvetica Chimica Acta* **1984**, *67*, 105-112.
(213) Marrocchi, A.; Minuti, L.; Taticchi, A. and Scheeren, H. W. *Tetrahedron* **2001**, *57*, 4959-4965.
(214) Fieser, M. *Fieser and Fieser's Reagents for Organic Synthesis. Wiley, 2007; Vol. 1-23*.
(215) Begouin, A. and Hesse, S. *10th International Electronic Conference on Sythetic Organic Chemistry (ECSOC-10)* **2006**.
(216) Boberg, F.; Bruns, W.; Kaller, R. and Mußhoff, D. *Phosphorus, Sulfur, and Silicon* **1992**, *72*, 33-47.
(217) Ali, S. M.; Findlay, J. W. A. and Turner, A. B. *Journal of the Chemical Society-Perkin Transactions 1* **1976**, 407-410.
(218) Gonzales, A. G.; Rodriguez, C. M. and Luis, J. G. *Journal of Chemical Research (S)* **1988**, 114-115.
(219) Andersson, J. T.; Schräder, W.; Traulsen, F. and Werlich, S. *Polycyclic Aromatic Compounds* **2001**, *18*, 351-360.
(220) Lee, C. G.; Lee, K. Y.; Kim, S. C. and Kim, J. N. *Bulletin of the Korean Chemical Society* **2005**, *26*, 485-487.
(221) Mukhopadhyay, S.; Rothenberg, G.; Wiener, H. and Sasson, Y. *New Journal of Chemistry* **2000**, *24*, 305-308.
(222) Kuznetsova, E. A.; Postnova, M. V.; Koshel', S. G.; Lebedeva, N. V.; Yun'kova, T. A. and Koshel', G. N. *Russian Journal of Organic Chemistry* **2004**, *40*, 1288-1290.
(223) Parihar, J. A. and Ramana, M. M. V. *Chinese Journal of Chemistry* **2004**, *22*, 1196-1199.
(224) Anastassiadou, M.; Baziard-Mouysset, G. and Payard, M. *Synthesis* **2000**, 1814-1816.
(225) Ramana, M. M. V. and Potnis, P. V. *Synthesis* **1996**, 1090-1092.
(226) Cossy, J. and Belotti, D. *Organic Letters* **2002**, *4*, 2557-2559.
(227) Nagy, G.; Hancsók, J.; Varga, Z.; Pölczmann, G. and Kalló, D. *Topics in Catalysis* **2007**, *45*, 195-201.
(228) Tedjamulia, M. L.; Tominaga, Y. and Castle, R. N. *Journal of Heterocyclic Chemistry* **1983**, *20*, 1485-1495.
(229) House, W. T. and Orchin, M. *Journal of the American Chemical Society* **1960**, *82*, 639-642.
(230) Silverwood, H. A. and Orchin, M. *Journal of Organic Chemistry* **1962**, *27*, 3401-3404.
(231) Das, B.; Vankateswarlu, K.; Mahender, G. and Mahender, I. *Tetrahedron Letters* **2005**, *46*, 3041-3044.
(232) Tanemura, K.; Suzuki, T.; Nishida, Y.; Satsumabayashi, K. and Horaguchi, T. *Chemical Communications* **2004**, 470-471.
(233) Aoyama, T.; Takido, T. and Kodomari, M. *Synlett* **2005**, 2739-2742.

(234) Meille, V.; Schulz, E.; Lemaire, M.; Faure, R. and Vrinat, M. *Tetrahedron* **1996**, *52*, 3953-3960.
(235) Kuehm-Caubère, C.; Adach-Becker, S.; Fort, Y. and Caubère, P. *Tetrahedron* **1996**, *52*, 9087-9092.

Lebenslauf

Name:	**Magdalena Ulman**
Geburtsdatum:	26. 09. 1977
Geburtsort:	Białystok
Staatsangehörigkeit:	polnisch
Eltern:	Alina Anna Olszewska (geb. Gąsowska)
	Marek Józef Olszewski
Schulausbildung	
1984 - 1992	J. Korczak-Grundschule Nr. 31 in Białystok. Polen
1992 - 1996	III Allgemeinbildente K. K. Baczyński-Lyzeum in Białystok, Polen
23. 05. 1996	Allgemeine Hochschulreife Abschlussnote: sehr gut
Studium	
1996 - 2001	Studium der Chemie an der Universität Białystok, Polen
10. 2000 - 06. 2001	Diplomarbeit in Chemie zum Thema: “Oberflächenlipide aus getrockneten Blättern verschiedener Typen der Tabakpflanze *Nicotiana tabacum*”
19. 06. 2001	Diplomprüfung Abschlussnote: sehr gut
Promotionsstudium	
01. 10. 2005	Beginn der Dissertation in der NRW Graduate School of Chemistry am Institut für Anorganische und Analytische Chemie unter Betreuung von Prof. Jan T. Andersson
Berufstätigkeit	
11. 2001 - 09. 2005	Wissenschaftliche Mitarbeiterin am Institut für Chemie an der Universität Białystok, Polen
02. 2001 - 08. 2001	Wissenschaftliche Hilfskraft am Labor des Zollamts in Białystok, Polen

Acknowledgement

First of all I would like to thank my supervisor Prof. Jan T. Andersson for his continuous support, scientific guidance and contagious enthusiasm. The successful completion of my scientific work was possible by his valuable suggestions and hours of discussion. His optimistic attitude and pleasant nature made my stay here truly nice. Being one of the members of AK Andersson has been an honor to me.

I would like to thank Prof. Uwe Karst and Prof. Günter Haufe for their consent to be my mentors.

I thank the NRW Graduate School of Chemistry at the University of Münster (GSC-MS) for providing the financial support and all the members of GSC-MS, in particular Prof. Hellmut Eckert, Dr. Hubert Koller, Dr. Stefan Elbers, Uta Bröcker, Christiana Bäumer und Simone Ulke for their support and help in the bureaucracy procedure during my stay in Germany.

The work was accomplished in collaboration with the Max-Planck-Institute of Coal Research in Mülheim an der Ruhr (Germany). Special thanks to PD Dr. Wolfgang Schrader for the coordination of the work and Dr. Saroj Panda for FT-ICR MS measurements.

All my colleagues from AK Andersson: Dr. Thomas Schade, Dr. Kishore Sripada, Dr. Saroj Panda, Dr. Nina Kolbe, Dr. (soon) Markus Penassa, Dr. (soon) Ansgar Japes, Thies Nolte, Stefan Hildebrandt, Margarete Nocun, Dr. Eiman Fathalla, Dr. Abdelrahman Hegazi, Peni Handayani, Claudia Sill, Karin Weißenhorn and Daniel Plothe created a pleasant atmosphere in the working environment and were always helpful, encouraging and motivating. Many thanks for all critical comments in the improvement of my thesis.

I would like to thank certain people from AK Karst: Torsten Vielhaber and Björn Meermann for the possibility of fluorescence spectroscopy measurement, Jens Künnemeyer for his support both in scientific and personal matters, Marianne Lüttmann for being always ready to help in the official matters.

Many thanks to three very important members of the GSC-MS: Kasia Koroniak, Aarón Flores-Figueroa and Tülay Aslı Tumay for being my close friends.

Special acknowledgement belongs to my family. Without its support and love I would not be able to achieve that all.

And the last but not the least I would like to thank very special person in my life, Sven Dorprigter, for motivation, help, teaching German (habe ich doch etwas gelernt, oder?), Snowboard, and just for being :)

Versicherung nach § 2 Absatz 4

Hiermit versichere ich, dass ich die vorgelegte Dissertation selbst und ohne unerlaubte Mittel angefertigt, alle in Anspruch genommenen Quellen und Hilfsmittel in der Dissertation angegeben habe und die Dissertation nicht bereits anderweitig als Prüfungsarbeit vorgelegen hat.

Münster, 26. September 2008 ……

(Magdalena Ulman)